

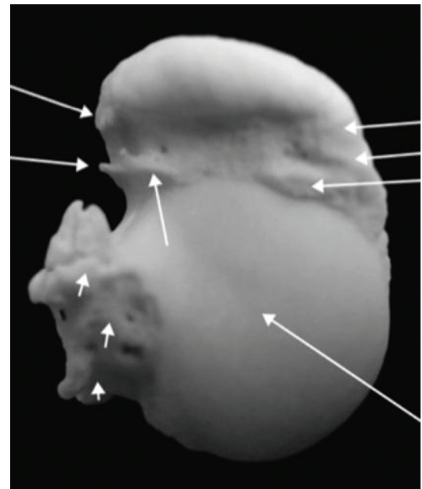
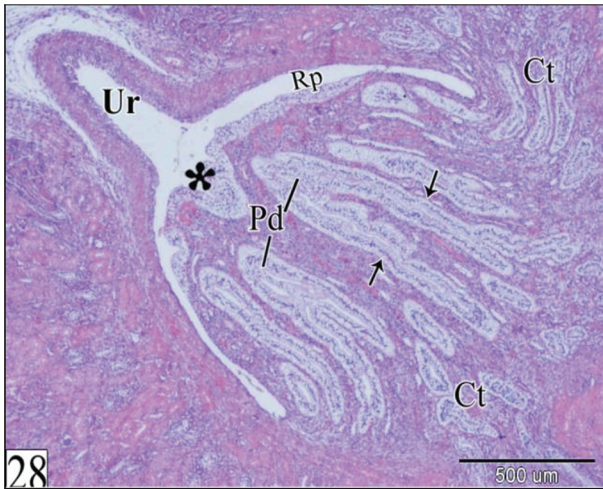
Journal of Veterinary Anatomy

Volume 10

October 2017

Number 2

Published by the African Association of Veterinary Anatomists



Asila for designing and publishing

Manuscripts and other related correspondence may be sent to:

Prof. Dr. Ashraf S. Saber
Editor, *Journal of Veterinary Anatomy*
Department of Anatomy and Embryology,
Faculty of Veterinary Medicine,
University of Sadat City, Sadat City, EGYPT
Phone : 00202 227 190 72
Mobile : 01204888019
E-mail : saberashraf_2@yahoo.com

Subscription : Annual subscription are advised to be sent for the year 2010 and onwards in favor of "Asela for designing and Publishing", Cairo. Renewal should be done before December every year so that the number of subscribers may be ascertained before the next issue of the journal (*J Vet. Anat.*) is published.

Subscription Rates

Annual : LE. 600 or US\$ 120
Three Years : LE. 1500 or US\$ 350
Life time : LE. 6.000 or US\$ 1200

Notice: Subscriptions in Egyptian Pounds is applicable to Egyptian Institutions and subscribers only.

Publisher: Asila for designing and Publishing
32 Mohamad Awad Street, Makram Ebeed, Nasr City, Cairo, EGYPT
Phone & Fax: 02 227 425 09
Website: www.tashkila.net

Cover Design: Prof. Ashraf S. Saber

Cover Photos: Unipapillary metanephros of rabbit embryo (upper left) & Proximal humerus of red fox (upper right) & Skull of obese blue fox (lower row)

Journal of Veterinary Anatomy



Editor

Ashraf S. Saber

*Department of Anatomy and Embryology,
Faculty of Veterinary Medicine, University of Sadat City,
Sadat City, EGYPT*

Members of the Advisory Board

<i>Prof. Dr. Christoph Muelling</i>	<i>(Germany)</i>
<i>Prof. Dr. Johanne Plendl</i>	<i>(Germany)</i>
<i>Prof. Dr. Karl Dietrich Weyrauch</i>	<i>(Germany)</i>
<i>Prof. Dr. Larry Freeman</i>	<i>(USA)</i>
<i>Prof. Dr. Marco A. Sampaio</i>	<i>(Brazil)</i>
<i>Prof. Dr. Mohamed El Sakhawy</i>	<i>(Egypt)</i>
<i>Prof. Dr. Nicola Mirabella</i>	<i>(Italy)</i>
<i>Prof. Dr. Rudolf Leiser</i>	<i>(Germany)</i>
<i>Prof. Dr. Robert Henry</i>	<i>(USA)</i>
<i>Prof. Dr. Sanaa Mokhtar</i>	<i>(Egypt)</i>
<i>Prof. Dr. Safwat Ragab</i>	<i>(Egypt)</i>
<i>Prof. Dr. Tom Caceci</i>	<i>(USA)</i>
<i>Prof. Dr. Wael Khamas</i>	<i>(USA)</i>
<i>Prof. Dr. Yoshiharu Hashimoto</i>	<i>(Japan)</i>

Contents

Volume 10

October 2017

Number 2

1) Anatomical Guide for Regional Anesthesia in the Buffalo in Egypt (*Bos bubalis* L.)

Farag, F.M., Daghash, S.M., El-Bably, S. H., Sary, R.G. and Hagrass S.M. 1-15

2) Anatomic and Radiographic Studies on the Paranasal Sinuses of the Buffalo in Egypt (*Bos bubalis*, L.)

Farag, F.M.M., Hagrass S.M., Daghash, S.M., El-Bably, S. H. and Sary, R.G. 17-35

3) Significant Diseases of Two Very Aged Red Foxes (*Vulpes vulpes*, Demarest 1820)

Dennis Lawler^{a,d,e,f*}, Julia Becker^b, Patricia Goodman^c, Richard Evans^d, Luci Kohn^e 50-37

4) Skeletal Pathology of Farm-Reared Obese Juvenile Blue Foxes (*Vulpes lagopus*)

Anne-Mari Mustonen^{a,b}, Dennis F. Lawler^c, Leena Ahola^d, Tarja Koistinen^{d,e}, Liisa Jalkanen^f, Jaakko Mononen^e, Marja-Leena Lamidi^g, Petteri Nieminen^{a,b} 51-74

5) Macro-anatomic Investigation of Larynx, Trachea and Lungs in Martens (*Martes Foina*)

Yasin Demiraslan^{1*}, Iftar Gurbuz¹, OzcanOzgel¹ 75-83

6) Morphological and Craniometric Features of the Skull of African Savanna Hare (*Lepus microtis*) Found in North-Central Nigeria

Fatima O. Oyelowo¹, Ifukibot I. Usende^{1*}, Idris A. Azeez² and Abdulsalam E. Aminu¹ 85-107

7) Development of the Rabbit (*Oryctolagus cuniculus*) Metanephros

W. Gaber 109-130

Anatomical Guide for Regional Anesthesia in the Buffalo in Egypt (*Bos bubalis* L.)

Farak, F.M., Daghash, S.M., El-Bably, S. H., Sary, R.G. and Hagrass S.M.

Anatomy and Embryology Department, Faculty of Veterinary Medicine, Cairo University

With 9 figures

Received October 2016, accepted for publication in April 2017

Abstract

The present study was conducted on eight buffaloes (*Bos bubalis* L.) of ages ranging between 2-7 years. The specimens were prepared by the routine anatomical methods used for fixing and manually dissected to expose the topographic arrangement of the nerves of flank and face of most clinical importance and commonly subjected to nerve block in cases of the surgical approaches to the flank as well as for the minute surgical operation in the head involving the nostrils, lips and horns. The definite site of injection of anesthetic drug was also suggested for each nerve. The study revealed that, the regional anesthesia of the mid paralumbar fossa in the buffalo was achieved through three distal paravertebral injections. The most cranial one for anesthesia of the costoabdominal nerve, at the upper part of the flank about 5 cm from the free end of the second lumbar transverse process and 7 cm caudal to the

last rib and at a depth of about 3 cm. The middle one for blocking the iliohypogastric was indicated 5 cm below the 3rd lumbar transverse process midway between the last rib cranially and tuber coxae caudally, while the most caudal one for anesthesia of the ilioinguinal nerve inserts was applied about 5 cm cranial to the tuber coxae, 5 cm below the free end of the 4th lumbar transverse process.

The infra-orbital, mental and cornual nerves were the most clinically important sensory nerves in the head region. For anesthesia of the infra-orbital nerve the anesthetic drug was injected in the vicinity of the infra-orbital foramen which was situated 1.5 cm dorsal to the first cheek tooth and about 6 cm rostral to the facial tubercle. For anesthesia of the mental nerve the needle was inserted at the middle distance of the lateral surface of the interalveolar space of the mandible between the lateral incisor and

first premolar teeth. For anesthesia of the cornual nerve, the site of this regional block was midway between the orbital rim and the base of the horn, 4cm medial to the frontal crest.

The results obtained were photographed, described and discussed with those of bovine species.

Keywords: Anatomy, Regional anesthesia, Buffalo,

Introduction

The Egyptian water buffalo (*Bos bubalis* L) was a unique species of buffalo all over the world, which could accommodate different weather changes. Egypt had not less than 3 million water buffalos, which could solve feed problems from meat and milk. Buffalos constitute an important part of the array of domestic animal resources in Egypt and many other African countries (Bhatt, 1999; Wilson, 2012). The buffalos were descended from two distinct types, swamp buffalos and riverine buffalos. The riverine buffalos found mainly at the Mediterranean area from which the Egyptian buffalos were descended and they were hold for milk and meat production (Shalash, 1988; Soliman, 2009).

Due to their size and anatomy, cattle are not very good candidates for general anesthesia meaning that many procedures performed use the local

techniques. Most surgeries performed on these patients can be done standing with a small amount of sedation and regional nerve blocks (Edmondson, 2008). Several features of local anesthesia render it particularly useful in veterinary practice and many surgical procedures could be carried out satisfactorily under local anesthesia (Lee, 2006).

In buffalo, the available data about anesthetic techniques and surgical affections considered scarce. While in cattle, several methods of anesthesia for flank laparotomy have been described. In addition, each of them has some advantages and disadvantages for clinical use (Roberts, 1986; karda, 1996; Hall, et al., 2001). The present study is therefore an attempt to provide an anatomical guide indicating the accurate site of each nerve supplying the flank region, horns and lips in relation to bony prominences. Advantages of this approach: very easy when we know the morphometric study of the region, economic not consumes a large amount of anesthetic drug and in the same time more effective.

Materials and Methods

The present study was conducted on eight buffaloes (*Bos bubalis* L.) of ages ranging between 2 -7 years. Six of these animals were recently dead

three of each sex and the remaining two animals were live one of each sex. The animals were collected from different area in Giza and transported to the laboratory of the Anatomy and Embryology Department Faculty of Veterinary Medicine, Cairo University. Both common carotid arteries were thoroughly flushed with warm (40c°) saline solution and the specimens were then injected with formalin solution (10% formalin, 4% phenol, 1% glycerin), and left to fix for 3-4 days then manually dissected to investigate the nerves under investigation. Measurements were applied using Vernier Calliper to indicated the accurate site of each nerve in relation to the nearest bony prominence to decide the best site for injection of the anaesthetic drug. The nerves were then coloured by acrylic colours and photographed.

The two live buffaloes were used for testing the anaesthetic effect after and the area of desensitization for each nerve under investigation. The animals were tranquilized by 10 mg/kg b.wt. Xylazine HCL 2% (Xylaject HCL 2 %, Adwia Co. S.A.E.). The needle of 22 gauges was inserted into the indicated site for each nerve under investigation and 10- 15 ml of lidocaine HCL 2 % (Debocaine HCL 2%, Al-Debeiky Pharmaceutical Industry Co.-A.R.E) was injected and waited for 10

minutes for detection of the anesthetic drug effect.

The nomenclature used was adopted according to the Nomina Anatomica Veterinaria (2012).

Results

Regional anesthesia of the abdominal wall comprised 3 ventral rami of the last intercostal, first and second lumbar nerves; namely the costoabdominal, iliohypogastric and ilioinguinal nerves respectively.

N. costoabdominalis

The costoabdominal nerve (Figs 1/1 & 2/2), represented the ventral branch of the last intercostalis nerve. It descended in zigzag pattern in a ventrolateral direction with slight caudal inclination in the abdominal wall alongside the M. transverses abdominis at a distance of about 6.0-7.0 cm caudal to the last rib. Near the ventral end of the last rib it divided into lateral and medial branches. The lateral branch penetrated the aponeuroses of the oblique abdominal muscles and distributed to the M. cutaneous trunci and skin of the lateral abdominal wall. The medial branch distributed to the oblique abdominal muscles and terminated in the M. rectus abdominis as well as the skin of the ventral abdominal wall. The definite site for blocking the costoabdominal nerve

(Fig 3/1) was indicated at the upper part of the flank about 5 cm below the free end of the second lumbar transverse process and 7 cm caudal to the last rib (Figs 1/2 & 2/1) and at depth of about 3 cm penetrating the skin, fascia and oblique abdominal muscles. The desensitized area (Fig 3/4) comprised the cranial part of the flank and skin and fascia of the ventral abdominal wall.

N. iliohypogastricus

The Iliohypogastric nerve (Figs 1/3 & 2/3) constituted the ventral branch of the first lumbar spinal nerve. It descended in zigzag pattern in a ventrolateral direction with slight caudal inclination in the abdominal wall alongside the M. transverses abdominis at the middle of the distance between the last rib and the tuber coxae (Fig 1/4) and divided at the level of the ventral end of the last rib into lateral and medial branches which followed the same course and distribution of the corresponding branches of the costoabdominal nerve. The accurate site for blocking the iliohypogastric (Fig 3/2) was indicated 5 cm below the 3rd lumbar transverse process at the mid-distance between the last rib cranially and tuber coxae caudally, about 22-24 cm from each of the later two points at a depth 3 cm. The desensitized area (Fig 3/5) comprised the

middle part of both the flank ventral abdominal wall.

N. Ilioinguinalis

The Ilioinguinal nerve (Figs 1/5 & 2/4) represented the ventral branch of second lumbar spinal nerve. It descended in zigzag pattern in a ventrolateral direction with slight caudal inclination in the abdominal wall alongside the M. transverses abdominis at about 5 cm cranial to the tuber coxae. It divided on a level with the ventral end of the last rib into lateral and medial branches which followed the same course and distribution of the corresponding branches of the costoabdominal nerve. The accurate site for blocking the ilioinguinal nerve (Fig 3/3) was indicated at the upper part of the flank about 5 cm cranial to tuber coxae and about 5 cm below the 4th lumbar transverse process. The area of destination (Fig 3/6) of the ilioinguinal nerve comprised the skin and muscles in the caudal part of the lateral and ventral abdominal wall and to some extent front of the hip and thigh, lateral surface of the stifle, the skin of the external genital organs and the surrounding skin in the inguinal region and mammary gland (Fig 1/7).

Regional anesthesia was also applied in the head region and mostly involved the infraorbital, mental and cornual nerve block

N. infraorbitalis

The infraorbital nerve (Fig 4/1) represented the continuation of the maxillary branch of the fifth cranial nerve after it enters the infraorbital canal. It emerged on the face as a flat band through the infraorbital foramen where it was covered by the levator nasolabialis muscle and soon divided into several rami that distributed to the nasal region and maxillary lip. For blocking the infraorbital nerve (Fig 9/1) the anesthetic drug was injected in the vicinity of the infraorbital foramen (Fig 5/3) which was situated 1.5 cm dorsal to the first cheek tooth (Fig 5/2) and about 6 cm rostral to the facial tubercle (Fig 5/1). The drug was injected deep into the levator nasolabialis muscle and the injection should be repeated on the opposite side. The desensitized field (Fig 9/4) comprised the dorsum nasi and diverticulum nasi, the nasal vestibule as well as the maxillary lip.

N. mentalis

The Mental nerve (Fig 4/2) was a branch of the mandibular alveolar nerve that emerged via the mental foramen (Fig 6/2) and divided into three branches below the depressor anguli oris muscle. These branches distributed to the skin of the chin as well as the skin and mucous membrane of the lower lip. For blocking of mental nerve (Fig 9/2) the needle was inserted in

the vicinity of the mental foramen at the middle distance of the lateral surface of the interalveolar space of mandible between the lateral incisor (Fig 6/1) and first premolar teeth (Fig 6/3) and the injection should be repeated on the opposite side. Injection of the drug rostral to the level of the mental foramen induced blocking of the mental nerve and the desensitized field (Fig 9/5) comprised the mandibular lip and chin without teeth or gum anesthesia. In another trial the needle was inserted in a rostro-caudal direction into the mental foramen and 10 ml of the drug was injected deeply through the mandibular canal resulting in additional anesthesia of the mandibular cheek and incisor teeth and gum.

N. cornualis

The cornual nerve (Fig 7/1) emerged from the caudal opening of the supra-orbital foramen (Fig 8/2) and proceeded caudolaterally in a special groove (Fig 8/3) reaching the base of the horn undercover of the M. orbicularis oculi and M. frontalis. For blocking the cornual nerve, the agent was deposited subcutaneously midway between the orbital rim and the base of the horn 4cm medial to the frontal crest (Fig 9/3).

Discussion

According to Thomas and Lerche (2016) the anesthesia of the paralumbar fossa and abdominal wall in cattle can be achieved by several techniques. These techniques include the proximal paravertebral nerve block, the distal paravertebral nerve block, the inverted L block and infusion of the incision or line block. These anesthetic techniques are commonly used for abdominal procedures such as omentopexy, abomasopexy, rumenotomy, cesarean section or other surgical approaches using a paralumbar fossa approach. The current investigation in buffalo indicated the accurate site for injection of anesthetic drug for each nerve supplying the flank region and aimed to consume smaller amount of anesthetic drug, produced fast action and in the same time more effective and also indicated the actual area innervated by each nerve. According to the present study the main nerves supplying the flank region were T13, L1 and L2. For anesthesia of the costoabdominal nerve (T13) best site was indicated at the upper part of the flank about 5 cm from the free end of the second lumbar transverse process and 7 cm caudal to the last rib and at depth of about 3 cm. The site for blocking the iliohypogastric (L1) was indicated 5 cm below the 4th lumbar transverse process midway between the last rib cranially and tuber coxae caudally, about 22-24 cm from each of

the later two points at depth 3 cm. For anesthesia of ilioinguinal nerve (L2) the needle was inserted in the upper part of the flank about 5 cm cranial to tuber coxae and 5 cm below the 5th lumbar transverse process. However, the indicated site for blocking each of these nerves could be compared favorably with the distal paravertebral anesthesia recommended by Edmondson (2008) and Thomas and Lerche (2016). In this concern Vermont (1999) reported that, for analgesia of the right and left paralumbar region, an area approximately 20 cm wide and 30 cm long should be prepared for aseptic surgery and analgesia provided by a line, an inverted 'L' or paravertebral block. The paracostal incision should be started 5 to 7.5 cm ventral to the transverse process of the second lumbar vertebrae and proceed ventrally and parallel to the last rib for about 20 cm.

Edmondson (2008) added that, the inverted L block is a nonspecific regional block in cattle in which a 18-gauge 3.8-cm needle was used to inject up to a total of 100 ml of local anesthetic solution in multiple small injection sites into the tissues bordering the dorsocaudal aspect of the thirteenth rib and ventrolateral aspect of the transverse processes of the lumbar vertebrae. The author also added that the disadvantages of this technique include incomplete analgesia

and muscle relaxation of the deeper layers of the abdominal wall (particularly in obese animals); possible toxicity after larger doses of anesthetic; and increased cost because of larger doses of local anesthetic. Nuss et al (2012) compared two methods of local anesthesia for laparotomy in cattle including the modified infiltration anesthesia (MIA) technique consisting of an incision line block combined with an inverted L-block, and the proximal paravertebral anesthesia (PPVA). They concluded that, both techniques required a mean of 8 minutes to complete but the MIA method was considered more difficult than the PPVA. The PPVA required significantly less procaine than the MIA (144 vs. 195ml). Comparison of the two techniques with respect to different types of pain reactions (no reaction, non-specific reaction, specific reaction) during cutting of the different layers of the abdominal wall revealed that PPVA provided significantly better analgesia than the MIA. After PPVA, pain reactions to incision of the external oblique abdominal muscle were more severe, but reactions to abdominal exploration and to suturing the two oblique abdominal muscles were significantly milder than after MIA.

In the present study anesthesia of the infraorbital nerve was achieved by injection of 5 ml procaine hydrochloride

2% in the vicinity of the infraorbital foramen which was situated 1.5 cm dorsal to the first cheek tooth and about 6 cm rostral to the facial tubercle on the same frontal level. The desensitized area comprised the dorsum nasi and diverticulum nasi, the nasal vestibule and superior lip, the maxillary lip, and labial mucous membrane. Edward (2001), Edmondson (2008) and Hussain et al (2009) reported that the infraorbital nerve was the continuation of the maxillary branch of the fifth cranial nerve after it entered the infraorbital canal and emerged on the face as a flat band through the infraorbital foramen where it was covered by the levator nasolabialis muscle. The infraorbital nerve was blocked as it emerged from the infraorbital canal. The nerve is difficult to palpate but is located rostral to the facial tuberosity on a line extending from the nasomaxillary notch to the second upper premolar. The latter author added that the infraorbital nerve block may be used for the repair of nasal lacerations and the placement of a nose ring.

In agreement with Park et al (2014) and Jaber et al (2013) the mental nerve was a branch of the mandibular alveolar nerve that emerged via the mental foramen and divided into three branches which are distributed to the skin of the chin and as well as the skin and mucous membrane of the lower

lip. They added that, the mental nerve block is a simple technique to supply anesthesia to this area and that the lacerations of the lower lip and of the facial soft tissues in the lower chin require proper anesthesia to ensure adequate cosmetic closure. The present study indicated the accurate site for applying the mental nerve block at the middle distance of the lateral surface of the interalveolar space of the mandible between the lateral incisor and first premolar teeth. Mohamed and Fathy (2015) indicated the site of the mental nerve in donkey just rostral to the 1st premolar.

In agreement with Allouch (2014) in bovine and Kataba et al. (2014) in goat, the parameters of the mental foramen were vital landmarks for injection of local anesthetic drugs in the mandibular canal via the mental foramen for blocking the infra-alveolar nerve, so desensitization of the lower jaw with its teeth and the lower lip will be occurred and this method was easier and avoided all risks of blood vessel injures in case of the mandibular alveolar nerve block.

In agreement with Navarre (2006) and Edmondson (2008) in cattle and Prasad et al (2016) in buffalo the cornual nerve block is used for anesthesia for dehorning cattle. The horn and the skin around the base of the horn are

innervated by the cornual branch of the lacrimal or zygomaticotemporal nerve, which is part of the ophthalmic division of the trigeminal nerve. The cornual nerve passes through the periorbital tissues dorsally and runs along the frontal crest to the base of the horns. The authors mentioned that the cornual nerve was blocked by injection of the anesthetic drug midway between the lateral canthus of the eye and the base of the horn along the zygomatic process. Similar observations were recorded in the present study that revealed that the cornual nerve in buffalo follows a relatively higher course about 4cm medial to the frontal crest. Elmore (1980) added that well-developed horns require additional anesthetic infiltration along the caudal aspect of the horn, in the form of a partial ring block, to desensitize subcutaneous branches of the second cervical nerve.

References

- Allouch, G.M. (2014):** Applied anatomy on the maxilla and mandibular regions of the bovine with special reference to its important in regional anesthesia. *Int. J. Food, Agricult. Veter. Sci.*
- Bhatt, P. N. (1999):** Buffaloes. In: W.J.A. Payne and R.T. Wilson (authors), an introduction to animal hus-

bandry in the tropics, 5th ed. Blackwell Science, Oxford: 325–404.

Edmondson M.A. (2008): Local and regional anesthesia in cattle. *Vet Clin North Am Food AnimPract.* Jul; 24(2): 211-26

Edwards B. (2001): Regional anesthesia techniques in cattle. In *Pract;* 23:142–9

Elmore R.G. (1980): Food animal regional anesthesia, bovine blocks: corneal. *Vet Med;* 75:1610–2.

Hall, L. W., Clarke, K. W., Trim, C. M. (2001): *Veterinary Anesthesia*, 10th ed. Saunders, London: 315-339.

Hussain, S.S., Tahseen, L. and Moulvi, B.A. (2009): International Book Distributing co. (Publishing Division) Khushnuma Complex Basement7, MeerabaiMarg (Behind Jawahar Bhawan) Lucknow 226 001 u.P. (INDIA): 91-522

Jaber, A, Whitworth, J.M., Corbett, I. P., Al-Baqshi, B., Jauhar, S. and Meechan, J. G. (2013): Effect of Massage on the Efficacy of the Mental and Incisive Nerve Block. *Anesth Prog.* Spring; 60(1):15-20

Karda, R. T. (1996): Local and regional anesthetic techniques: ruminants and swine. In: Thurmon, J. C,

Tranquilli, W. J, Benson, G. J. (Eds.). *Lumb & Jones 'Veterinary Anesthesia*, 3rd ed. Williams & Wilkins, Baltimore: 479-514

Kataba, A., Edwell, S.M., Humphrey, S., Casanova, P.M. (2014): Clinical anatomy of the head region of Gwembe Valley Dwarf goat in Zambia. *Int. J. Veter. Sci.*, 3(3): 142 146.

Lee L. (2006): Local Anesthesia & Analgesia. *Veterinary Surgery I, VMED* 7412

Navarre C. (2006): Numbing: nose to tail. *Proceedings from the 39th Annual Convention of AABP;* 39: 53–5.

Mohamed R.A. and Fathy M.Z. (2015): Applied anatomy of the head region of donkey (*Equus asinus*) in Egypt and its clinical value during regional anesthesia. *Inter. J. Curr. Res. Aca. Rev.* Volume 3 Number 4: 45-58

Nomina Anatomica Veterinaria (2012): 5th edition Revised version. Prepared by the International Committee on Veterinary Gross Anatomical Nomenclature (I.C.V.G.A.N.) and authorized by the General Assembly of the World Association of Veterinary Anatomists (W.A.V.A.) Knoxville, TN (U.S.A.) 2003 Published by the Editorial Committee Hannover (Germany),

Columbia, MO (U.S.A.), Ghent (Belgium), Sapporo (Japan).

Nuss, K., Eiberle, B.J., Louis, S. C. (2012): [Comparison of two methods of local anesthesia for laparotomy in cattle]. Tierarztl Prax Ausg G Gross-tiere Nutztiere. 40(3): 141-9.

Park,H.G., Park,P.G., Kim,W.J., Park, Y.H., Kang, H. Baek, C.W. Jung, Y.H. Woo,Y. C., Koo,G.H. and Shin, H.Y. (2014): Ultrasound-Assisted Mental Nerve Block and Pulsed Radiofrequency Treatment for Intractable Post herpetic Neuralgia: Three Case Studies. Korean J Pain., 27(1): 81–85.

Prasad, V.D. Kumar, P.R. Harikrishna, N.V.V. Sreenu, M. Vidyasagar, P. Mahesh R. and Bhagyaraju, D. (2016): A comprehensive study on surgical affections of horns in buffaloes (*Bubalus bubalis*). Journal of Livestock Science (ISSN online 2277-6214) 7: 280-287

Roberts, S. J. (1986): Veterinary Obstetrics and Genital Diseases (Therigenology), 3rd ed: 294-296.

Shalash, M. R. (1988): The water buffalo of Egypt. Acta Veterinaria Scandi-

navia, 83 Supplements. 1:66-79.

Soliman, I. (2009): Present situation and future perspective of buffalo production in Africa. In: Buffalo—prospective animals for milk and meat enterprise, 6th Asian Buffalo Congress. Lahore, Pakistan.

Thomas,J. A.and Ierche,P.(2016): Anesthesia and Analgesia for Veterinary Technicians, 5th Edition. Columbia, MD, U.S.A

Vermunt, J. (1999): Exploratory laparotomy in cattle. Journal of Veterinary Surgery (IJVS). NZ Vet script 12 (7): 6-7. IRANIAN

Wilson, R.T. (2012): The past and present of and potential for the domestic (water) buffalo in Africa. Trop. Anim. Health Prod. 44: 1367–137.

Corresponding author

Farag, F.M.M.

Email: fouad.farag@cu.edu.eg

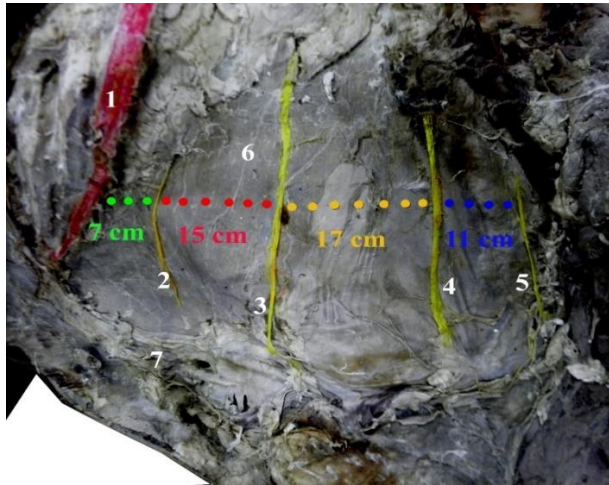


Fig (1): A photograph showing the nerves of the flank region in the buffalo.

1N. costoabdominalis, 2 Last rib, 3 N. iliohypogastricus, 4 Tuber coxae, 5 N. Ilioinguinalis, 6 Genitofemoralis, 7 Mammae.

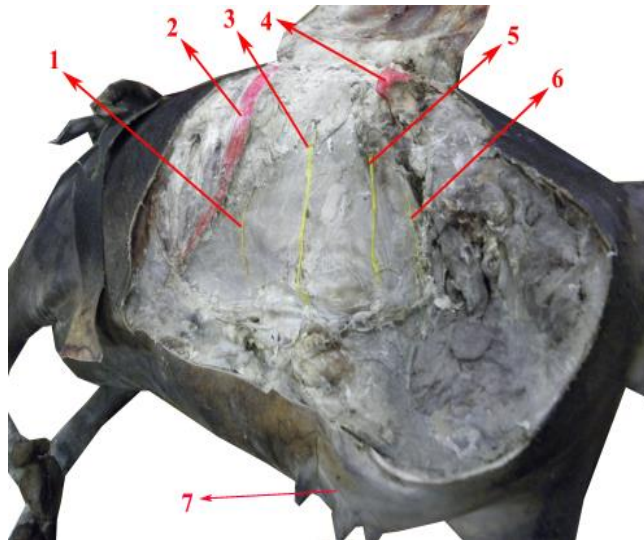


Fig (2): A photograph for a dissected flank of buffalo showing the distance between each nerve.

1 Last rib, 2 N. costoabdominalis, 3 N. iliohypogastricus, 4 N. ilioinguinalis, 5 N. genitofemoralis, 6 M. obliquus externus abdominis, 7 M. rectus abdominis.

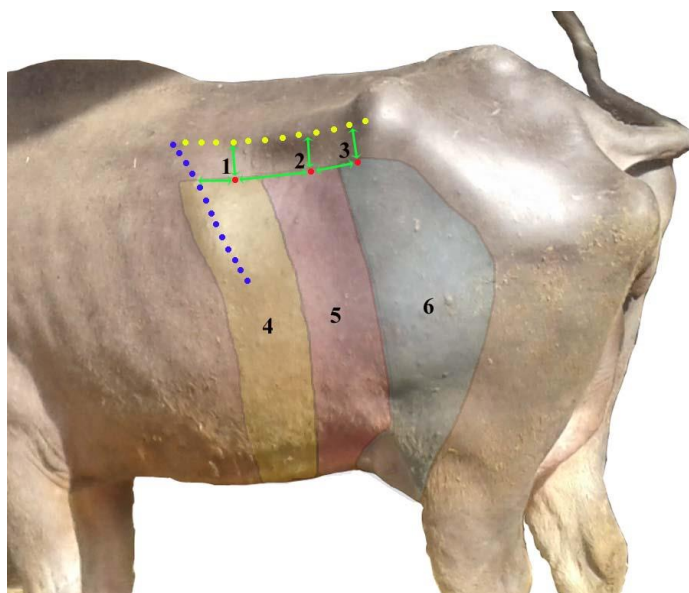


Fig (3): A photograph showing sites of nerve block of each nerve in the flank of buffalo.

1 Site for block of N. costoabdominalis, 2 Site for block of N. iliohypogastricus, 3 Site for block of N. ilioinguinalis, 4 Desensitized area of N. costoabdominalis, 5 Desensitized area of N. iliohypogastricus, 6 Desensitized area of N. ilioinguinalis.

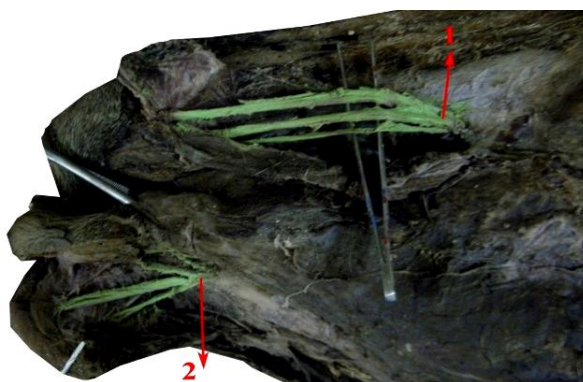


Figure (4): A photograph showing the infraorbital and mental nerve of buffalo.

1. N. infraorbitalis. 2. N. mentalis.

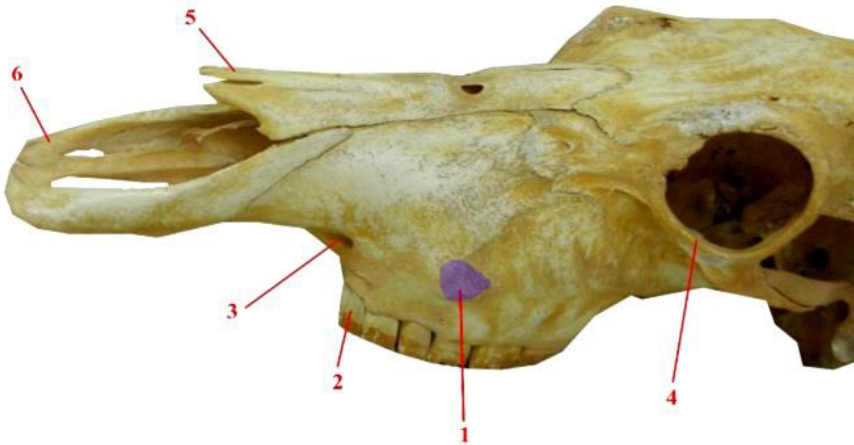


Figure (5): A photograph for the skull of buffalo showing the infraorbital foramen and its relation to the facial tubercle.

1 Tuber faciale, 2 Dentes premolars I, 3 Foramen infraorbitale, 4 Orbital rim, 5 Os nasale, 6 Os incisivum.



Figure (6): A photograph for the mandible of buffalo showing the mental foramen.

1 Dentes incisivi lateralis, 2 Foramen mentalis, 3 Dentes premolars I.

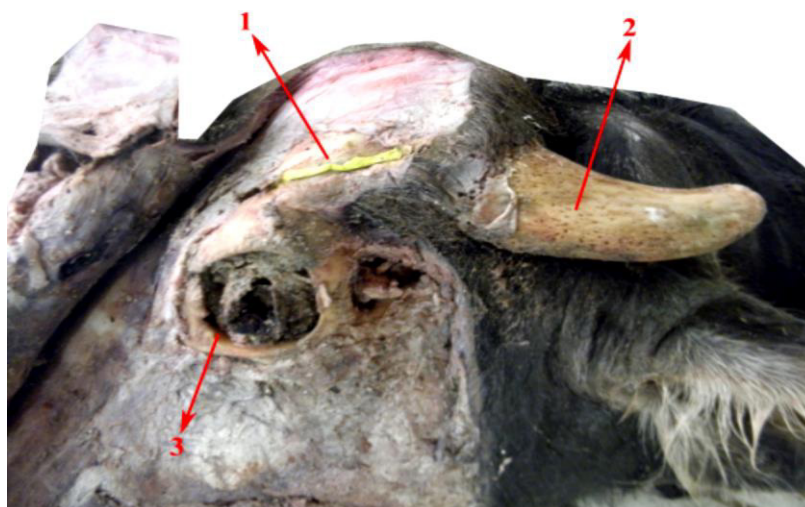


Figure (7): A photograph for a dissected head of buffalo showing the cornual nerve.
1 N. Cornualis, 2 Processus cornualis, 3. Orbital rim

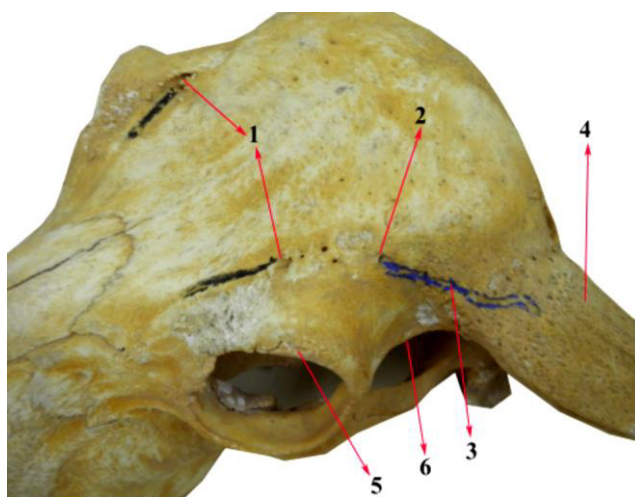


Figure (8): A photograph for the skull of buffalo showing the course of the cornual nerve.
1 Foramen supraorbitalis caudalis, 2 Foramen supraorbitalis rostralis, 3 Groove for N. cornualis, 4 Processus cornualis, 5 Orbital rim, 6 Linea temporalis.

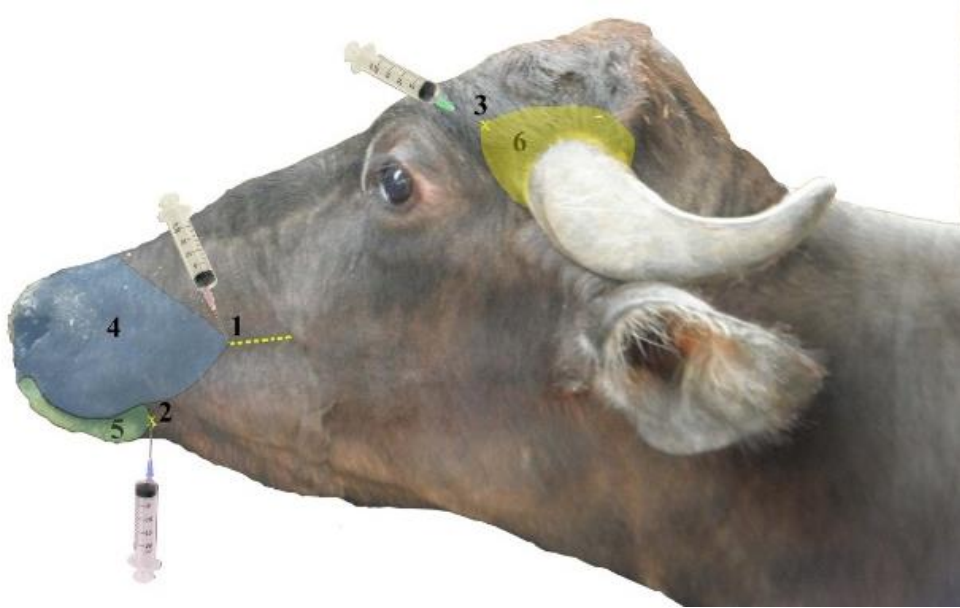


Figure (9): A photograph showing sites of nerve blocks in the head of buffalo.

1 Site for block of N. infraorbitalis, 2 Site for block of N. mentalis, 3 Site for block of N. cornualis, 4 Desensitized area of N. infraorbitalis, 5 Desensitized area of N. mentalis, 6 Desensitized area of N. cornualis.

Animal species of this issue

Water buffalo (*Bubalus bubalis*)



Kingdom: Animalia & Phylum: Chordata & Class: Mammalia & Order: Artiodactyla & Family: Bovidae & Subfamily: Bovinae & Tribe: Bovini & Genus: *Bubalus* & Species: *B. bubalis*

The **water buffalo** or **domestic Asian water buffalo** (*Bubalus bubalis*) is a large bovine animal, frequently used as livestock in southern Asia, and also widely in South America, southern Europe, north Africa, and elsewhere.

Buffalo are used as draft, meat, and dairy animals. Their dung is used as a fertilizer and as a fuel when dried. In Chonburi, Thailand, and in South western region of Karnataka, India, there are annual water buffalo races known as Kambala. A few have also found use as pack animals carrying loads even for special forces.

Adult Water Buffalo range in size from 400 to 900 kg for the domestic breeds, while the wild animals are nearly 3 m long and 2 m tall, weighing up to 1,200 kg; females are about two-thirds this size.

River buffalo are usually black and have long curled horns, whereas swamp buffalo can be black or white, or both, with gently curved horns. The largest recorded horns are just under 2 metres long.

Source: Wikipedia, the free encyclopaedia

Anatomic and Radiographic Studies on the Paranasal Sinuses of the Buffalo in Egypt (*Bos bubalis*, L.)

Farag, F.M.M., Hagrass S.M., Daghash, S.M., El-Bably, S. H. and Sary, R.G.

Anatomy and Embryology Department, Faculty of Veterinary Medicine, Cairo University

With 9 figures

Received March 2016, accepted for publication April 2017

Abstract

This survey was applied on the paranasal sinuses of the Buffalo in Egypt (*Bos bubalis* L.) and its surgical approach. Ten adult buffaloe heads of ages ranging between 2 -7 years were used. Six of these heads were used for dry skull preparation while the other four were used for radiography and cross sections. The study concluded that, in addition to sinuses conchales, four paranasal sinuses have been found to occur in adult buffalo comprising the sinus frontalis, sinus maxillaris, sinus palatinus and sinus lacrimalis. The anatomical and radiographic description of these paranasal sinuses as well as its dimensions and communications has been mentioned. Two sites for trephination of the frontal sinus could be indicated. Trephining the rostral frontal sinus through was indicated at the middle of a transverse line extending between the caudal margins of the orbital rim to the median plane while trephination site to gain the caudal frontal sinus was in-

dicated at the middle of another transverse line extending from the middle of the base the horn to the median plane. Surgical approach of the maxillary sinus for trephining could be indicated on a vertical line extending upward from the caudal margin of the 2nd premolar for about 4.0-4.5 cm.

Keywords: Anatomy, Radiography, Paranasal Sinuses, Buffalo.

Introduction

The paranasal sinuses are air-filled spaces located within the bones of the skull and face. They are centered on the nasal cavity and have various functions, including lightening the weight of the head, humidifying and heating inhaled air, increasing the resonance of speech (in human), and serving as a crumple zone to protect vital structures in the event of facial trauma (Reddy and Dev, 2012; Dalgorf and Harvey, 2013). However, their role in increasing the thermal and mechanical

protection of the brain, without concurrently increasing the weight of the skull, being proposed. It is to add that the hypothesis that these sinuses are functionless and are formed as result of the removal of mechanically unnecessary bone, a process which was designated as opportunistic pneumatisation' (Farke, 2010).

The paranasal sinuses in bovine comprised the frontal, maxillary, lacrimal, palatine, sphenoid and nasal conchal sinuses. Some of these sinuses communicate with each other while others open independently into the nasal meatus. In cattle, the paranasal sinuses continue to develop, changing in shape and size, up to seven years of age (Dyce et al. 2010). Alsafy et al (2012) studied a computed tomography of paranasal sinuses and their communications in the Egyptian buffalo while Basso et al (2016) compared between three techniques for videosinuscopy in cattle.

Among the pathologies of the sinuses, an inflammatory process called sinusitis stands out. In cattle, the leading cause of frontal sinusitis is associated with dehorning, as about 2% of surgically dehorned animals develop this disease (Silva, 2008). It can also be associated with respiratory infections, trepanations or fractures with frontal sinus exposure, cysts or nasal cancer (Smith, 2006).

However, this study is undertaken to extend knowledge of the topography of the paranasal sinuses in the buffalo and suggest best sites for surgical approach to these sinuses, which may be helpful for surgeons in trephining of the sinuses and dehorning.

Materials and Methods

The present study was applied on ten heads of buffaloes of age 2 -7 years collected from the slaughterhouses in Giza and transported to the laboratory of the Anatomy and Embryology Department Faculty of Veterinary Medicine, Cairo University. Six of these heads were used for dry skull preparation while the other four were used for radiography and cross sections.

Anatomical cross sections were performed on two buffalo's heads (one fresh and one frozen) by using table of a band saw and transverse sections were cut at the level of last molar check tooth, first premolar check tooth and middle of interdental space. Slices were numbered and gently cleaned from debris with water and light brushing and were photographed immediately with the caudal and cranial surfaces of each slice facing the camera. Radiographs were performed on two other fresh heads at 55 k v 30-70 MA, 0.5 second and FFd 70 cm.

Skulls preparation was adopted according to Hildebrand (1968) and Lee post (2005). Manual and electric saws were used for sagittal sections in three skulls and another three skulls were used for exposure of frontal, maxillary, palatine and lacrimal sinuses. Vernier caliper was used to measure different dimensions of each sinus. The access to the sinuses was carried out by a trephining technique, first with a drill, making a small skull opening, then amplified by rotational moves with a 20mm circular trephine. The chosen sites for trephination were based on the anatomy and measurements of the frontal and maxillary sinuses. The nomenclature used was adopted according to the *Nomina Anatomica Veterinaria* (2012).

Results

The major paranasal sinuses in buffalo comprised the frontal, maxillary, palatine, and lacrimal sinuses.

Sinus frontalis

The frontal sinus is the largest of the paranasal sinuses in the buffalo. It was extensive, excavated almost all the frontal bone (Fig 3/10), and a large part of the caudal and lateral wall of the cranium, invading also the parietal, interparietal and extended for a variable distance into the core of the cornual process (Figs 1/4 & 2/3). A complete median septum

separated the right and left sinuses. It was in the form of a rectangular space, narrow at its rostral portion and widen gradually in caudal direction. The outer limit of each sinus could be indicated rostrally by an imaginary line extending transversely through the rostral margin of the orbits passing through the rostral end of the rostral supraorbital groove. It was bounded caudally by the occipital bone and laterally by the frontal crest and temporal bone and extended medially to the median plane which indicates the site of the interfrontal septum. The cavity of the frontal sinus was divided into two main sinuses, rostral and caudal by an inverted V- shaped incomplete septum (Fig 1/10) which started from the middle of the base and extended rostromedially to about the middle of the sinus where it formed an acute angle, then redirected caudomedially to join the interfrontal septum. The rostral frontal sinus was larger and further divided by two irregular incomplete sagittal partitions into three compartments; lateral, intermediate and medial. Each of these compartments was further subdivided by fine boney plates into minor compartments. The lateral compartment (Fig 1/1) was the longest one, wide near its middle and narrowed both rostrally and caudally.

The supraorbital canal (Fig 1/9), extended as short canal passing

through the lateral margin of this compartment through an irregular bony septum. From this compartment extended two diverticula; a postorbital diverticulum and cornual diverticulum. The **postorbital diverticulum** was situated about the middle of the lateral compartment and was about 2.5-3.0 cm in depth and was divided by 2-3 smaller lamellae. The **cornual diverticulum** extended from the caudal part of the lateral compartment into the core of the cornual process where it divided into two recesses a rostral and a caudal one. The rostral recess (Fig 1/5) was shorter measuring about 9 cm long from the base of the horn while the caudal recess (Fig 1/6) was longer extended for about 14 cm into the cornual process. The intermediate compartment (Fig 1/2) was the narrowest and shortest of the three subdivisions of the rostral frontal sinus. The medial compartment (Fig 1/3) was a narrow space adjacent to the interfrontal septum. It was wider rostrally and narrow caudally.

The caudal frontal sinus (Fig 1/7) was in the form of wide triangular space with its apex rostrally and the base caudally situated. Its apex could be indicated by a transverse line extending from the middle of the distance between the caudal margin of the orbital rim and base of the horn to the midline, while its base towards the occipital bone. The cau-

domedial portion of the sinus formed the nuchal diverticulum (Fig 1/8) in the form of transverse excavation of about 3.5 cm in depth. It invaded the well-developed parietal bone to the level of the nuchal crest and was divided by 3-4 lamellae into smaller sub compartments. Measurements revealed that the frontal sinus measured about 18-20 cm in length. Its width was about 5.0 - 6.5 at its rostral part and widen gradually in caudal direction reaching its maximum width on the level of the middle of the horn base where it measured 9.0-10.0 cm. Its maximum height measured about 3.0-4.0 cm near its middle portion. The rostral frontal sinus was communicated with the cavity of the dorsal turbinate through the conchofrontal opening and with the lacrimal sinus through small frontolacrimal opening and communicated with the nasal cavity through a nasofrontal opening into the ethmoidal meatuses. No direct connection of the caudal frontal sinus with either the nasal cavity or other sinuses could be observed.

Two sites for trephination of the frontal sinus could be indicated. Trephining the rostral frontal sinus (Fig 2/1) is at the middle of a transverse line extending between the caudal margins of the orbital rim to the median plane. Trephination site to gain the caudal frontal sinus (Fig 2/2) is the middle of another trans-

verse line extending from the middle of the base the horn to the median plane.

Sinus maxillaris

The maxillary sinus (Fig 3/6 and 4) was an extensive excavation which occupied entirely the maxilla (Fig 3/1) and extended into the adjoin part of the lacrimal (Fig 5/4) and zygomatic bones (Figs 3/7 & 5/5). It was nearly triangular in outline with its apex rostrally coincided the facial tuberosity (Fig 3/2) at the level of the caudal margin of the 2nd premolar. It widen gradually in caudal direction till reaching its maximum width at the level of the last molar tooth where it began to be narrowed at its most caudal portion where it embraced the rostral and ventral margin of the orbital rim and continued caudally into the thin-walled lacrimal bulla (Fig 5/6). The dorsal limit of the sinus was indicated by a line extending from the facial tuberosity to the rostral margin of the orbital rim (Fig 4/5), while the ventral limit was about 2.5 cm above alveolar border (Fig 4/6) of the maxillary cheek teeth.

The cavity of the maxillary sinus was nearly prismatic in shape and not divided by any partition. Its average length was about 10.0-11.5 cm while its height was about 1.0 cm at its apex and its maximum height at the level of the last molar tooth was about 7.0-8.0 cm. The transverse width of the sinus also increases in

caudal direction from about 0.8 cm at its rostral part to about 3.5 cm at its caudal part. The floor of the sinus was irregular where the roots of the last three or four cheek teeth project up, being covered by a plate of bone. In cross section of the head, the maxillary sinus began to appear at the level of caudal margin of the 2nd premolar tooth.

The maxillary sinus was communicated with the nasal cavity through the small slit-like 0.4-0.5 cm in length, **nasomaxillary orifice**, near its rostral portion on the level of the 3rd premolar at a height of about 2.0 cm from the floor of the sinus. This location was relatively high and might hinder the natural drainage of the pus or other fluids from the maxillary sinus. It was also communicated with the caudal part of the palatine sinus through an extensive **maxillopalatine opening** (Fig 4/3) which was an oval opening located over the infraorbital canal (Fig 4/4) just caudal to the nasomaxillary orifice, at a level extending between the caudal margin of the 3rd premolar to the caudal margin of the 2nd molar teeth. It was also communicated with the lacrimal sinus through **maxillolacrimial opening** on a level with the last molar tooth. Surgical approach of the maxillary sinus for trephining (Fig 5/3) could be indicated on a vertical line extending upward from the caudal margin of the 3rd premolar for about 4.0-4.5 cm.

Sinus palatinus

The palatine sinus (Figs 6, 7/1, 8/6) was represented by an extensive excavation in the horizontal part of the palatine bone and the palatine process of the maxilla and considered the second in size after the frontal sinus. The right and left sinuses were separated by an, undulant interpalatine septum. Its caudal limit coincided the caudal border of the palate bone, about 4 cm caudal to the last molar tooth while its rostral limit extended to a level about 2.5-3.5 cm in front of the first premolar tooth. The sinus cavity was subdivided into two unequal compartments caudal and rostral by incomplete transverse bony partitions (Fig 6/4) arising from the floor of sinus. The caudal part of the sinus (Fig 6/5) was the largest of the two compartments and appeared quadrilateral in sagittal section of the palate. It measured about 7.5-8.5 cm long and 3.5-4.0 cm width. It was traversed obliquely by the palatine canal, and communicated with the maxillary sinus by maxillopalatine opening (Fig 4/3) over the infraorbital canal (Fig 4/4). The rostral compartment (Fig 6/3), appeared triangular in the sagittal section of the palate with its narrow apex rostrally and wide base caudally. It measured about 6.5- 7.5 cm in length and maximum width about 3.5 cm at its base. In cross section, the palatine sinus appeared at the level of last molar

tooth (Fig 7), at the level of the first premolar check tooth (Fig 8).

Sinus lacrimalis

The lacrimal sinus (Fig 3/9) was in the form of small quadrilateral excavation mainly in the lacrimal as well as the small adjoin portion of the frontal bone while its medial wall was formed by lateral mass of the ethmoidal bone at the rostromedial portion of the orbit. It measured about 3.5-5.0 cm in length and about 2.0-2.5 cm width. The nasolacrimal duct traversed its lateral wall and it was communicated at its rostral end with the maxillary sinus through maxillo-lacrimal opening and at its caudal end with the lateral compartment of the rostral frontal sinus through frontolacrimal opening and thus the lacrimal sinus considered as an indirect communicator between the maxillary and frontal sinuses.

Discussion

In accordance with Saigal and Khatra (1977) and Eshrah (2006) the paranasal sinuses in the buffaloes comprised the frontal, maxillary, palatine and lacrimal, while the sphenoid sinus was not observed in any of the examined specimens. Alsafy et al. (2012) mentioned that the sphenoid sinus was noticeable small and shallow only in two specimens. On the other hand, Eshrah (2006) and Alsafy et al. (2014) mentioned that the latter sinus was well devel-

oped in camel while the palatine sinus was absent. He added that, the palatine sinus was absent in camel while the lacrimal sinus was absent in donkey. Budras et al. (2011) classified the paranasal Sinuses of the ox into two groups. Group I were those sinuses which open into the middle nasal meatus and comprised the maxillary, lacrimal, palatine in addition to the dorsal and ventral conchal sinuses while group II were those sinuses that open in the ethmoidal meatuses and constituted the frontal and sphenoid in addition to the middle conchal sinuses.

The present study declared that the frontal sinus in the buffalo was extensive and excavated almost all the frontal bone and a large part of the caudal and lateral wall of the cranium, invading also the parietal, interparietal bones. Budras et al. (2011) in ox mentioned that the frontal sinus also excavated part of the occipital and temporal bones an, observation which could not be ascertained in buffalo. In agreement with Alsafy et al. (2012) in buffalo, Budras et al. (2011) in ox, and Farke (2010) in Bovidae the right and left frontal sinuses were separated by complete interfrontal septum. In this respect, in cattle, El-Hagri (1967) found a communication between the two frontal sinuses caudally where the interfrontal septum was deficient.

The present study revealed that, the frontal sinus was divided into two

main sinuses, rostral and caudal by an inverted V- shaped incomplete septum which started from the middle of the base and extended rostromedially to about the middle of the sinus where it formed an acute angle then redirected caudomedially to join the interfrontal septum. Budras et al. (2011) mentioned that the division of the sinus in the ox was achieved through an oblique transverse septum that runs from the middle of the orbit caudomedially to join the median septum in the transverse plane of the caudal margin of the orbit. In this respect Eshrah (2006) and Alsafy et al. (2012) in the buffalo mentioned that, a transverse oblique septum at the level of the perpendicular plate of the ethmoid bone separated the larger caudal frontal sinus from the smaller rostral frontal sinus. However, in accordance with the latter authors the rostral frontal sinus was further divided into medial, intermediate and lateral sinuses. Saigal and Khatra (1977) added that the caudal frontal sinus was divided into medial and lateral compartments by an oblique septum and also mentioned that the frontal sinus was divided into numerous interconnected diverticula by ridges and partial septa. Eshrah (2006) and Alsafy et al. (2012) in buffalo added that an incomplete oblique transverse septum divided the caudal frontal sinus into large caudolateral and small rostromedial sinuses was present. Moreover, Osman et al.

(2012) and Kareem and Sawad (2016) mentioned that in goat, the frontal sinus was demarcated into large lateral frontal sinus caudally, and small medial frontal sinus rostrally.

The present study reported that, supraorbital canal invaded the rostral frontal sinus as short canal passing through the lateral margin of the lateral compartment through an irregular bony septum. On the contrary, Budras et al. (2011) in ox, as well as in the buffalo of this study, mentioned that this canal traversed the caudal frontal sinus.

In Accordance with Budras et al. (2011) in cattle, the frontal sinus had three clinically important diverticula: the nuchal, cornual, and postorbital diverticula. However, the latter authors and Alsafy et al. (2012) mentioned that these three diverticula were derived from the caudal frontal sinus while the present study revealed that only the nuchal diverticulum was partitioned from the caudal frontal sinus while the cornual and postorbital diverticula were protracted from the rostral frontal sinus. The current investigation recorded an extensive nuchal diverticulum, which excavated the well-developed parietal bone. It is further subdivided by 3-4 lamellae into smaller subcompartments, which is in agreement with the findings of Saigal and Khatra (1977), Kumar and Dhingra (1980) and Alsafy et al (2012) in buffalo. Kumar and Dhingra (1980) added

that both the cornual and nuchal diverticula were absent in the buffalo calf.

In buffalo the rostral frontal sinus was communicated with the cavity of the dorsal turbinate through the conchofrontal opening and with the lacrimal sinus through small frontolacrimal opening and communicated with the nasal cavity through the nasofrontal opening into the ethmoidal meatuses but no direct connection of the caudal frontal sinus with either the nasal cavity or other sinus could be observed. In this respect, Alsafy et al. (2012) in buffalo reported that all rostral frontal sinus compartments communicated separately with the ethmoidal meatus and rostrally with the dorsal nasal conchal sinus by nasofrontal opening. Budras et al. (2011) in cattle added that also the caudal frontal sinus has only one aperture: at its rostral extremity, there is a small outlet to an ethmoid meatus. A result, which could not observed in any of the examined buffalo specimens.

The present work indicated two sites for trephination of the frontal sinus. Trephining the rostral frontal sinus through was indicated at the middle of a transverse line extending between the caudal margins of the orbital rim to the median plane while trephination site to gain the caudal frontal sinus was indicated at the middle of another transverse line ex-

tending from the middle of the base of the horn to the median plane. The site for trephination of the caudolateral compartment of the sinus is at the mid-distance between the base of the horn and the median plane. Saigal and Khatra (1977) and Alsafy et al. (2012) mentioned that the most suitable site of trephining the maxillary sinus could be located at about the midpoint between the infraorbital margin and the facial tuber. They also added that the most suitable trephining site of frontal sinus is on a line joining the middles of temporal regions about midway between the median plane and the lateral margin of the head. Basso et al. (2016) in bovine mentioned that the trephination areas and sinuses were selected based on anatomy, but they may be modified according to the purposes of the exam. The authors identified three main areas for trephination comprising the nuchal diverticulum, the caudal region of the sinus as well as postorbital region and added that exploration of the rostral portion of the sinus was complicated by the presence of large numbers of intrasinus lamellae resulting in irregular areas which prevent the insertion of endoscopes through the proposed access. Eshrah (2006) indicated the suitable site for trephination of frontal sinus in buffalo was located on both sides of intersection point of a line joined between the rostral borders of base of horns and midline. While in

camel the point of trephination was located on both sides of intersection point of a line joined between the caudal border of orbits and midline. While in donkey it was located on both sides of intersection point of a line joined between the supraorbital foramen and midline.

In agreement with Eshrah (2006) and Alsafy et al. (2012) in buffalo, the maxillary sinus was nearly triangular in outline and extended from the facial tuberosity rostrally to the orbital rim caudally and extended into the thin walled lacrimal bulla. Similar the observation of Eshrah (2006) the maxillary sinus in buffalo was a single sinus had no partition, while the same author mentioned that, in donkey it divided unequally by an oblique osseous partition into a rostral maxillary sinus and a caudal maxillary sinus. The present study revealed that, maxillary sinus was communicated with the nasal cavity through the small slit-like 0.4-0.5 cm in length, nasomaxillary orifice near its rostral portion on the level of the 3rd premolar at height of about 2.0 cm from the floor of the sinus. This location was relatively high and might hinder the natural drainage of the pus or other fluids from the maxillary sinus. It was also communicated with the caudal part the palatine sinus through an extensive maxillopalatine opening and with the lacrimal sinus through maxillolacrima open-

ing. Alsafy et al. (2012) in buffalo mentioned that, the nasomaxillary opening was situated on the medial wall midway between the orbit and facial tuber at a level from 1st molar to 3rd molar teeth. According to Saigal and Khatra (1977), the nasomaxillary opening was not distinguishable because of its continuity with the defect in the roof of palatine sinus, whereas in ox, it was much narrower and lied dorsal to the maxillopalatine opening. In small ruminants, it lied in dorsal passage of the middle conchal meatus caudally (Nickel et al., 1986). Eshrah (2006) mentioned that the maxilloacrimonasal opening was not observed in buffalo but present in camel.

Eshrah (2006) declared that the suitable site for trephination of the maxillary sinus in buffalo was located at a point 2.5 cm caudal to infraorbital foramen and 2.5 cm dorsal this foramen. In this respect Saigal and Khatra (1977) and Alsafy et al. (2012) in buffalo mentioned that the most suitable site of trephining the maxillary sinus could be located at about the midpoint between the infraorbital margin and the facial tuber. In the view of the morphometric studies applied in the present study the suggested sites were considered rostral to the rostral limit of the sinus and mostly leads to the nasal cavity, and the accurate site for trephining the sinus was indicated on a vertical

line extending upward from the caudal margin of the 2nd premolar for about 4.0-4.5 cm.

The current investigation confirmed the observation of Alsafy et al. (2012) in buffalo that the palatine sinus was located within the horizontal part of the palatine bone and the palatine process of the maxilla and that the right and left sinuses were separated by an, undulant interpalatine septum and the sinus cavity was subdivided into two compartments caudal and rostral by incomplete transverse bony partitions. Eshrah (2006) reported that in buffalo and donkey the cavity of sinuses partly were divided by bony specules into several diverticulae 3-4 in buffalo and 2 -3 in donkey. The author also added that, the palatine sinus in buffalo lacked bony roof that permit mucous membrane of nasal cavity to lie back to back against that of palatine sinus. An observation, which was not documented in the present study. Kareem and Sawad (2016) recorded pyramidal shaped palatine sinus in goat.

In accordance with Alsafy et al. (2012) in buffalo, the lacrimal sinus was in the form of small excavation mainly in the lacrimal as well as the small adjoin portion of the frontal bone while its medial wall was formed by lateral mass of the ethmoidal bone at the rostromedial por-

tion of the orbit and that the nasolacrimal duct traversed its lateral wall. Eshrah (2006) mentioned that the cavity of the lacrimal sinus in buffalo was irregular due to the presence of bony specules divided it into 3-4 diverticulae. In confirmation with Eshrah (2006) and Alsafy et al. (2012) in buffalo the lacrimal sinus was communicated with the maxillary sinus by maxillo-lacrimal opening. In addition, the present study revealed that the lacrimal sinus was also communicated with the lateral compartment of the rostral frontal sinus through frontolacrimal opening and thus the lacrimal sinus is considered as an indirect communicator between the maxillary and frontal sinuses. Such communication was achieved through direct frontomaxillary opening in the donkey as recorded by Eshrah (2006) and El-Gendy and Alsafy, (2010) and in the Arabian foal by Bahar et al. (2014).

References

- Alsafy, M. A. M, El-Gendy, S. A. A. and El Sharaby, A. A. (2012):** Anatomical Reference for Computed Tomography of Paranasal Sinuses and Their Communication in the Egyptian Buffalo (*Bubalus bubalis*). *Anat. Histol. Embryol.* 42(3): 220-231.
- Alsafy, M. A. M, El-Gendy, S. A. A. and Abumandour, M.M.A. (2014):** Computed Tomography and Gross Anatomical Studies on the Head of One-Humped Camel (*Camelus dromedarius*). *Anatomical Record* 297: 630–642
- Bahar, S., Bolat, D., Dayan, M.O. and Paksoy, Y. (2014):** Two- and Three-Dimensional Anatomy of Paranasal Sinuses in Arabian Foals. *J. Vet. Med. Sci.* 76(1): 37–44.
- Basso, F.Z., Busato, E.M., da Silva, J.R., Guedes, R.L., Filho, I.R. and Dornbusch, P.T. (2016):** Comparison between three techniques for videosinuscopy in cattle. *Ciência Rural, Vol.46, No.7, jul.*
- Budras, K.D., Habel R.E., Mülling, C.K.W., Greenough, P.R. (2011):** Bovine Anatomy: An Illustrated Text. 2nd ed, Schluetersche, Germany.
- Dalgorf, D.M. and Harvey R.J. (2013):** Chapter 1: Sinonasal anatomy and function. *Am J Rhinol Allergy.* May-Jun. 27 Suppl 1: S3-6. [Medline].
- Dyce, K.M., Sack, W.O, Wensing C. J. G. (2010).** Textbook of Veterinary Anatomy published in China library of Congress cataloging in. WB Saunders Comp.
- El-Gendy, S. A., and Alsafy, M. A. M. (2010):** Nasal and paranasal sinuses of the donkey: gross anatomy

and computed tomography. *J. Vet. Anat.* 3, 25–41.

El-Hagri, M. A. A., (1967): Splanchnology of Domestic Animals. 1st public organization for books and scientific publications, Giza: Cairo University Press. pp. 23–30.

Eshrah, E.A.I. (2006): Some comparative anatomical studies on the nasal cavity and the larynx in the buffalo (*Bos bubalis*), the camel (*Camellus dromedarius*) and the donkey (*Equus asinus*). Ph.d. Thesis, Faculty of Veterinary Medicine, Benha University.

Farke, A.A. (2010): Evolution and functional morphology of the frontal sinuses in Bovidae (Mammalia: Artiodactyla), and implications for the evolution of cranial pneumaticity. *Zool J Linnean Soc.*, 159: 988–1014.

Hildebrand (1968): Anatomical preparations. University of California Press. Berkeley and Los Angeles, California.

Kareem, D.A. and Sawad, A.A. (2016): Silicon polymer for cast of paranasal sinuses of Iraqi local goat (*Capra hircus*) *Bas.J.Vet.Res.* Vol. 15, No. 1

Kumar, S. and Dhingra, L.D. (1980): Paranasal sinuses of buffalo

(*Bubalus bubalis*). *Haryana Agricult Univ J Res* 10: 267–282.

Lee post, (2005): The Moose Manual, How to Prepare and Articulate Large Hoofed Mammal Skeletons Bone Building Books, Volume 6.

Nomina Anatomica Veterinaria (2012): 5th edition Revised version. Prepared by the International Committee on Veterinary Gross Anatomical Nomenclature (I.C.V.G.A.N.) and authorized by the General Assembly of the World Association of Veterinary Anatomists (W.A.V.A.) Knoxville, TN (U.S.A.) 2003 Published by the Editorial Committee Hannover (Germany), Columbia, MO (U.S.A.), Ghent (Belgium), Sapporo (Japan).

Osman, M.M., Kamal El-Deen, M.M., Kamel, H.M. and Youssef, H.A.Z. (2012): Study on goat as animal model for endoscopic sinus surgery training. *the Journal of PAN Arab Rhinology.* October, Vol 2, No 2, pp. 66-70.

Reddy, U.D., Dev, B. (2012): Pictorial essay: Anatomical variations of paranasal sinuses on multidetector computed tomography-How does it help FESS surgeons? *Indian J Radiol Imaging.* Oct. 22(4): 317-24.

Saigal, R. P. and Khatra, G. S. (1977): Paranasal sinuses of the

Paranasal sinuses of the buffalo

Farag et al.

adult buffalo (*bubalus bubalis*). Anat. Anz. 141, 6–18.

Silva, L. (2008): Estudo retrospectivo sobre fatores de risco e avaliação de quatro protocolos terapêuticos para sinusite em um rebanho de 2491 bovinos. In CONGRESSO BRASILEIRO DE MEDICINA VETERINÁRIA (Vol. 35).

Smith, B.P. (2006): Doenças do Sistema Respiratório. In: **Medicina interna de grandes animais**. Barueri: Manole, : 479-592.

Corresponding author

Farag, F.M.M.

email: fouad.farag@cu.edu.eg

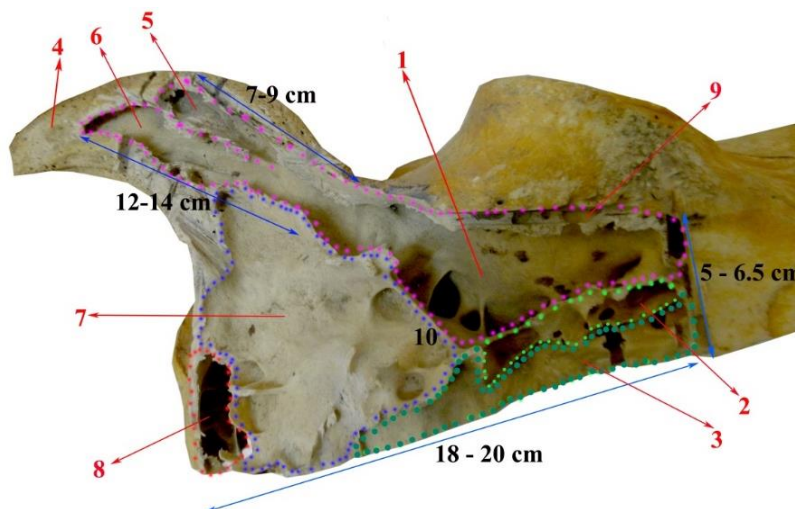


Fig (1): A photograph showing the frontal sinus of buffalo, dorsal view.

1 Sinus frontalis rostralis lateralis, 2 Sinus frontalis rostralis intermedius, 3 Sinus frontalis rostralis medialis, 4 Processus cornualis, 5 Recess rostralis, 6 Recess caudalis, 7 Sinus frontalis caudalis, 8 Diverticulum nuchalis, 9 Canalis supraorbitalis, 10 Inverted V- shaped incomplete septum.

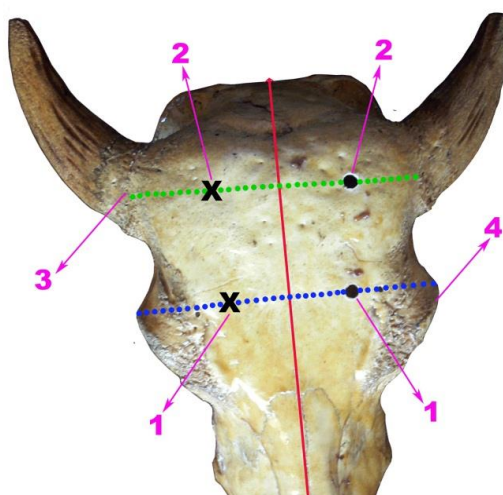


Fig (2): A photograph of a skull of buffalo, dorsal view, showing the sites of approach of frontal sinus.

1 Site for trephining of Sinus frontalis rostralis, 2 Site for trephining of Sinus frontalis caudalis, 3 Processus cornualis, 4 Margo orbitalis.

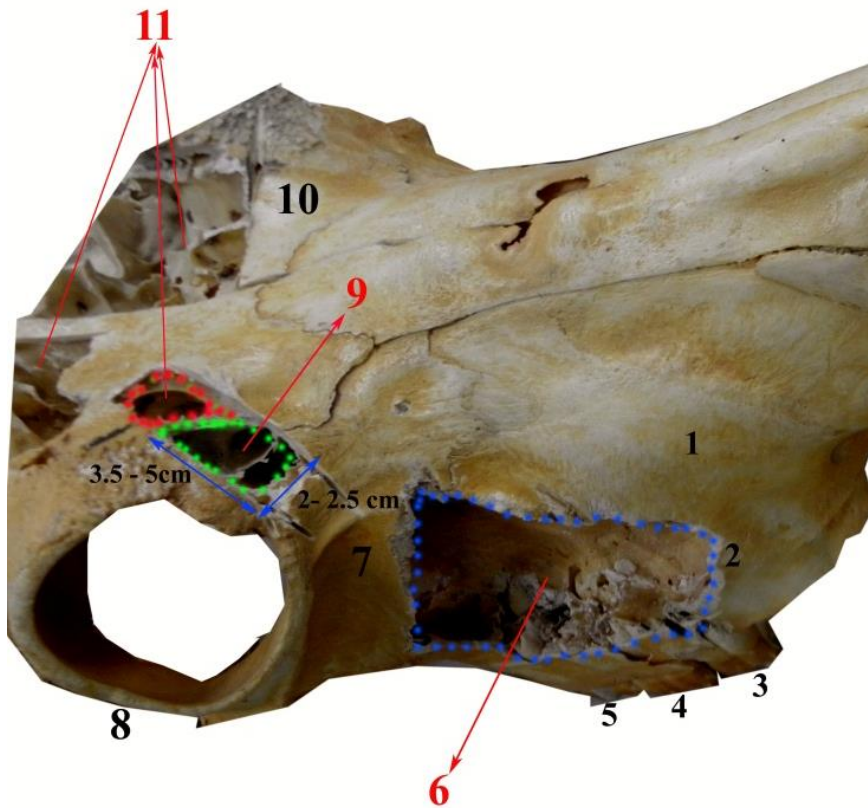


Fig (3): A photograph showing the maxillary and lacrimal sinus of buffalo.

1 Maxilla, 2 Tuber faciale, 3 Dentes molars I, 4 Dentes molars II, 5 Dentes molars III, 6 Sinus maxillaris, 7 Os zygomaticum, 8 Margo orbitalis, 9 Sinus lacrimalis, 10 Os frontale, 11 Sinus frontalis.

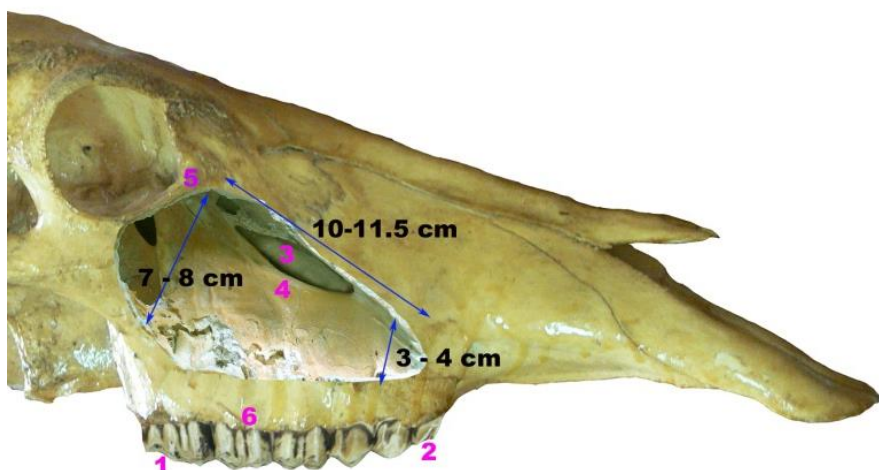


Fig (4): A photograph showing the maxillary sinus in a skull of buffalo, lateral view.

1 Dentes molars III, 2 Dentes premolars I, 3 Apertura maxillopalatina, 4 Canalis infraorbitalis, 5 Margo orbitalis, 6 Margo alveolaris.

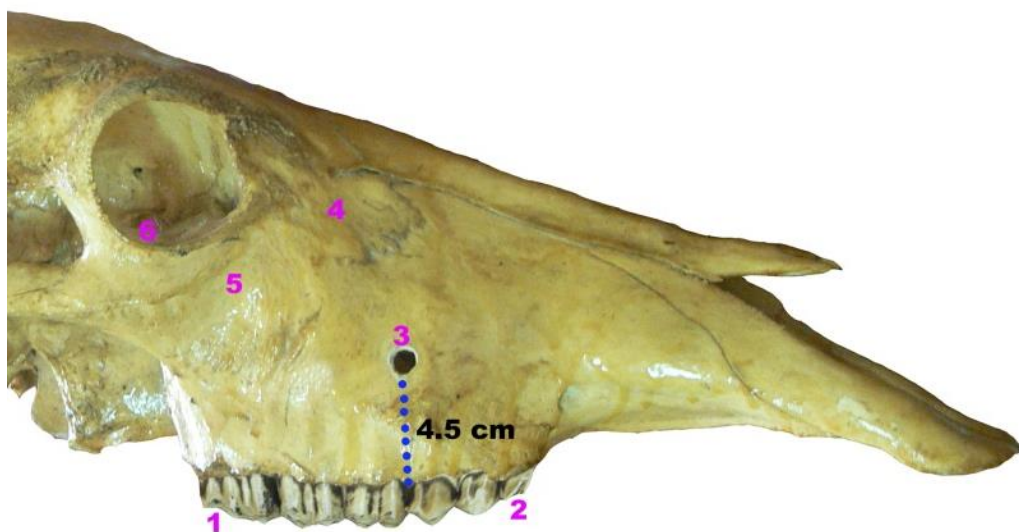


Fig (5): A photograph of a skull of buffalo, lateral view, showing the site of approach of maxillary sinus.

1 Dentes molars III, 2 Dentes premolars I, 3 Site for trephining of sinus maxillaris, 4 Os lacrimale, 5 Os zygomaticum, 6 Bulla lacrimalis.

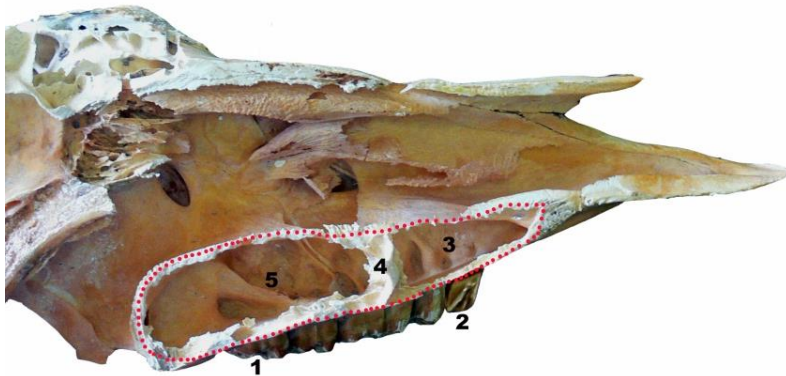


Fig (6): A photograph of a sagittal section in a skull of buffalo showing the palatine sinus.

1 Dentes molars III, 2 Dentes premolars I, 3 Sinus palatinus rostralis, 4 Incomplete transverse bony partitions, 5 Sinus palatinus caudalis.

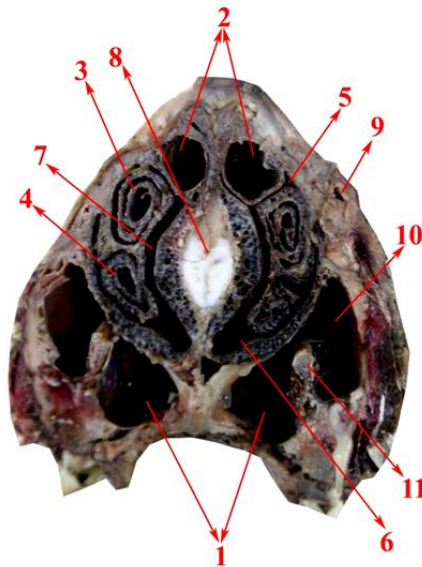


Fig (7): A photograph showing a cross section in the nasal cavity of buffalo at the level of last molar tooth.

1 Sinus palatinus, 2 Concha nasalis dorsalis, 3 Dorsal part of Concha nasalis ventralis, 4 ventral part of Concha nasalis ventralis, 5 Meatus nasi medius, 6 Meatus nasi ventralis, 7 Meatus nasi communis, 8 Septum nasi osseum, 9 canalis nasolacrimalis, 10 sinus maxillaris, 11 canalis infraorbitalis.

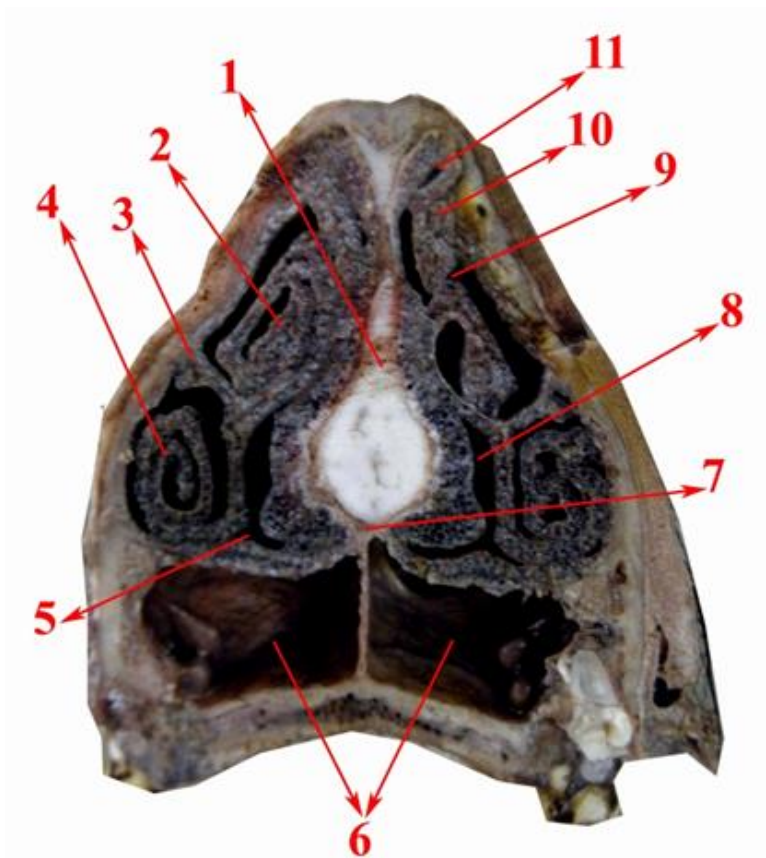


Fig (8): A photograph showing a cross section in the nasal cavity of buffalo at the level of first premolar tooth.

1 Septum nasi osseum, 2 Dorsal part of Concha nasalis ventralis, 3 Basal lamella, 4 ventral part of Concha nasalis ventralis, 5 Meatus nasi ventralis, 6 Sinus palatinus, 7 Vomer, 8 Meatus nasi communis, 9 Meatus nasi medius, 10 Concha nasalis dorsalis, 11 Meatus nasi dorsalis.

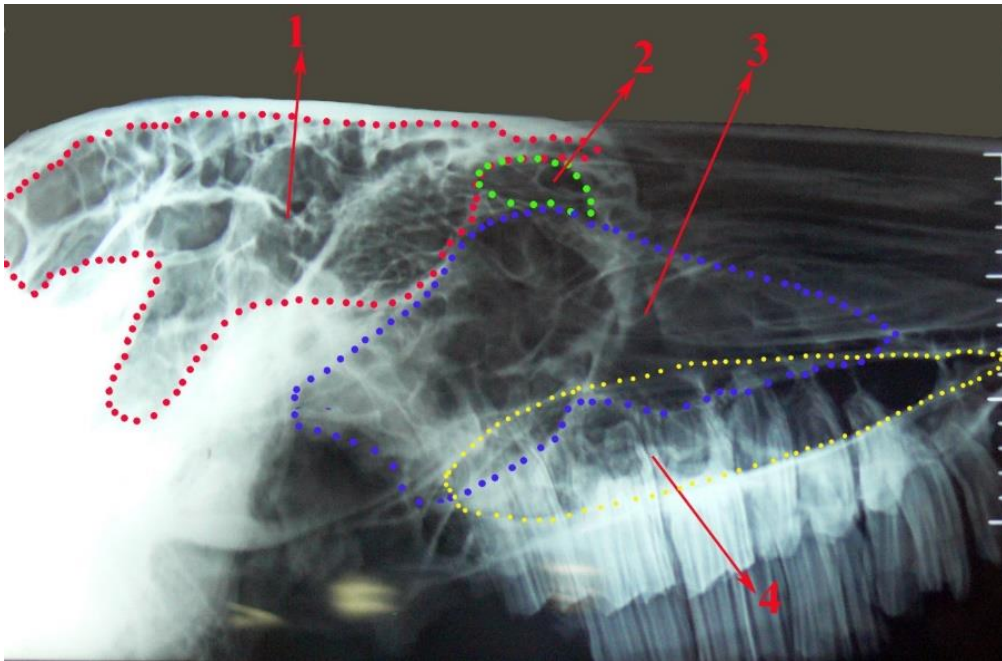


Fig (9): A photograph of X-ray on the head of buffalo, lateral view.
1 Sinus frontalis, 2 Sinus lacrimalis, 3 Sinus maxillaris, 4 Sinus palatinus.

Animal species in this Issue

Red Fox (*Vulpes vulpes*, Demarest 1820)



Kingdom: Animalia & Phylum: Chordata & Class: Mammalia & Order: Carnivora & Family: Canidae & Genus: ***Vulpes*** & Species: *V. Vulpes* (Demarest 1820)

The **red fox** (*Vulpes vulpes*), largest of the true foxes, has the greatest geographic range of all members of the Carnivora order, being present across the entire Northern Hemisphere from the Arctic Circle to North Africa, North America and Eurasia. Apart from its large size, the red fox is distinguished from other fox species by its ability to adapt quickly to new environments. Despite its name, the species often produces individuals with other colourings, including albinos and melanists. Forty-five subspecies are currently recognized, which are divided into two categories: the large northern foxes, and the small, basal southern foxes of Asia and North Africa.

The species has a long history of association with humans, having been extensively hunted as a pest and furbearer for many centuries, as well as being represented in human folklore and mythology. Because of its widespread distribution and large population, the red fox is one of the most important furbearing animals harvested for the fur trade.

The largest red fox on record in Great Britain was a 17.2 kg (38.1 lbs), 1.4-metre (4 ft 7 in) long male, killed in Aberdeenshire, Scotland, in early 2012.

Source: Wikipedia, the free encyclopaedia

Significant Diseases of Two Very Aged Red Foxes (*Vulpes vulpes*, Demarest 1820)

Dennis Lawler^{a,d,e,f*}, Julia Becker^b, Patricia Goodman^c,
Richard Evans^d, Luci Kohn^e

^aIllinois State Museum, 1011 E. Ash St., Springfield IL 62703 USA

^bTippecanoe Animal Hospital, 3818 State Rd. 38 E, Lafayette, Indiana 47905 USA

^cWolf Park, 4004 E 800 N, Battle Ground, Indiana 47920 USA

^dPacific Marine Mammal Center, 20612 Laguna Canyon Rd., Laguna Beach, CA 92561 USA

^eDepartment of Biology, Southern Illinois University, Edwardsville, IL 62025 USA

^fCenter for American Archaeology, Rt. 100, Kampsville IL USA 62053

With 5 figures & 1 table

Received April, accepted for publication June 2017

Abstract

Wild mammal survival rarely approaches ages that are possible in genomic terms. Thus, sheltered environments present unique opportunities to study wild mammal aging and compare aging-related disorders to those of similar domestic animals. We evaluated two aged red fox vixens that had lived in a park setting where they were not caged, and were provided an environment that reflected a natural setting as closely as possible, while providing for proper nutrition and health care. During their 14th year, both foxes developed symptoms suggesting orthopedic and renal deterioration. After diagnosis, monitoring, and humane euthanasia,

postmortem evaluation revealed degenerative joint and renal disease, each closely resembling organ-specific pathology of aged domestic dogs.

Based on evaluation of these foxes and other recent reports, we hypothesize that underlying mechanisms for late life pathological changes reflect broadly and deeply conserved response capacities and not artificial environments, provided that shelter, nutrition, and health care are adequate to minimize stochastic mortality that prevails in the wild.

Keywords: Aging, hip, kidney, osteoarthritis, red fox, shoulder, *Vulpes vulpes*

Introduction

Background

The red fox (*Vulpes vulpes [fulva]*, Demarest 1820) is highly successful, having the largest global distribution of any extant terrestrial carnivore (Henry 1996; Cypher 2003). Its dispersal patterns appear related to population density, interspecies competition, and habitat change (Allen and Seargeant 1999). Adult size is variable with mature body weight 3.0-8.0 kilograms, but on average it is the largest among North American foxes (Cypher 2003). Longevity of 8.6 years in the wild has been reported for a tagged red fox, but in free-living populations, survival as long as 6 years is uncommon (Allen and Seargeant 1999; Storm et al. 1976; Tuller 1983). Since survival in the wild rarely approaches true species limits of longevity, elucidating the aging process in wild species remains a very difficult task. Considering available observational methods, establishing control populations of "normal" free-roaming subjects for comparative studies is nearly impossible because of the natural delay between biological onset of many late life diseases and onset of overt symptoms, and because of the ability of wild mammals to disguise pain and symptoms of organ disease. Thus, the most pressing need is to report all species-related

aging observations to build a database from which to clarify late life diseases in wild mammals.

In this regard, we report examination of shoulder and hip joints, and kidneys, of two red fox vixens that were euthanized during their 14th year because of orthopedic and renal disease. The observations, along with other recent studies, contribute to expanding our understanding of the mammalian aging process.

Life histories

The two females (vixens), named Devon and Ember (not siblings), were born in the spring of 2000. They were habitat-reared and maintained together. They were fed a natural diet consisting of deer meat and small rodents, occasional rabbits, fruits and vegetables, and they regularly caught small rodents and insects such as cicadas. They resided at Wolf Park, Battle Ground IN, in an enclosure measuring 60 x 40 feet, with ladders and decks for climbing and jumping, thus allowing natural fox behavior. They were vaccinated for rabies, distemper, leptospirosis, parvovirus, coronavirus, adenovirus, parainfluenza virus, and lyme disease, and were monitored daily. Health history of each fox was unremarkable until late life.

A few weeks prior to humane euthanasia in their 14th year, both foxes exhibited signs of reduced activity and declining range of joint motion, resulting in end-of-life maintenance indoors. Biochemical evaluation indicated progressive renal failure in both foxes (Table 1). Following humane euthanasia, postmortem examinations were done by the attending veterinarian as a part of normal health care practices. The foxes were not part of a research study, and Institutional Animal Care and Use Committee clearance was not required.

Materials and Methods

Tissue harvest and processing

Gross postmortem examination of both foxes revealed pale yellow, rough-surfaced kidneys that were not contracted or nodular. The left kidney from Ember was preserved in formalin and sent to the consulting pathologist for routine histological evaluation, to parallel routine veterinary clinical practices.

Harvest of shoulder and hip joints was done *en bloc*, followed by freezing at -4°C. Other remains were buried with ceremony, according to Park practices. The frozen bone specimens were transferred to the Illinois State Museum Research and Collections Center, Springfield IL. Bone processing was continued by trimming soft tissue and incubating in hot

water (40-45°C) to macerate remaining non-ossified tissue by bacterial action, with filtering and water replacement as needed. Following several weeks' incubation, soaking in 15-20% ammonia solution promoted further removal of fat from bone. A final brushing step in detergent was done to remove tightly adhered exuded fat. Following clearing, bones were rinsed in tap water and dried. Evaluation of joint components included scapular, humeral, acetabular, and femoral articular surfaces and margins, and periarticular structure. Lumbar vertebrae 5-7 and the sacrum were available from Ember. All harvested bone components were photographed and descriptions recorded.

Results

Renal disease

Renal histopathology (Ember) yielded diffuse, moderate-severe, chronic, glomerular and tubular, calcinosis and interstitial fibrosis (Table 1, Fig 1).

Scapular glenoid

Glenoid fossae were bordered or impinged by encircling articular margin / periarticular prominence, rimming, or osteophytes that were severe in Devon and mild in Ember. Glenoid articular surfaces (Devon) revealed circular caudolateral features (3mm, left side affected more severely) characterized by loss of articular

bone and exposure of thickened underlying trabeculae (Fig 2). Ember was affected similarly but less severely. Both foxes also revealed right glenoid pinpoint depression caudolateral (Devon) or craniocentral (Ember), consistent with focal ossification failure.

Proximal humerus

Proximal humeral articulations were bordered or impinged by encircling articular margin/periarticular prominence, rimming, or osteophytes. The features were severe in Devon (Fig 3) and milder in Ember. Both intertubercular (bicipital) grooves revealed severe osteophytes in Devon (Fig 4), while similar lesions in Ember were less severe. The latter features are compatible with degrees of co-morbid biceps tendonitis. Ember also revealed a 1x3 mm mid-lateral articular surface defect on the left humerus.

Acetabulum

Acetabular fossae of both foxes revealed bone formation suggesting enthesiophytes. The new bone formation was more severe in Devon, impinging the dorsomedial articular surface bilaterally (Fig 5). The medial acetabular articular margins were prominent in both foxes, while Devon had small osteophytes at each caudal acetabular margin.

Proximal femur and spine

The dorsal femoral necks revealed very mild filling with new bone (Devon), and prominent femoral head articular margins (Devon and Ember, with greater severity in Devon). Ember had severe spondylosis deformans of cranial and caudal aspects of lumbar vertebrae 6 and 7, and cranial sacrum.

Discussion

Behaviors and osteoarthritis

The red fox hunts small prey by pouncing and pinning the prey with its forefeet, killing it with a bite. Suddenly attacking small prey from brush cover also is a common behavior. Somewhat larger prey (rabbits) are stalked and attacked with jumping or sprinting behaviors (Scott 1943). Other normal fox behaviors include brisk walk as the normal gait; trotting up to several kilometers and jumping to about 4 meters; occasional swimming or climbing; and active defense of a home range (Pasitschniak-Arts and Pasitschniak-Arts 1996). At Wolf Park, very similar behaviors (especially in young foxes) include jumping from heights of 1.3-2.0 m; climbing fences, play-ladders, or trees; pouncing on insects such as cicadas; and playing on a trampoline.

Given an active lifestyle and carnivorous behaviors, significant prevalence of arthropathy might be expected in the uncommon event that a free-living fox survives to advanced age. Obesity is a well-known risk for osteoarthritis in several mammalian species (Anderson and Felson 1988; Davis *et al*, 1988; van Saase *et al*, 1988; Bendele and Hulman 1991; Popovitch *et al*, 1995; Lawler *et al*, 2008), but obesity is unusual in wild canids. In the foxes we evaluated, only seasonally-expected fluctuations in body condition were observed, without obesity at any time during life. Thus, environmental and nutritional influences seem insufficient to explain the disease observations. The latter is interesting, considering the similarities to the parallel conditions among elderly domestic dogs.

Renal disease

The similarity of the fox renal morphology to late-life renal disease in domestic dogs prompts hypotheses that (a) soft organ diseases of aged Canidae may be more universal consequences of simple chronology than has been supposed; and (b) immediate environments may be correspondingly less influential provided that nutrition, shelter, and health care are adequate. Additional late life biochemical studies of wild canids that live to species-possible ages should

be conducted and published, to explore more completely the chronological prevalence of diseases across related individuals in non-domestic populations.

Joint disease – shoulder

In a cross-sectional study of 88 randomly-selected domestic dogs (mean age 8.2 years, range 1-12), shoulder radiography revealed primary age-related osteoarthritis in 31% of the group (mean age 10.2 years)(Ljunggren and Olsson 1975). A cross-sectional study of skeletal remains of 16 adult raccoon dogs (*Nyctereutes procyonoides*) revealed 100% prevalence of the same glenoid features that were observed in the two vixens, with severity ranging from near-normal to mild osteoarthritis, while 81% of proximal humeral articulations also reflected the fox observations (Lawler *et al*, 2012). Recently, lesions of scapular glenoid articular cartilage were related spatially to underlying pathology of articular bone in 7 gray wolves (ages 5-19 years), and the nature and spatial distribution of the osteoarthritis changes were again the same as the foxes and raccoon dogs (Lawler *et al*, 2016).

A longitudinal study of 149 domestic dogs revealed 53% radiographic prevalence of age-related shoulder osteoarthritis at mean age 13.8 years

(Morgan *et al*, 1987). In another longitudinal study, 43 Labrador retrievers had more radiographic shoulder osteoarthritis at age 8 years than elbows, hips, and stifles of the same dogs (Kealy *et al*, 2000).

Joint disease – hip & spine

One left femoral head lesion (Devon) is compatible with an early circumferential femoral head osteophyte (Szabo *et al*, 2007). The red fox osteoarthritis-related pathology of acetabula and proximal femoral articulations mimic observations of domestic dogs (Lawler *et al*, 2008) and raccoon dogs (Lawler *et al*, 2012). A report of femoral head radiographic pathology in a gray wolf (*Canis lupus lupus*) described very similar features (Lawler and Evans 2016). The intra- and extra-articular spatial locations of these features are consistent across canids examined to date, with the expected age-related variation in severity.

Spondylosis refers to osteophyte formation around cranial and/or caudal vertebral end plates, secondary to degenerative disease of the adjacent intervertebral disk (Morgan and Biery 1985). The intervertebral disk space may be narrowed and adjacent vertebrae become unstable, prompting osteophyte reaction. Older large domestic dogs develop spondylosis more frequently, but smaller dogs also are affected. Some affected

dogs experience pain and difficult movement, while others remain relatively asymptomatic (Prada 1993). We are not aware that this pathology has been investigated in red foxes, but the strong similarity between fox and other canid features again is striking.

Studies of domestic dogs demonstrate that radiography significantly underestimates diarthrodial joint pathology (Morgan *et al*, 1987; Runge *et al*, 2008; Lawler and Evans 2016), and radiographic diagnosis of joint pathology in other canids introduces these same limitations (Lawler *et al*, 2016). We suggest that comparative joint biology studies of Canidae have been impeded by (a) limitations inherent in most imaging modalities; (b) hazards of anesthetizing wild animals for examination; (c) relative infrequency of highly detailed postmortem study of wild mammal diarthrodial joints.

Integrative joint development and function

Studies of morphological integration examine relationships among anatomical structures (Cheverud 1982, 1995, 1996). Common functional attributes, such as the shape of the proximal humerus and scapular glenoid fossa, lead to functional integration with muscle actions that are necessary for proper function, implying

common developmental influences during formation and growth (integration). These influences may be hormonal, or they may relate to interaction of developing tissues.

Integrated structures evolve together because of correlated inheritance and shared influence from natural selection. Functional and developmental morphological integration occur at the individual level, and evolutionary integration occurs at the population level (Cheverud 1982, 1995, 1996).

Integrated traits are expected to exhibit a significant correlation among traits within the anatomical module, based on their shared influences (Cheverud 1982, 1995, 1996; Hallgrímsson *et al*, 2002). Morphological integration studies of mammalian scapulae have examined the developmental, functional, and evolutionary structure of the scapular glenoid and blade (Young 2004, 2006, 2008). Scapula studies of seven primate species (Young 2004) and six mustelid species (Norman 2016) identified significant integration within the glenoid, as well as within the blade and acromion. Locomotion influences on integration were observed in 17 primate species (Young 2008). Developmental influences of the *Hoxc6* gene on glenoid (Olivier *et al*, 1990); *Emx2* gene influencing the scapula blade (Pellegrini

et al, 2001); and *Pax1* gene influencing the scapular blade and acromion (Timmons *et al*, 1994; Wilm *et al*, 1994), help to elucidate the genomic integration of these developmental and functional regions. It follows that associated soft tissue structures should be governed under common developmental and functional influences.

Further evaluations of integrated diarthrodial joint components, based on phylogeny and functional morphology, should further clarify why degenerative joint pathology tends to occur at nearly identical foci within the same joint, across species.

Conclusions

It is clear that aging-related osteoarthritis is not unique to the domestic dog and occurs among other Canidae, in similar joint-specific spatial patterns. Primary influences on expression of late life diseases among canids appear to reflect (a) species-related achievable longevity; (b) the balance among disease onset and the subsequent time that symptoms develop to be observed; and (c) genome-mediated responses to insults that appear to be conserved phylogenetically.

Acknowledgements

Specimens and histories were provided by Wolf Park (Battle Ground,

Indiana). The Illinois State Museum research and Collections Center (Springfield IL) provided specimen-processing facilities for this work. This work was conducted pro bono and was unfunded.

References

Allen, S.H., Sargeant, A.B. (1999): Dispersal patterns of red foxes relative to population density. *Journal of Wildlife Management* 57: 526-533.

Anderson, J.J., Felson, D.T. (1988): Factors associated with osteoarthritis of the knee in the first national health and nutrition examination survey (Hanes I). *American Journal of Epidemiology* 128: 179-189.

Bendele, A.M., Hulman, F.J. (1991): Effects of body weight restriction on the development of and progression of spontaneous osteoarthritis in guinea pigs. *Arthritis and Rheumatism* 34: 1180-1184.

Cheverud, J.M. (1982): Phenotypic, genetic and environmental morphological integration in the cranium. *Evolution* 36: 499-516.

Cheverud, J.M. (1995): Morphological integration in the saddle-back tamarin (*Saguinus fuscicollis*) cranium. *American Naturalist* 145: 63-89.

Cheverud, J.M. (1996): Developmental integration and the evolution of pleiotropy. *American Zoologist* 36: 44-50.

Cypher, B.L. (2003): Foxes. In: Feldhamer, G.A., Thompson, B.C., Chapman, J.A. (eds.). *Wild Mammals of North America*, 2nd edition. *Johns Hopkins University Press*, Baltimore, pp. 511-546.

Davis, M.A., Ettinger, W.H., Neuhaus, J.M., Hauck, W.W. (1988): Sex differences in osteoarthritis of the knee. *American Journal of Epidemiology* 127: 1019-1030.

Hallgrímsson, B., Willmore, K., Hall, B.K. (2002): Canalization, developmental stability and morphological integration in primate limbs. *Yearbook of Physical Anthropology* 45: 131-158.

Henry, J.D. (1996): Foxes: Living on the Edge. In: *Northwood Wildlife Series*. Minocqua, Wisconsin.

Kealy, R.D., Lawler, D.F., Ballam, J.M., Lust, G., Biery, D.N., Smith, G.K., Mantz, S.L. (2000): Evaluation of the effect of limited food consumption on radiographic evidence of osteoarthritis in dogs. *Journal of the American Veterinary Medical Association* 217: 1678-1680.

- Lawler, D., Becker, J., Reetz, J., Goodman, P., Evans, R., Rubin, D., Tangredi, B., Widga, C., Sackman, J., Martin, T., Kohn, L., Smith, G. (2016):** Pathology of grey wolf shoulders: Lessons in species and aging. *Anatomical Review* doi: 10.1002/ar.23380
- Lawler, D.F., Larson, B.T., Ballam, J.M., Smith, G.K., Biery, D.N., Evans, R.H., Greeley, E.H., Segre, M., Stowe, H.D., Kealy, R.D. (2008):** Diet restriction and aging in the dog. Summary of major observations over two decades. *British Journal of Nutrition* 99: 793-805.
- Lawler, D.F., Evans, R.H., Nieminen, P., Mustonen, A.-M., Smith, G.K. (2012):** Lessons from a non-domestic canid: joint disease in captive raccoon dogs (*Nyctereutes procyonoides*). *Veterinaria Italiana* 48(4): 367-378.
- Lawler, D.F., Evans, R.H. (2016):** Evaluation of femoral head and neck new bone from a grey wolf (*Canis lupus lupus*): When is it pathology? *Journal of Veterinary Anatomy* 9(1): 9-46.
- Ljunggren, G., Olsson, S.-E., (1975):** Osteoarthritis of the shoulder and elbow joints in dogs: a pathologic and radiographic study of necropsy material. *Journal of the American Veterinary Radiological Society* 16: 33-38.
- Morgan, J.P., Pool, R.R., Miyabayashi, T. (1987):** Primary degenerative joint disease of the shoulder in a colony of beagles. *Journal of the American Veterinary Medical Association* 190: 531-540.
- Morgan, J.P., Biery, D.N. (1985):** Spondylosis deformans. In: Newton, C.D., Nunamaker, D.H. (eds.). *Textbook of Small Animal Orthopedics. JB Lippincott*, Philadelphia. pp. 773-788.
- Norman, S. (2016):** Morphometric analysis of scapula morphology within the Mustelidae family. Masters Thesis. *Southern Illinois University, Edwardsville IL USA*.
- Olivier, G., de Robertis, E.M., Wolpert, L., Tickle, C. (1990):** Expression of a homeobox gene in the chick wing bud following application of retinoic acid and grafts of polarizing region tissue. *EMBO Journal* 9: 3093-3099.
- Pasitschniak-Arts, S., Pasitschniak-Arts, M. (1996):** *Vulpes vulpes*. In: *American Society of Mammalogists: Mammalian Species*. No. 537: 1–11.

- Pellegrini, M., Pantano, S., Fumi, M.P., Lucchini, F., Forabosco, A. (2001):** Agenesis of the scapula in *Emx2* homozygous mutants. *Developmental Biology* 232: 149-156.
- Popovitch, C.A., Smith, G.K., Gregor, T.P., Shofer, F.S. (1995):** Comparison of susceptibility to hip dysplasia between Rottweilers and German Shepherd dogs. *Journal of American Veterinary Medical Association* 206: 648-650.
- Prada, R. (1993):** Cauda Equina Syndrome. In: Slatter, D. (ed.). *Textbook of Small Animal Surgery*, 2nd edition, Volume 1. WB Saunders, Philadelphia. pp. 1094-1105.
- Runge, J.J., Biery, D.N., Lawler, D.F., Gregor, T.P., Evans, R.H., Kealy, R.D., Szabo, S.D., Smith, G.K. (2008):** The effects of lifetime food restriction on the development of osteoarthritis in the canine shoulder. *Veterinary Surgery* 37: 102-107.
- Scott, T.G. (1943):** Some food coactions of the northern plains red fox. *Ecological Monographs* 13: 427-473.
- Storm, G.L., Andrews, R.D., Phillips, R.L., Bishop, R.A., Siniff, D.B., Tester, J.R. (1976):** Morphology, reproduction, dispersal and mortality of midwestern red fox populations. *Wildlife Monographs* 49: 1-82.
- Szabo, S.D., Biery, D.N., Lawler, D.F., Shofer, F.S., Powers, M.Y., Kealy, R.D., Smith, G.K. (2007):** Evaluation of a circumferential femoral head osteophyte as an early indicator of osteoarthritis characteristic of canine hip dysplasia in dogs. *Journal of the American Veterinary Medical Association* 231(6): 889-892.
- Timmons, P.M., Wallin, J., Rigby, P.W., Balling, R. (1994):** Expression and function of *Pax1* during development of the pectoral girdle. *Development* 120: 2773-2785.
- Tullar, B.F., Jr. (1983):** An unusually long-lived red fox. *New York Fish and Game Journal* 30: 227.
- van Saase, J.L., Vandenbroucke, J.P., van Romunde, L.K.J., Valkenburg, H.A. (1988):** Osteoarthritis and obesity in the general population. A relationship calling for an explanation. *Journal of Rheumatology* 15: 1152-1158.
- Young, N. (2004):** Modularity and integration in the Hominoid scapula. *Journal of Experimental Zoology (Molecular Development and Evolution)* 302B: 226-240.
- Young, N. (2006):** Function, ontogeny and canalization of shape variance in the primate scapula. *Journal of Anatomy* 209: 623-636.

Young, N. (2008): A comparison of the ontogeny of shape variation in the anthropoid scapula: functional and phylogenetic signal. *American Journal of Physical Anthropology* 136: 247-264.

Academy of Sciences USA 95: 8692-8697.

Wilm, B., Dahl, E., Peters, H., Balling, R., Imai, K. (1994): Targeted disruption of Pax1 defines its null phenotype and proves haploinsufficiency. *Proceedings of the National*

Corresponding author:

Dennis Lawler
Illinois State Museum, 1011 E. Ash St.,
Springfield IL 62703 USA
dlawler11@yahoo.com

Table (1): Biochemical documentation of progressive renal disease in two elderly female *Vulpes vulpes*

Ember

	<u>Urea nitrogen (mg/dl)</u>	<u>Creatinine (mg/dl)</u>	<u>Phosphorus (mg/dl)</u>	<u>Hematocrit (%)</u>
8/29/2014	222	4.7	16.5	18
7/23/2014	201	5.3	13.4	30
6/14/2014	154	5.0		35
5/28/2014	136	5.0	11.7	21
5/15/2014	149	4.6		34
5/01/2013	68	1.7		48
7/11/2012	64	1.1	3.9	48
2/27/2011	59	1.0		46
1/30/2010	26	0.6	2.6	47

Devon

	<u>Urea nitrogen (mg/dl)</u>	<u>Creatinine (mg/dl)</u>	<u>Phosphorus (mg/dl)</u>	<u>Hematocrit (%)</u>
7/22/14	195	7.5	13.9	28
6/14/14	162	5.3		36
5/15/14	182	4.7		39
9/11/13	83	1.3	4.4	39
5/01/13	65	0.8		49
7/11/12	48	0.9	3.9	43
7/27/11	46	0.7		46
3/05/11	32	0.7	3.6	57
8/24/10	48	0.7		37

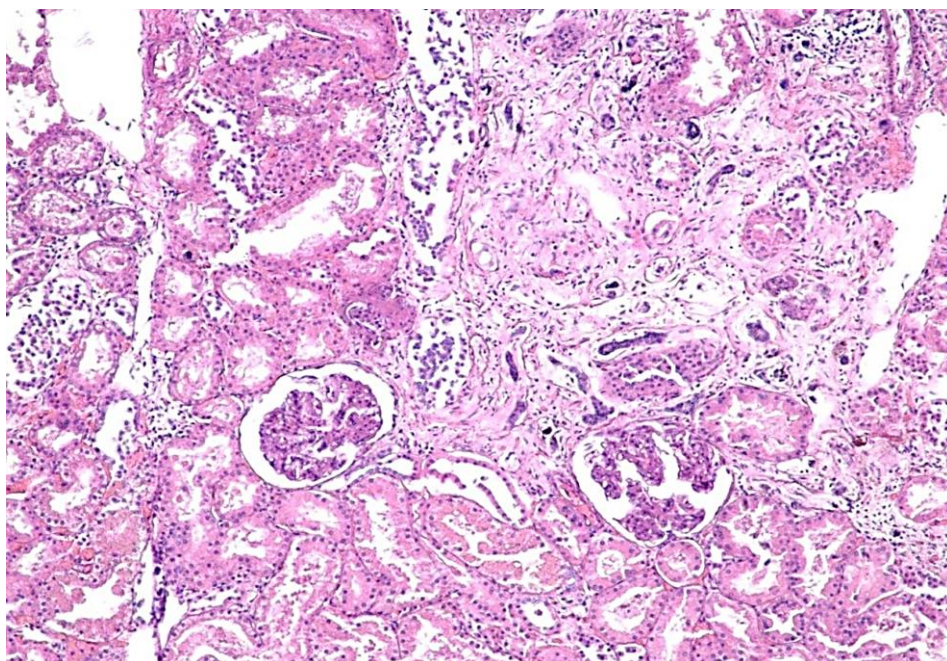


Fig (1): Ember, left kidney. Nephropathy, glomerular and tubular, dystrophic with calcinosis, chronic, moderate-severe, diffuse (H&E).

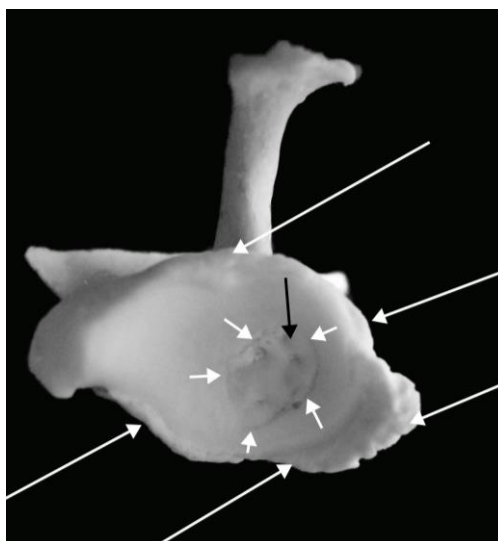


Fig (2): Devon, left scapula glenoid cavity. Severe encircling osteophytes (long white arrows); Bone loss mid-caudal fossa (short white arrows); Exposed thickened subarticular trabeculae (black arrow)

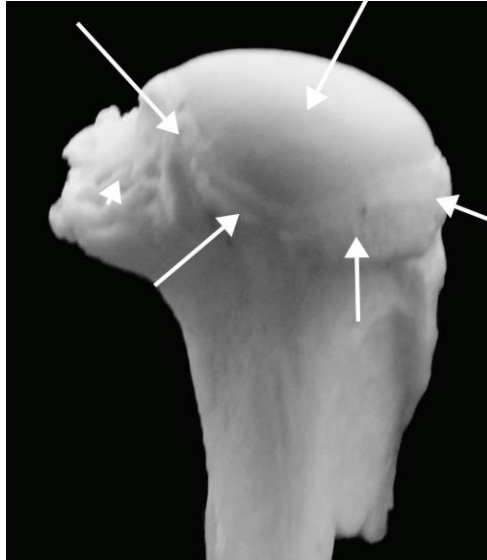


Fig (3): Devon, right proximal humerus, caudolateral view. Normal caudolateral articular surface (long white arrow); Severe encircling articular margin & periarticular osteophytes impinging margin of articular surface (short white arrows); osteophytes on lesser tubercle (white arrowhead).

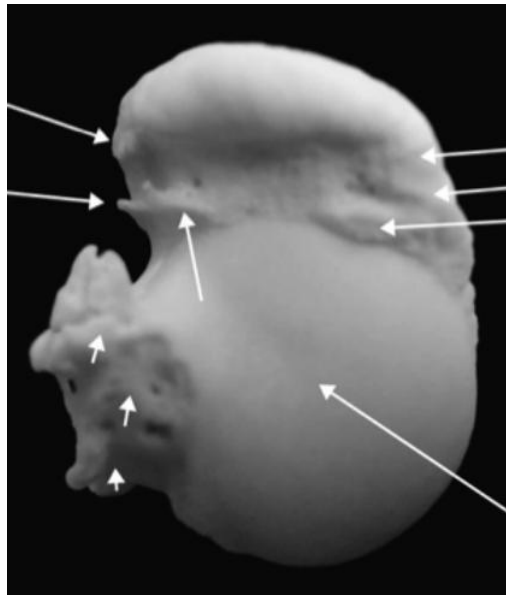


Fig (4): Devon, right proximal humerus, articular surface, dorsal view. Normal articular surface (long white arrow); Osteophytes on lesser tubercle (white arrowheads); Severe osteophytes medial & lateral margin & floor of intertubercular (bicipital) groove (short white arrows).

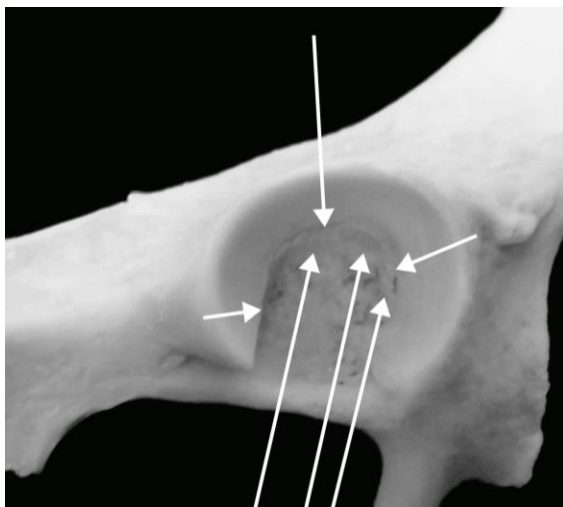


Fig (5): Devon, right acetabulum, lateral view. Severe new bone craniodorsal fossa, probable enthesiophytes (long white arrows); Impinging of medial articular surface (medium arrow); Prominent medial articular margin (short white arrows).

Skeletal Pathology of Farm-Reared Obese Juvenile Blue Foxes (*Vulpes lagopus*)

Anne-Mari Mustonen^{a,b}, Dennis F. Lawler^c, Leena Ahola^d,
Tarja Koistinen^{d,e}, Liisa Jalkanen^f, Jaakko Mononen^e,
Marja-Leena Lamidi^g, Petteri Nieminen^{a,b}

^a University of Eastern Finland, Faculty of Health Sciences, School of Medicine, Institute of Biomedicine/Anatomy, P.O. Box 1627, FI-70211, Kuopio, Finland

^b University of Eastern Finland, Faculty of Science and Forestry, Department of Environmental and Biological Sciences, P.O. Box 111, FI-80101, Joensuu, Finland

^c Illinois State Museum Research and Collections Center, 1011 East Ash St., Springfield, IL 62703, USA

^d University of Eastern Finland, Faculty of Science and Forestry, Department of Environmental and Biological Sciences, P.O. Box 1627, FI-70211, Kuopio, Finland

^e Natural Resources Institute Finland (Luke), Green Technology, Halolantie 31A, FI-71750, Maaninka, Finland

^f Punaturkki Veterinary Clinic, Satamakatu 20, FI-70100, Kuopio, Finland

^g University of Eastern Finland, Faculty of Health Sciences, P.O. Box 1627, FI-70211, Kuopio, Finland

With 8 figures & 1 table Received June, accepted for publication September 2017

Abstract

Orthopedic abnormalities of farm-reared blue foxes (*Vulpes lagopus*) have increased recently, creating new concerns about their welfare. Therefore, skeletal condition of obese juvenile blue foxes was evaluated for relationships to degree of obesity. Two pilot study groups included less obese foxes (N = 5) and more obese foxes (N = 5); the latter group had visible carpal joint laxity and locomotor deficits. The principal aims were to examine forelimb deformities and abnormal locomotion

in light of degree of obesity. Overt and incipient (mild or developing) pathology were prevalent and reflected degree of obesity. It is likely that genetic selection and feeding practices were primary underlying problems, but disrupted mineral nutrition and housing practices may have been involved as well. These observations underscore the importance of new actions and additional studies of breeding, nutrition, and housing practices, with the ultimate goal of enhancing the welfare of farmed foxes.

Keywords: blue fox, obesity, radiography, skeletal pathology, *Vulpes lagopus*.

Introduction

Eight decades of diet restriction research have contributed significantly to the understanding of obesity. Body fat now is recognized as an active endocrine organ with the capacity to influence metabolism by (a) contributing to oxidative stress; (b) secreting several hormones; and (c) releasing inflammatory cytokines (Laflamme 2012). Excess body fat in domestic dogs (*Canis lupus familiaris*) increases risk of (a) glucose intolerance and insulin resistance (Larson et al. 2003; de Godoy and Swanson 2013); (b) osteoarthritis; (c) earlier onset of aging-related diseases; (d) shortened lifespan (Kealy et al. 2002; Lawler et al. 2008); (e) reduced respiratory tidal volume, as well as increased respiratory rate and bronchoreactivity (Manens et al. 2012).

The blue fox is a color variant of the wild arctic fox (*Vulpes lagopus*). Blue foxes have been farm-reared for approximately 100 generations (Einarsson and Skrede 1989). Size, body mass, and obesity of blue foxes have increased dramatically in recent decades due to strong selec-

tion for large pelt size, and unrestricted feeding (body mass 5–7 kg in Nes et al. 1988; 13–14 kg in Kempe et al. 2009, 2013; 13–19 kg in Korhonen et al. 2014). Today, body condition at pelting most often is obese to extremely obese (Kempe et al. 2009).

Welfare problems that may relate to obesity, such as foot deformities and abnormal locomotion, are observed frequently on blue fox farms (Kempe et al. 2010; Ahola et al. 2012). In the survey by Ahola et al. (2012), 47% of Finnish foxes especially the blue fox showed degrees of abnormal locomotion, while 23% displayed severe forelimb bending. Kempe et al. (2010) observed that 67% of juvenile blue foxes had poor or very poor forelimb structure.

In this primarily observational pilot study, full skeletons of ten blue foxes were evaluated. The aims were: (a) examine the relationship of visible skeletal pathology to observed limb deformities and locomotor deficits of farm-reared blue foxes; (b) evaluate the contributing role of excessive obesity. The hypotheses were: (a) skeletal pathology contributes to carpal joint laxity and abnormal locomotion; (b) obesity causes or exacerbates musculoskeletal conditions of juvenile blue foxes.

Materials and Methods

Experimental animals and housing

Ten male farm-reared blue foxes were selected at age seven months, based on their body condition, forelimb structure, and locomotor characteristics as of 8 December 2011. The foxes had been housed as sibling pairs in 1.2 m² wire-mesh cages with an elevated observation platform and at least one activity object. The cages were in outdoor sheds at natural ambient temperature and photoperiod, in Eastern Finland (63°N, 29°E).

The foxes were fed ad libitum with commercial fur animal diets (Ylä-Karjalan Rehu, Valtimo, Finland; raw protein 9.1–10.7%; raw fat 10.8–11.6%; raw carbohydrates 15.7–17.6% of fresh weight; metabolizable energy 6.9–7.4 MJ/kg fresh weight). Vitamin–mineral supplements were added to the diet to approximate official recommendations for foxes (Finnish Fur Breeders' Association 2011). Water was provided ad libitum with an automatic watering system.

Fox body condition scores were evaluated visually by one researcher (TK) on 8 December 2011, according to Kempe et al. (2009), as 1 = very thin; 2 = thin; 3 = ideal; 4 = heavy; 5=extremely fat. Carpal laxi-

ty was evaluated by TK based on WelFur assessment categories 0 = no bent feet; 1 = slightly bent feet; 2 = severely bent feet (WelFur 2015). Locomotion was evaluated by TK based on WelFur assessment categories (WelFur 2015).

Five less obese foxes (body condition score 3–4) had normal to mildly abnormal forelimb structure (WelFur score 0–1) and no clear locomotor deficit or unwillingness to move. Five more obese foxes (body condition score 5) had severely bent forelimbs (WelFur score 2) and abnormal locomotion and/or unwillingness to move. Since the study location was a commercial fox farm, no non-obese foxes were available and the selection process could not be randomized.

Euthanasia and radiography

All the foxes were reared on a commercial farm until they were harvested at age seven months, during the normal pelting season. They were sacrificed by electrocution according to recommended farming practices (Council of the European Union 2009), on the same day that their body condition, forelimb conformation, and locomotion were evaluated. No animal ethics license was required, based on the instructions of the National Animal Experiment Board. The foxes were pelted manually and the car-

carcasses were transported to the University of Eastern Finland to be frozen at -20°C .

Radiographic examination was done in a single-blind manner at the Tuhatjalka Veterinary Clinic (Kuopio, Finland) by an experienced veterinarian (LJ). The radiographs were taken using the Sedecal APR-VET model no. A6504-01 (Algete, Spain). Multiple radiographic images were taken of each cadaver. The spine was examined using a lateral projection focused at mid-lumbar, and forelimb images included cervical and thoracic vertebrae. The cranium and forelimbs were imaged using ventrodorsal and lateral projections, both centered on the elbow joints. The hind limbs were examined using two ventrodorsal projections, focused on the hips and tibias. The radiographs were evaluated by an experienced veterinarian (DL) who was unaware of group assignment.

Skeletal clearing and skeletal analysis

After radiography, the carcasses were weighed, and initial soft tissue clearing was done to remove abdominal and thoracic soft tissue. The remainder of each carcass was frozen and shipped on dry ice to the Illinois State Museum Research and Collections Center (Springfield, IL, USA). The carrier replenished dry

ice as required, and the carcasses arrived frozen and intact. They were transferred to a -4°C freezer until further processing.

Detailed skeletal clearing was completed by thawing for 24 hours at room temperature, manual defleshing, and disarticulation (DL). Disarticulated skeletal components were incubated in covered, water-filled stainless steel containers at 45°C , with periodic discard of macerated remaining soft tissue, and water replacement. Following maceration, defatting was continued as needed in 20% ammonia solution at room temperature, followed by drying for about seven days.

Skeletal observations were characterized as normal, incipient pathology, or pathology. Incipient pathology was contrasted from overt pathology by being (a) occult by direct physical examination and radiography; (b) recognized occasionally at gross necropsy and recognized frequently on cleared bone; (c) evidently early or very mild stages of development (Lawler and Evans 2016).

Pathology was graded as present or absent. Findings for right and left sides of the body first were classified separately, but if overt/incipient pathology was identified, the structure diagnosis was assigned ac-

ording to the worse side. A pathological finding even in the minority of the ribs (or other skeletal structures with multiple parts) was considered sufficient for this anatomical region to be classified as pathological. All structures were photographed.

Statistical analysis

The goal of statistical evaluation was to estimate differences between less obese and more obese foxes, since degrees of obesity influence health and longevity of dogs (Lawler et al. 2008). Effects of obesity on prevalence of radiographic and skeletal findings were tested by binary logistic regression with generalized estimating equations, to account for the correlation structure of the data due to the repetitions (SPSS v19.0 software, IBM, Armonk, NY, USA). Pathology classifications were selected as the response, with obesity and anatomical region as predictors. Radiographic observations were tested as pooled data, and skeletal observations (axial skeleton, forelimbs, hind limbs) were tested separately. The vertebral column also was tested separately from the axial skeleton, with vertebral groups as predictors.

In some cases, the distribution of either incipient or overt pathology between the less and more obese

foxes could not be tested with the model because there were too few assignments to a particular classification in the group and/or anatomic area. In these instances, the model was simplified by not including the interaction of group-by-anatomic area. The results are presented as N of foxes in each category (Table 1).

Linear regression analysis was done on the combined and average pathology scores of each individual as dependent variables and the carcass weight as the independent variable. The weights of skinned carcasses were compared between the groups using the Mann–Whitney *U*-test, as the data were not normally distributed. The $p < 0.05$ was considered statistically significant.

Results

Carcass weights

All ten carcasses were much larger, with much more body fat than is observed in free-roaming *V. lagopus*. Weights of skinned carcasses differed between the groups (less obese median 8.96 kg; more obese median 13.08 kg; Mann–Whitney *U*-test, $p = 0.009$). The regression analyses for carcass weights and pathology scores of combined anatomical areas were not statistically significant ($p = 0.111$ – 0.123).

Radiography

Radiographic examinations suggested one or more narrowed intervertebral disk spaces in four less obese foxes and one more obese fox. However, the observations could not be confirmed from disarticulated skeletal components.

Scapular radiography revealed glenoid subchondral sclerosis (three less obese; two more obese) and periarticular bony prominence (one more obese). Humeral shoulder articulations suggested flattened articular surface (one less obese) and prominent articular margin (one less obese). Incongruent elbow joint spaces were observed in four more obese foxes, and wide carpal joint space was suggested in one more obese fox. One more obese fox had a healing humeral shaft fracture that caused a short and deformed bone, elbow osteoarthritis (Fig 1), and mild deformity of the carpal joint.

Hip radiography suggested shallow acetabulum (two less obese; three more obese) with subchondral sclerosis (three less obese; three more obese), and prominent articular margin (one more obese). The femoral articular margin revealed circumferential osteophytes (three less obese; two more obese). Caudal femoral neck osteophytes (three less obese; two more obese) also were observed. Other observations

included (a) hip joint laxity (three less obese) or subluxation (two less obese; five more obese); (b) flattened or misshaped femoral head (four less obese; four more obese); (c) prominent femoral head articular margin (one less obese).

The distribution of normality vs. pathological radiographic observations differed significantly according to group and anatomic location (generalized linear model with binary logistic; experimental group $p < 0.001$, anatomic region $p < 0.001$, interaction $p = 0.484$). The frequency of suspected abnormal observations was higher in the more obese group (44 vs. 48%).

Skeletal findings: Axial skeleton

The entire skeleton of each of the ten foxes was evaluated (DL) without knowledge of group assignment. To facilitate reader evaluation of welfare-associated observations, sums for normality, incipient pathology, and overt pathology are reported for each structure (Table 1), along with a qualitative summary of primary observations in the text.

Skull: Pathology observations included (a) fragility, porosity, thin bone structure; (b) dental alveolar wall thinning; (c) perialveolar prominence or overt rim formation; (d) rough perialveolar bone; (e) prominent alveolar margin (Fig 2).

Thorax and Vertebrae: Pathology observations included (a) fragile ribs and costochondral flaring (Fig 3); (b) vertebral articular osteophytes. Incipient pathology included (c) prominent/sharp vertebral articular margin or periarticular rim. Vertebral lateral asymmetry occurred at high frequency.

Degree of obesity did not affect distribution of normality vs. incipient pathology in the axial skeleton (group $p = 0.668$, region $p < 0.001$). The distribution of normality vs. overt pathology differed significantly based on group and location (group $p = 0.001$, region $p < 0.001$, interaction $p = 0.515$). The frequency of pathological observations was higher in the more obese group. The distribution of observations also differed when categories of pathology were pooled (normality vs. pooled incipient *and* overt pathology; group $p < 0.001$ [less obese 48%; more obese 62%], region $p < 0.001$, interaction $p = 0.550$).

There was no effect of obesity on vertebrae (normality vs. incipient pathology: group $p = 0.668$, region $p = 0.005$; normality vs. pooled incipient *and* overt pathology: group $p = 0.548$, region $p = 0.002$).

Skeletal findings: Appendicular skeleton, forelimbs

Scapula: Pathology observations included (a) rough or irregular articular or periarticular bone; (b) deepened caudolateral glenoid fossa. Incipient pathology included (c) prominent/sharp/rimmed articular margin; (d) prominent or thickened periarticular bone; (e) focal delayed ossification.

Humerus: Pathology observations included:

(a) prominent/sharp/thickened articular margin; (b) prominent or rimmed periarticular margin (distal humerus); (c) increased shaft curvature or distorted shaft (Supplementary Figure S1A); (d) rough/irregular bone surface; (e) articular surface depression; (f) healed fracture (Supplementary Figure S1A). Incipient pathology included (g) prominent periarticular margin (proximal humerus); (h) rim at articular/periarticular margin (proximal humerus); (i) flattened or thickened articular margin (proximal humerus); (j) thickened lateral margin of the intertubercular groove; (k) focal abnormal wear (distal humerus).

Radius: Pathology observations included proximal (a) osteophytes; (b) prominent/thickened articular/periarticular margin (Fig 4a); (c) periarticular prominence or proliferation; (d) articular surface depression; (e) bone shaft increased curvature (Fig 4a) or distortion; distal

(f) rough articular bone surface or surface defect; (g) periosteal reaction; (h) wide, rough, and indistinct epiphyseal bone (Fig 4a, Supplementary Figure S2). Incipient pathology included (a) incomplete articular margin ossification with mild rim; (b) prominent periarticular margin; (c) irregular articular margin; (d) irregular bone surface.

Ulna: Pathology observations included (a) osteophytes (Supplementary Figure S1B); (b) periosteal reaction; (c) increased shaft curvature or distortion; (d) impinged/distorted articular surface; (e) rough, thickened bone surface; (f) wide, rough, indistinct/elongated/ thickened epiphyseal or metaphyseal bone. Incipient pathology included (g) thickening or prominence of the periarticular margin; (h) rimming of articular/periarticular margin; (i) prominent articular margin; (j) incomplete ossification of articular surface. The more obese fox with a partly healed humeral shaft fracture (Supplementary Figure S1A) also revealed significant osteoarthritis and deformity of the associated proximal radius and ulna (Supplementary Figure S1B).

Distal limb: Pathology observations in phalanges consisted only of bone porosity. Incipient pathology consisted of prominent articular margin. Among metacarpals and

metatarsals, periarticular prominence was the only pathology observation, while rough bone surface occurred as incipient pathology. All carpal joint bones were normal. Incomplete ossification was observed in tarsal joint bones.

Obesity influenced the distribution of normality and incipient pathology in the forelimbs (group $p = 0.027$, region $p < 0.001$), with a higher frequency of incipient pathology in the more obese group. The distribution of normality vs. overt pathology differed significantly (group $p < 0.001$, region $p < 0.001$, interaction $p = 0.999$). The distribution also was different when the categories of pathology were pooled (normality vs. pooled incipient *and* overt pathology; group $p < 0.001$ [less obese 52%; more obese 64%], region $p < 0.001$, interaction $p = 1.000$).

Skeletal findings: Appendicular skeleton, hind limbs

Acetabulum: Pathology observations consisted of medial or dorsomedial acetabular periarticular rim. Incipient pathology included (a) prominent/rough/sharp lateral articular margin (Supplementary Figure S3); (b) rough or incompletely ossified articular surfaces; (c) fossa new bone deposition suggesting enthesiophytes.

Femur: Pathology observations included (a) caudal femoral neck osteophyte; (b) bony filling/ thickening of the dorsal femoral neck; (c) rough periarticular bone surfaces; (d) prominent/sharp articular/ periarticular margins (Supplementary Figure S4); (e) incomplete ossification; (f) rough or porous bone; (g) wide, rough surfaces of epiphyseal and metaphyseal bone (Supplementary Figure S4); (h) increased femoral shaft curvature (Fig 4b); (i) mild bony proliferation of the patella. Incipient pathology included (j) femoral head flattening; (k) rough, irregular periarticular margins.

Tibia, fibula: Pathology observations included (a) prominent/rough articular/periarticular margin; (b) rough/prominent bone surface; (c) increased shaft curvature; (d) incomplete ossification; (e) articular surface depression or suspected erosion; (f) wide, rough, and indistinct epiphyseal and metaphyseal bone. Incompletely fused tibial crest occurred as incipient pathology. Fibular observations included (g) wide, rough, and indistinct epiphyseal and metaphyseal bone; (h) incomplete ossification; (i) increased shaft curvature or bowing.

The distribution of normality vs. overt pathology in the hind limbs differed significantly according to group and location (group $p <$

0.001, region $p <$ 0.001, interaction $p =$ 0.875), with the more obese group having higher frequency of pathology observations. The distribution also was significantly different when the categories of pathology were pooled (normality vs. pooled incipient *and* overt pathology; group $p <$ 0.001 [less obese 48%; more obese 58%], region $p <$ 0.001, interaction $p =$ 0.876).

Discussion

Radiography

Direct examination of cleared bones is known to be more sensitive than radiography for detecting pathological changes (Lawler and Evans 2016). In the blue foxes, routine radiographs accurately reflected direct observations only when pathology was at least moderately advanced. Similar outcomes occurred in a previous study of shoulder joints of gray wolves (*Canis lupus lupus*; Lawler et al. 2016a). Suwankong et al. (2006) reported that computed tomography and magnetic resonance imaging of canine degenerative lumbosacral stenosis aligned well with one another, but both agreed less well with direct observations at surgery.

Interpretation of radiographs in this study likely was complicated by (a) inability to achieve completely correct positioning flexion secondary to large focal subcutaneous fat depos-

its; (b) joint alterations caused by excessive body weight on an immature skeleton. Radiographic interpretation also may be complicated by lack of species-specific reference data (Lawler and Evans 2016); post-mortem rigor mortis (Lawler et al. 2016a); and forces applied during pelting.

Incipient skeletal pathology of farm-reared canids likely would be interpreted from radiography only as increased bone density (Lawler et al. 2015), or as within normal limits. Thus, radiography alone is insufficient as a diagnostic approach to assessing orthopedic disease in farm-reared canids.

Skeletal effects

Skeletal pathology often is subtle at early or mild stages. Thus, diagnoses by any approach are partly subjective. An observation at some early point could be diagnosed as a minor anatomic variant, later becoming suspected incipient pathology, or overt pathology at a still more advanced stage. Therefore, outcomes of evaluation depend partly on age of the individual at examination, stage of the pathology, and rate of progression. In the context of age, the observed frequencies of pathology in these seven-month juvenile blue foxes were unexpectedly high.

Previous data on musculoskeletal disorders of juvenile blue foxes are scarce. Korhonen et al. (2015) reported that evaluation of carpal and elbow joints did not reveal damage or disease, and no curving of ulna or radius was noted. These observations suggest the possibility of interacting or co-contributing causes for the blue fox observations.

We observed few changes in metapodial, carpal, or tarsal bones, and the bone curvatures that we documented were insufficient (subjectively) to cause locomotor disorders. The large sizes and young ages of the blue foxes, and the fact that long bone deformity was mild, suggest a hypothesis that forelimb bending was related mainly to tendon and ligament stress because body weight was excessive and thus could not be supported by still-maturing skeletal elements. The extreme size departure from that of wild arctic foxes (Audet et al. 2002) results at least partially from genetic selection for large size, to yield a large pelt (Kempe et al. 2013).

Housing condition is another factor that requires new studies. Korhonen et al. (2001) documented a tendency for better leg structure in blue foxes that were reared in large earthen-floor pens (15 m²) rather than in smaller wire-mesh cages (0.5/1.3 m²). The possibility of inter-

acting or co-contributing causes for the observations is suggested strongly.

Nutritional influences

Obesity is a significant risk for musculoskeletal disorders of domestic dogs, especially osteoarthritis (Kealy et al. 2000; Marshall et al. 2009). Dämmrich (1991) documented that overnutrition can lead to growth rates that are too rapid for proper skeletal development. In large-breed dogs, carpal hyperextension, increased distal radial and ulnar size, and roughness of periosteal and medullary contours, are among changes that can result from excessively rapid growth (Hedhammar et al. 1974). In rapidly growing puppies, malnutrition or overnutrition can lead to pathology of extensor and flexor muscle groups and, thus, joint laxity (Çetinkaya et al. 2007). The blue foxes revealed compatible joint pathology.

In addition to overnutrition, the findings also suggest disrupted mineral nutrition, again raising the possibility of interacting or co-contributing causes. Calcium:phosphorus (Ca:P) imbalance can induce severe disturbances of skeletal development, growth, and bone mineralization in large dog breeds (Schoenmakers et al. 2000). Korhonen et al. (2015) have connected forelimb bending with dietary Ca:P 1.5:1 in

juvenile blue foxes, although confirming data are needed (Korhonen et al. 2005).

Unfortunately, the composition of the diet in the present study could not be examined in detail. Some of the observations, such as skull fragility, could derive from nutritional secondary hyperparathyroidism (de Fornel-Thibaud et al. 2007), underscoring the need for additional nutritional studies of farmed foxes.

An observation that likely was not obesity-related was the fiber-like shredding of costochondral bone that, based on experience, probably represents a processing effect of hot water maceration on the margins of inadequately mineralized bone.

Vertebral observations

Some cervical, thoracic, and lumbar vertebrae displayed at least incipiently pathological osteoarthritic changes in all foxes. Vertebral spinous process deviations were frequent; these may be incidental or pathological (Lawler et al. 2016b), but further clarifying diagnostics were not available for this pilot study.

Vertebral asymmetry can involve articular processes and surfaces, the spinous process, the vertebral arch, or the vertebral body. These

variants are common among skeletal remains of dogs and other canids (Lawler et al. 2016b and unpublished data), and appear to represent normal variation. Vertebrae from *V. lagopus*, *V. vulpes*, *Urocyon cinereoargenteus*, *Canis latrans*, and *C. lupus familiaris*, frequently reveal the same asymmetry without other pathology (Lawler DF, unpublished from specimens curated at the Illinois State Museum). Kharlamova et al. (2010) have demonstrated that skull, pelvis, and limbs of farm-reared silver foxes display directional asymmetry.

Conclusions

Incipient and overt skeletal pathology were common in these late juvenile blue foxes. Multiple skeletal components were involved. Obesity likely is the main direct etiological factor, but interacting or co-contributing influences cannot be excluded. Feeding practices now should be re-evaluated, to ensure that foxes do not develop overt locomotor and conformational abnormalities.

The data also indicate that genetic selection criteria for farmed fox rearing need to be redirected. In particular, selection for large body size may be significantly predisposing to other welfare and health concerns, and this practice needs to be

reconsidered. Housing practices may require revisions to facilitate increased daily locomotor activity for farmed foxes.

Dietary mineral balance as it relates to whole diet nutrient content and balance may be an under-recognized factor that contributes negatively to welfare and comfort, and thus new controlled nutritional studies clearly are needed urgently, likely along with evaluation for interacting genetic, nutritional, and housing influences. Studies of joint-related soft tissues would be useful to clarify histological characteristics of tendons, ligaments, and joint capsules of foxes that have visible carpal joint deformity.

Acknowledgments

The technical help of Jaana Auvinen, Kasper Heikkilä, Hobo Kukkonen, Olli Salmensuu, and the staff at the fur farm is greatly acknowledged. Labor allocated to this project by LA, TK, and JM, the costs for obtaining the carcasses and their delivery to the USA, as well as the radiographs were financially supported by the WelFur project funded by the European Fur Breeders' Association. The funding source had no involvement in the study design, in the collection, analysis and interpretation of data, in the writing of the report or in the

decision to submit the article for publication.

References

Ahola, L.K., Huuki, H., Hovland, A.L., Koistinen, T., Mononen, J. (2012): WelFur – foxes: the inter-observer reliability of the WelFur health measures, and the prevalence of health disorders on fox farms during the growth period. In: Larsen, P.F., Møller, S.H., Clausen, T., Hammer, A.S., Låssen, T.M., Nielsen, V.H., Tauson, A.H., Jepsen, L.L., Hansen, S.W., Elnif, J., Malmkvist, J., (Eds.). Proceedings of the Xth International Scientific Congress in Fur Animal Production. Wageningen Academic Publishers. Wageningen, pp. 441–447.

Audet, A.M., Robbins, C.B., Lari-vière, S. (2002): Alopex lagopus. Mamm. Species No. 713: 1–10.

Çetinkaya, M.A., Yardimci, C., Sağlam, M. (2007): Carpal laxity syndrome in forty-three puppies. Vet. Comp. Orthop. Traumatol. 20: 126–130.

Council of the European Union. (2009): Council regulation (EC) No 1099/2009 of 24 September 2009 on the protection of animals at the time of killing. Off. J. European Union 52(L 303): 1–30.

Dämmrich, K. (1991): Relationship between nutrition and bone growth in large and giant dogs. J. Nutr. 121: S114–S121.

de Fornel-Thibaud, P., Blanchard, G., Escoffier-Chateau, L., Segond, S., Guetta, F., Begon, D., Delisle, F., Rosenberg, D. (2007): Unusual case of osteopenia associated with nutritional calcium and vitamin D deficiency in an adult dog. J. Am. Anim. Hosp. Assoc. 43: 52–60.

de Godoy, M.R.C., Swanson, K.S. (2013): Companion Animals Symposium: Nutrigenomics: Using gene expression and molecular biology data to understand pet obesity. J. Anim. Sci. 91: 2949–2964.

Einarsson, E.J., Skrede, A. (1989): Avl og Fôring av Rev. Landbruksforlaget, Otta.

Finnish Fur Breeders' Association. (2011): Operation handbook 2010–2011. In: Fur 2011 Calendar. Saga Furs and Finnish Fur Breeders' Association. Vantaa, pp. 30–152.

Hedhammar, Å., Wu, F.-M., Krook, L., Schryver, H.F., de Lahunta, A., Whalen, J.P., Kallfelz, F.A., Nunez, E.A., Hintz, H.F., Sheffy, B.E., Ryan, G.D. (1974): Overnutrition and skeletal disease:

An experimental study in growing Great Dane dogs. *Cornell Vet.* 64 (suppl. 5): 5–160.

Kealy, R.D., Lawler, D.F., Ballam, J.M., Lust, G., Biery, D.N., Smith, G.K., Mantz, S.L. (2000): Evaluation of the effect of limited food consumption on radiographic evidence of osteoarthritis in dogs. *J. Am. Vet. Med. Assoc.* 217: 1678–1680.

Kealy, R.D., Lawler, D.F., Ballam, J.M., Mantz, S.L., Biery, D.N., Greeley, E.H., Lust, G., Segre, M., Smith, G.K., Stowe, H.D. (2002): Effects of diet restriction on life span and age-related changes in dogs. *J. Am. Vet. Med. Assoc.* 220: 1315–1320.

Kempe, R., Koskinen, N., Peura, J., Koivula, M., Strandén, I. (2009): Body condition scoring method for the blue fox (*Alopex lagopus*). *Acta Agric. Scand.* 59A: 85–92.

**Kempe, R., Koskinen, N., Mänty-
saari, E., Strandén, I. (2010):** The genetics of body condition and leg weakness in the blue fox (*Alopex lagopus*). *Acta Agric. Scand.* 60A: 141–150.

Kempe, R., Koskinen, N., Strandén, I. (2013): Genetic parameters of pelt character, feed efficiency and size traits in Finnish blue fox

(*Vulpes lagopus*). *J. Anim. Breed. Genet.* 130: 445–455.

Kharlamova, A.V., Trut, L.N., Chase, K., Kukekova, A.V., Lark, K.G. (2010): Directional asymmetry in the limbs, skull and pelvis of the silver fox (*V. vulpes*). *J. Morphol.* 271: 1501–1508.

Korhonen, H., Jauhiainen, L., Niemelä, P., Harri, M., Sauna-aho, R. (2001): Physiological and behavioural responses in blue foxes (*Alopex lagopus*): comparisons between space quantity and floor material. *Anim. Sci.* 72: 375–387.

Korhonen, H.T., Happo, M., Rekilä, T., Valaja, J., Pölönen, I. (2005): Effects of diet calcium:phosphorus ratio and metabolizable energy content on development of osteochondrosis, foot bending and performance in blue foxes. *Anim. Sci.* 80: 325–331.

Korhonen, H.T., Eskeli, P., Lappi, T., Huuki, H., Sepponen, J. (2014): Effects of feeding intensity and Ca:P ratio on foot welfare in blue foxes (*Vulpes lagopus*). *Open J. Anim. Sci.* 4: 153–164.

Korhonen, H.T., Eskeli, P., Huuki, H., Sepponen, J. (2015): Foreleg bending in blue foxes (*Vulpes lagopus*) as evaluated by radiography. *Open J. Vet. Med.* 5: 61–67.

- Laflamme, D.P. (2012):** Companion Animals Symposium: Obesity in dogs and cats: What is wrong with being fat? *J. Anim. Sci.* 90: 1653–1662.
- Larson, B.T., Lawler, D.F., Spitznagel, E.L. Jr., Kealy, R.D. (2003):** Improved glucose tolerance with lifetime diet restriction favorably affects disease and survival in dogs. *J. Nutr.* 133: 2887–2892.
- Lawler, D.F., Evans, R.H. (2016):** Evaluation of femoral head and neck new bone from a grey wolf (*Canis lupus lupus*): When is it pathology? *J. Vet. Anat.* 9: 39–46.
- Lawler, D.F., Larson, B.T., Balam, J.M., Smith, G.K., Biery, D.N., Evans, R.H., Greeley, E.H., Segre, M., Stowe, H.D., Kealy, R.D. (2008):** Diet restriction and ageing in the dog: major observations over two decades. *Br. J. Nutr.* 99: 793–805.
- Lawler, D.F., Evans, R.H., Reetz, J.A., Sackman, J.E., Chase, K., Widga, C.C., Smith, G.K. (2015):** Scapular glenoid observations of six *Canis lupus dingo*. *J. Vet. Anat.* 8: 47–58.
- Lawler, D., Becker, J., Reetz, J., Goodmann, P., Evans, R., Rubin, D., Tangredi, B., Widga, C., Sackman, J., Martin, T., Kohn, L., Smith, G. (2016a):** Pathology of grey wolf shoulders: Lessons in species and aging. *Anat. Rec.* 299: 1338–1347.
- Lawler, D.F., Widga, C., Rubin, D.A., Reetz, J.A., Evans, R.H., Tangredi, B.P., Thomas, R.M., Martin, T.J., Hildebolt, C., Smith, K., Leib, D., Sackman, J.E., Avery, J.G., Smith, G.K. (2016b):** Differential diagnosis of vertebral spinous process deviations in archaeological and modern domestic dogs. *J. Archaeol. Sci. Reports* 9: 54–63.
- Manens, J., Bolognin, M., Bernaerts, F., Diez, M., Kirschvink, N., Clercx, C. (2012):** Effects of obesity on lung function and airway reactivity in healthy dogs. *Vet. J.* 193: 217–221.
- Marshall, W.G., Bockstahler, B.A., Hulse, D.A., Carmichael, S. (2009):** A review of osteoarthritis and obesity: current understanding of the relationship and benefit of obesity treatment and prevention in the dog. *Vet. Comp. Orthop. Traumatol.* 22: 339–345.
- Nes, N., Einarsson, E.J., Lohi, O., Jarosz, S., Scheelje, R. (1988):** Vackra Pälsdjur – och dessas Färggenetik. Scientifur, Hillerød.
- Schoenmakers, I., Hazewinkel, H.A.W., Voorhout, G., Carlson, C.S., Richardson, D. (2000):** Effect

of diets with different calcium and phosphorus contents on the skeletal development and blood chemistry of growing great danes. *Vet. Rec.* 147: 652–660.

Suwankong, N., Voorhout, G., Hazewinkel, H.A.W., Meij, B.P. (2006): Agreement between computed tomography, magnetic resonance imaging, and surgical findings in dogs with degenerative lumbosacral stenosis. *J. Am. Vet. Med. Assoc.* 229: 1924–1929.

WelFur. (2015): WelFur Welfare Assessment Protocol for Foxes. WelFur Consortium, Brussels, <http://www.fureurope.eu/publications/welfur-welfare-assessment-protocol-for-foxes>.

Corresponding author:

Dennis F. Lawler,
dlawler11@yahoo.com

Table 1. Pathological skeletal features of two groups of obese blue foxes.

	Structure	Less Obese Foxes (N = 5)			More Obese Foxes (N = 5)		
		OP (N)	IP (N)	N (N)	OP (N)	IP (N)	N (N)
Axial Skeleton	skull, dorsal	3		2	3		2
	skull, palatine	3		2	4		1
	maxilla	4		1	5		
	mandible	2		3	5		
	teeth			5			5
	sternbrae*			5			4
	hyoid bones*			5			4
	ribs	2		3	4		1
	vertebrae cervical	1	4			5	
	vertebrae thoracic	1	4		1	4	
	vertebrae lumbar	1	4			5	
	sacrum	1	3	1	2	2	1
	vertebrae coccygeal			5		1	4
baculum*			4			3	
Appendicular Skeleton left, right hind limbs	phalanges			5	1	1	3
	nails			5			5
	retrieved sesamoids			5			5
	retrieved fabellae			5			5
	patellae	1		4			5
	metatarsals			5	1	1	3
	tarsal joint bones			5	2		3
	acetabula	1	2	2		5	
	prox femur & articular	4		1	5		
	femoral shaft	4		1	3		2
	distal femur & articular	5			5		
	prox tibia & articular	4		1	5		
	tibial shaft	3		2	3		2
	distal tibia & articular	5			5		
	prox fibula & articular	5			5		
fibular shaft	2		3	2		3	
distal fibula & articular	5			5			
Appendicular Skeleton left, right forelimbs	phalanges			5	1	1	3
	nails			5			5
	metacarpal bones			5		1	4
	retrieved sesamoids			5			5
	carpal joint bones			5			5
	scapula articular	2	3		3	2	
	prox humerus & articular	3	1	1	3	1	1
	humeral shaft	4		1	4		1
	distal humerus & articular	3		2	5		
	prox radius & articular	3		2	4	1	
	radial shaft	3		2	5		
	distal radius & articular	5			5		
	prox ulna & articular	4		1	3	1	1
	ulnar shaft	3		2	3		2
	distal ulna & articular	5			5		

OP = overt pathology, IP = incipient pathology, N = normal

*some small bones were not retrieved from all individuals after skeletal clearing



Fig (1): Dorsoventral forelimbs of more obese fox 42. Note the healing fracture of the distal aspect of the left humerus (long arrows) and the associated degenerative joint disease of the elbow (short arrows).

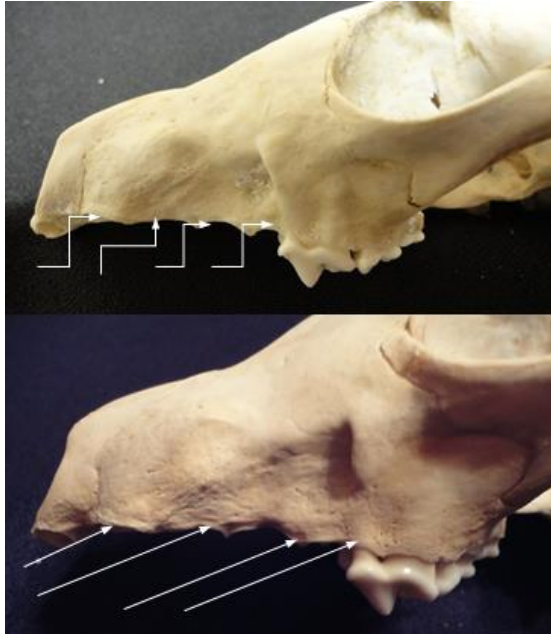


Fig (2): Top photo: Normal alveolar margins in left maxilla of less obese fox 20 (stepped arrows). Bottom photo: Mildly prominent alveolar margins in left maxilla of more obese fox 42 (straight arrows).

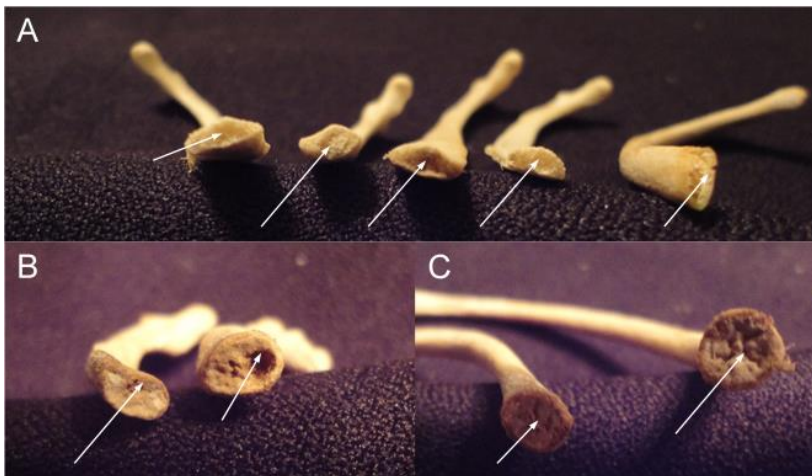


Fig (3): End-on view of costochondral junctions, rib cross-sectional aspect. (A) Less obese fox 10, all normal (arrows); (B) More obese fox 42, left is moderately affected; right is severely affected (arrows); and (C) More obese fox 42, both severely affected (arrows).

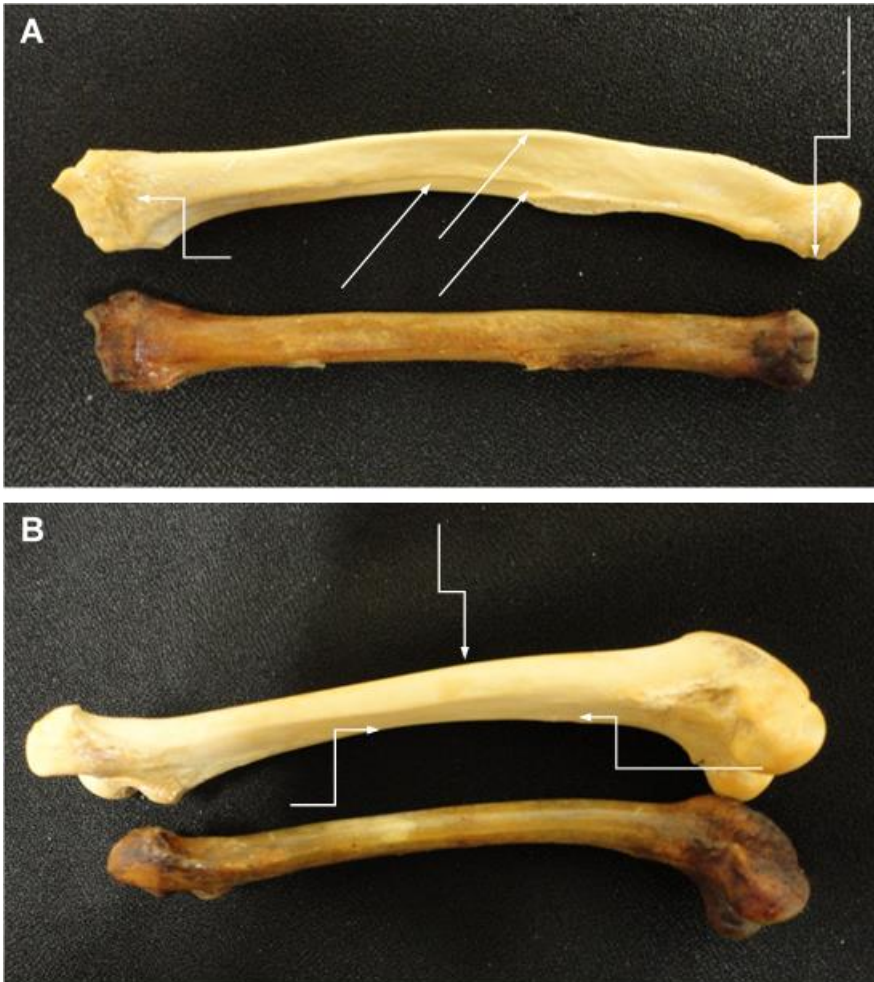
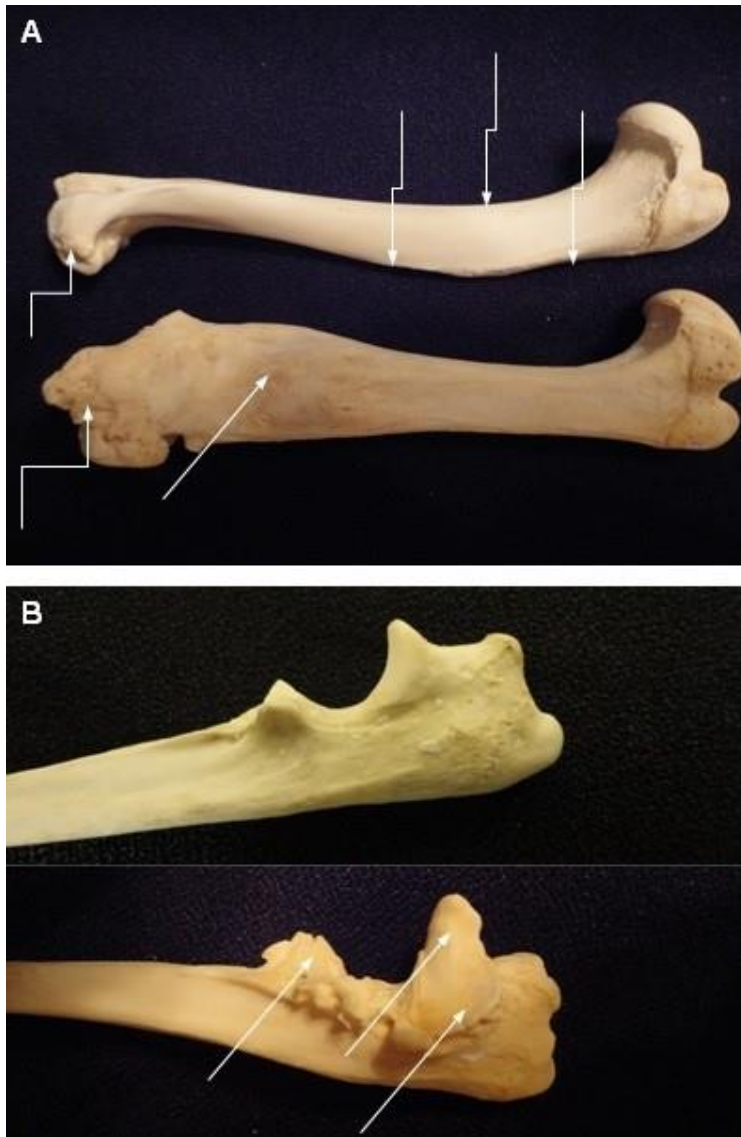
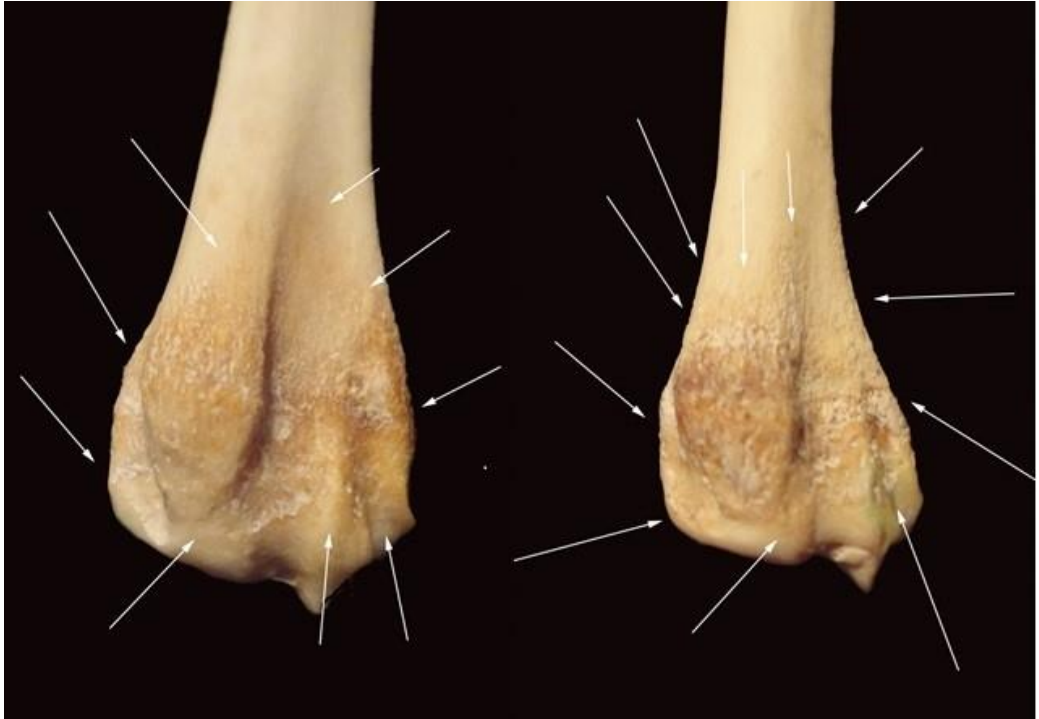


Fig (4): (A) Right radius, ulnar view (top) of more obese fox 12, compared with an adult arctic fox 615858 (Illinois State Museum zoology collections); distal is to the left. The more obese fox shows large size, severe mid-shaft curvature to medial (straight arrows), rough-surfaced distal epiphyseal and metaphyseal bone (short stepped arrow), and mild lateral prominence proximal periarticular margin (long stepped arrow). The bone of the wild fox is normal.

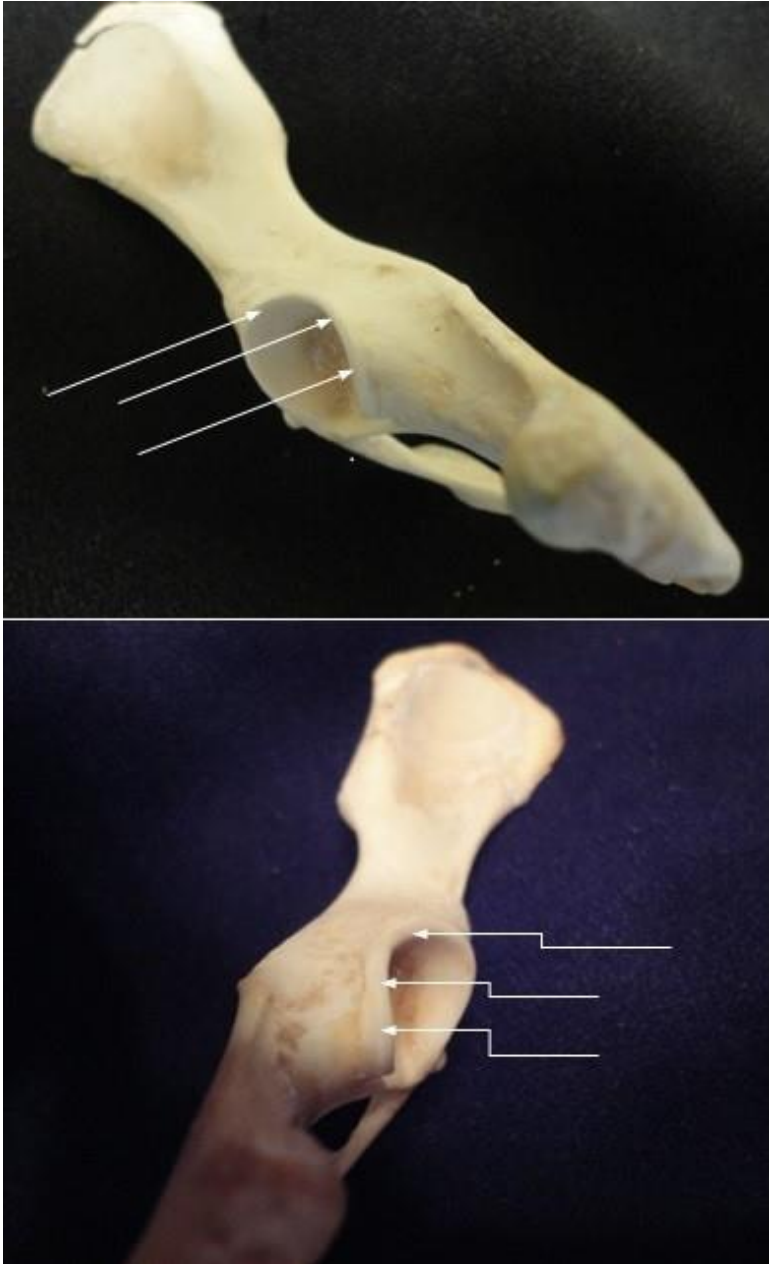
(B) More obese fox 12 right lateral femur (top), compared with arctic fox 615858 specimen. Distal is to the right. The more obese fox shows mildly increased mid-shaft curvature towards cranial (long stepped arrows).



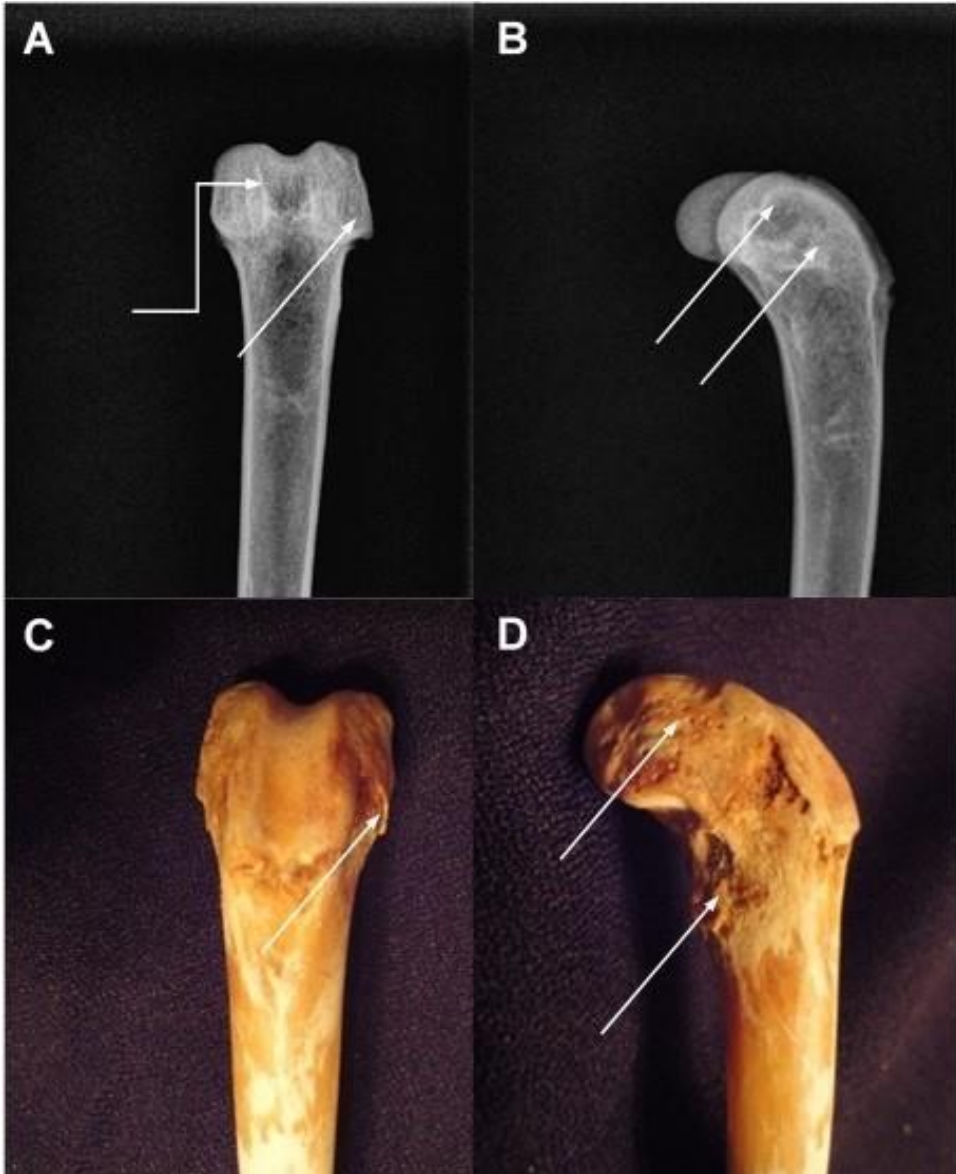
Supplementary Fig S1: (A): Right (top) and left (bottom) humerus of more obese fox 42; distal is to the left. The right humerus shows mild excess curvature to cranial at upper mid-shaft (long stepped arrows), with mild prominence of articular margin and periarticular features distally (short stepped arrow). The left humerus has a healed distal shaft pathological fracture (straight arrow) with bone thickening and remodelling. Distal articular features are deformed by osteophyte production secondary to humeral fracture-associated elbow joint deformity (stepped arrow). (B): The left proximolateral ulna of less obese fox 42 (bottom) displays very severe osteophyte production, secondary to humeral fracture and joint remodelling (arrows).



Supplementary Fig S2: Distal right radius, demonstrating mild (left: more obese fox 52) and severe rough bone (right; less obese fox 20) on epiphyseal and metaphyseal bone surfaces (arrows).



Supplementary Fig S3: Top photo: Straight arrows indicate lateral articular margin prominence that is normal in most foxes (example from less obese fox 50). Bottom photo: Stepped arrows indicate lateral articular margin prominence that represents mild–moderate increase, suggesting smooth osteophyte production in more obese fox 42.



Supplementary Fig S4: Comparison of radiographs and dry bone, distal left femur of more obese fox 42. **(A):** Distal left femur, cranio–caudal radiograph; **(B):** Distal left femur, latero–medial radiograph; **(C):** Gross photo cranial; and **(D):** Gross photo lateral. Epiphyseal and metaphyseal bone has rough surfaces on all sides, and both condyles reveal porosity-associated superficial bone loss (straight arrows). The lateral intercondylar articular margin is unusually prominent (A; stepped arrow). Articular surfaces are normal.

Macro-Anatomic Investigation of Larynx, Trachea and Lungs in Martens (*Martes Foina*)

Yasin Demiraslan^{1*}, Iftar Gurbuz¹, Ozcan Ozgel¹

¹Mehmet Akif Ersoy University Faculty of Veterinary Medicine Department of Anatomy 15030, Burdur, Turkey

With 3 figures

Received July, accepted for publication September 2017

Abstract

The purpose of this study is to determine the macroanatomic characteristics of larynx, trachea, and lungs in martens. In this study, six martens including three males and three females were used. It was found that the larynx of marten was consisted of totally five cartilages, one paired, and three unpaired. These cartilages were cartilago arytenoidea, cartilago thyroidea, cartilago cricoidea, and cartilago epiglottica. It was observed that trachea was consisted of averagely 56-58 cartilago trachealis and the length was measured as approximately 19 ± 2 cm. The pulmo dexter had four lobes: lobus cranialis, lobus medius, lobus caudalis, and lobus accessorius. On the other hand, the pulmo sinister had two lobes: lobus cranialis and lobus caudalis. As a result, it was expected that the macro-anatomic information regarding larynx, trachea, and pulmones would address the lack of literature in this area.

Keywords: Marten, Larynx, Pulmo (lung), Trachea.

Introduction

Marten (*Martes foina*) is a species of the family Mustelidae of the suborder Caniformia of the order Carnivora. This sub-species is represented by mink and badger (ITIS 2015).

Larynx is a tube-shaped organ that provides the connection between the pharynx and trachea. The function of the larynx is preventing the pass-age of foreign matters into the respiratory tract during respiration. Also, another essential function of the larynx is to create the sound (König and Liebich 2007). The skeleton of the larynx is combined with double-side symmetrical shaped cartilages (cart.). Larynx in a dog is consisted of seven cartilages. These cartilages are epiglottic, thyroid, arytenoid, cricoid, cuneiforme and corniculate. While cart. Arytenoidea is paired, the others are unpaired (Evans and

Christensen, 1993; Getty, 1975; Pasquini et al., 2003). In the cat, the larynx is shaped by the combination of totally five cartilages as one double (cart. arytenoidea) and three single (cart. cricoidea, cart. Epiglottica, cart. thyroidea), (Dyce et al., 2002; Getty, 1975; Pasquini et al., 2003).

Trachea is a flexible, cartilaginous, and membranous tube which forms the proximal part of the tracheobronchial tree (Getty, 1975). On the other hand, the dog trachea is formed by combination of 42-46 cart. trachealis, and the cat trachea is formed by 38-43 cart. trachealis (Getty, 1975 ; König and Liebich, 2007). It is stated that although trachea can be changed according to types of carnivores, its average length is 22.5 cm (Bahadır and Yıldız, 2005).

In cats and dogs; being larger than pulmo sinister, pulmo dexter is consisted of four lobes: lobus cranialis, lobus medius, lobus caudalis, and lobus accessorius. Pulmo sinister has two lobes: cranial and caudal (Evans, 2010; Getty, 1975).

In the available literature, while there are some related to the respiratory tracts of some carnivores, a study on the marten could not be found. Therefore, the aim of this study was to describe the

macroanatomic characteristics of the larynx, trachea, and lungs (pulmones) in the *Martes foina*.

Materials and Methods

In this study, six martens (three males and three females), which were killed in traffic accidents and brought to the Anatomy Department of Faculty of Veterinary Science of Mehmet Akif Ersoy University, were used. Permission was taken from Local Ethic Committee of Animal Experiments of Mehmet Akif Ersoy University in order to use the animals. Larynx and trachea were exposed by dissecting the neck skins and muscles of the martens. Then, the breast skins and muscles were dissected. The ribs were cut by using a costatome and the larynx, trachea, and pulmones were taken out as a whole. Findings were obtained by dissecting the laryngeal cartilages individually and a picture of each cartilage was taken. The number of the cartilagenous rings of the trachea were counted and transverse sections were photographed. Each lobe of the pulmo (lung) was separately weighed by using a precision scale. Findings regarding number, shape, and location of these lobes were obtained. Photos were taken by using a Canon 600D brand camera. Digimato brand digital caliper (150mm) was used to take

measurements. Weight dimensions were measured by a Precisa precision scale (S 125 SM). The terminology was based on the *Nomina Anatomica Veterinaria* (NAV 2012).

Results

In this study, the average length of the marten from the nose tip to tail root was 44 cm. The average body weight of marten was 2.20 kg. The larynx, trachea, and lungs of marten were viewed from cranial to caudal.

Larynx

The larynx of the marten consisted of four cartilages; one double and three single namely: cart. thyroidea (unpair), cart. arytenoidea (pair), cart. cricoidea (unpair), and cart. epiglottica (unpair). The cart. Thyroidea forms the base of the larynx. It has a cornu rostrale, cornu caudale, and lamina thyroidea. There was no evidence about significant linea obliqua and prominentia laryngea ventralis on this cartilage. The cart. Arytenoidea were simple pair of cartilages forming the cranio-dorsal aspect of the larynx. It was observed that there was a transition via membrana crico-tracheale between the first tracheal ring and the cart. cricoidea of the larynx and it has a significant processus muscularis. The apex of

the cart. epiglottica is wriggled in the ventral direction (Fig 1).

Trachea

The trachea was shaped by 56-58 cartilages and its length was approximately 19 ± 2 cm. It lies on the median line of the animal neck and was formed by two parts: cervical part and thoracic part. Examining transverse sections of the tracheal rings cleared that the rings were flattened dorso-ventrally, has a slightly oval shape and its ends were free. The free ends of the tracheal rings faced each other, and leaving a space of about 5.31 mm long between them. In the cervical part of the trachea the diameter was 8.32 mm for transversal and 5.94 mm for vertical lengths. In the mid part of the trachea these values were 7.00 mm for transversal and 5.23 for vertical lengths. At the trachea bifurcation level, the values were 8.49 mm and 5.24 mm for transversal and vertical respectively (Fig 1).

The thoracic part of the trachea entered the thorax at a level between the 4th and 5th ribs. The trachea was branched at the bifurcatio trachea into two main bronchi: bronchus principalis dexter and bronchus principalis sinister. The tracheal bifurcation angle was measured as 88.47° . It was determined that bronchus principalis

dexter splits into four bronchi ventilating the right lung lobes. These four bronchi were bronchus cranialis, bronchus medius, bronchus caudalis, and bronchus accessorius. It was also found that the bronchus principalis sinister splits into two bronchi: bronchus cranialis sinister and bronchus caudalis sinister.

Lung (Pulmo)

On opening the chest cavity in marten, the lungs were dark red-brown in colour and had the flat surfaces. The fissure interlobaris in martens was deep and the lobes were significantly distinct from each other.

a) The right lung (Pulmo dexter)

The right lung (pulmo dexter) was formed by four lobes: lobus cranialis, lobus medius, lobus caudalis, and lobus accessorius. The pulmo dexter was located at a level between the 2nd and 10th ribs. The lobus cranialis pulmonis dexter lies at the level between the 2nd and 7th ribs, the lobus medius pulmonis dexter at the level between 6th and 8th ribs, the lobus accessorius pulmonis dexter at the level between the 7th and 8th ribs, and lobus caudalis pulmonis dexter at the level between 5th and 10th ribs.

The shape of the lobus cranialis pulmonis dexter was long, dorso-

medially flattened and looked like a small tongue. The lobus medius pulmonis dexter was flat and pyramidal in shape. The lobus accessorius pulmonis dexter looked like a plump pyramid; whereas, the surface of the lobus caudalis pulmonis dexter was found to be similar to a stuffed and large triangle.

b) The left lung (Pulmo sinister)

The left lung (pulmo sinister) was formed by two lobes only: lobus cranialis and lobus caudalis (Fig 2). The pulmo sinister was observed between 2nd and 10th ribs. The lobus cranialis pulmonis sinister was determined at the level between 2nd and 6th ribs, while the lobus caudalis pulmonis sinister was observed to lie at the level between the 5th and 10th ribs.

Estimating the weight of the lung lobes revealed that; the lobus cranialis pulmonis dexter was 4.8 gr, the lobus medius pulmonis dexter was 1.9 gr, the lobus caudalis pulmonis dexter was 7.4 gr and the lobus accessorius pulmonis dexter was 2.3 gr. In the left lung, the lobus cranialis pulmonis sinister and lobus caudalis pulmonis sinister weighed 5.7 gr and 9.3 gr, respectively.

The upper surface of the lobus cranialis pulmonis sinister was large and narrowed ventrally; whereas,

the upper surface of the lobus caudalis pulmonis sinister was similar to a stuffed triangle (Fig 3).

Discussion

Larynx

Larynx of the dog was shaped by combination of seven cartilages: cart. epiglottica, cart. thyroidea, cart. arytenoidea (pair), cart. cricoidea, cart. cuneiformis and cart. Corniculate (Evans and Christensen, 1993; Getty, 1975; Pasquini et al., 2003). Larynx of the cat was shaped by combination of 5 (3 unpaired, 1 paired) cartilages: cart. cricoidea, cart. Epiglottica, cart. thyroidea, and cart arytenoidea (Dyce, 2002; Getty, 1975; Pasquini et al., 2003). In this study, the marten's larynx was shaped by combination of 5 cartilages as in the cat's larynx (3 unpaired, 1 paired). Cart. Cuneiformis and cart. corniculate cartilages, which were described in the larynx of the dog, were not observed in the larynx of the marten.

Getty (1975) reported that the appearance of cart. thyroidea was different in dogs and cats. While the laminae in dogs were similar to a rectangular, the laminae in cats were higher, narrower and extended obliquely towards the corpus to dorsocaudal. In martens, the laminae of cart. thyroidea were perpendicular and looked like rectangular as in dogs. Evans and

Christensen (1993) and Getty (1975) reported that in dogs there was a significant linea obliqua and prominentia laryngea ventralis on the cart. thyroidea. Getty (1975) noted that in cats the linea obliqua was not clear as in dogs and prominentia laryngea ventralis was not available. In agreement with what Getty (1975) stated in cats, the prominentia laryngea ventralis and linea obliqua were not also present in martens. König and Liebich (2007) and Getty (1975) stated that the apex of the epiglottis was sharp and triangular in carnivores. In the present study, the apex of the epiglottis was sharp and triangle, and also, curved in cranioventral direction.

Trachea

Evans and Christensen (1993) and Getty (1975) reported that while trachea in cats was consisted of 38-43 tracheal rings, the trachea in dogs was consisted of 42-46 tracheal rings (cartilago trachealis). The tracheal rings were 56-58 in martens. Getty (1975) stated that the ends of tracheal cartilages faced each other in uppe and there was an opening between them in transverse sections in the cervical part of the trachea. In martens, the ends of cartilages were faced each other and there was an opening as in the carnivores (mentioned in the

results). Getty (1975) stated that the trachea was separated into two bronchi towards the right of the median plane at the level between the 5th and 6th ribs and dorsal to the hearth base. These bronchi were bronchus principalis dexter and sinister. Similar bifurcation was found in martens at the level of the 4th and 5th ribs (mentioned before in the results). Bahadır and Yıldız (2005) reported that the average length of the trachea was 15-30 in carnivore species. In this study, this length was measured as 19 ± 2 cm for martens.

Lungs (Pulmones)

Getty (1975) and Dursun (2006) reported that the color of the blood drained the lungs could change from pink to orange according to the blood content. They also stated that when the lung is full with blood, its color was dark red, in addition, the carnivore lung had a flat surface. In marten of this study, the color of lungs was dark red-brown and its surface was flat. Getty (1975) stated that in cats and dogs, the pulmo dexter was consisted of four lobes which were lobus cranialis, lobus medius, lobus caudalis, and lobus accessorius and the pulmo sinister was consisted of two lobes: cranial and caudal. In the martens of the present study the lungs have the similar number of lobes as in cat

and dog. Getty (1975) and Dursun (2006) reported that lungs were divided into lobes by interlobar fissures (fissura interlobares) and these fissures were quietly deep in carnivores. In parallel with this information, the fissura interlobares in martens were deep and lobes were significantly distinct from each other (This piece of information was not mentioned in the results and was added there).

The study involves some limitations. Due to the fact that martens are wild animals, the lack of materials can be considered as a limitation. Since animal materials were arrived as dead, histological examination could not be performed. Also, owing to the fact that the lack of literature about some species in the same family (mink, badger, etc.), gives no chance to compare with animals in the same order could be regarded as a limitation of the study.

Conclusion

In conclusion, larynx, trachea and lungs of the martens were described macroscopically. The larynx was similar to the cat in felidae family; whereas, the trachea and lung were similar to canidae. It is expected that the information set forth regarding martens would address the lack of literature in this area.

References

Bahadır, A. and Yıldız. H. (2005): Veteriner Anatomi II -İç Organlar-. Ezgi Kitabevi, Bursa.

Dursun, N. (2006): Veterinary Anatomy II. Medisan Yayınevi, Ankara.

Dyce, K.M., Sack, W.O., Wensing, C.J.G. (2002): Textbook of Veterinary Anatomy. Third Edition, Saunders, Philadelphia.

Evans, H.E. and Christensen, G.C. (1993): Miller's Anatomy of the Dog. Third Edition. WB Saunders Company, Philadelphia.

Evans, L. (2010): Guide to the Dissection of the Dog. Seventh Edition, WB Saunders Company, Philadelphia, pp: 103.

Getty, R. (1975): Sisson and Grossman's The Anatomy of

Domestic Animals (Volume 2). Fifth Edition, pp: 1562-1575, W.B. Saunders Company, Philadelphia.

International Committee on Veterinary Gross Anatomical Nomenclature ICVGAN (2012): Nomina Anatomica Veterinaria. Hannover, Columbia, Ghent, Sapporo, (29.09.2015).

ITIS (2015): Integrated taxonomic information system *Martes foina*, (Erxleben 1777).

König, H.E., Liebich, H.G. (2007): Veterinary Anatomy of Domestic Mammals Textbook and Colour Atlas. Third edition. Schattauer GmbH, Stuttgart, Germany.

Pasquini, C., Spurgeon, T., Pasquini, S. (2003): Veterinary Anatomy of Domestic Animals Systematic and Regional Approach. Tenth Edition. Sudz Publishing, United States.

Corresponding Author:

yasindemiraslan@hotmail.com

Tel : +90 248 2132162

Fax : +90 248 2132001

Mehmet Akif Ersoy University, Faculty of Veterinary Medicine, Department of Anatomy 15030, Burdur, Turkey

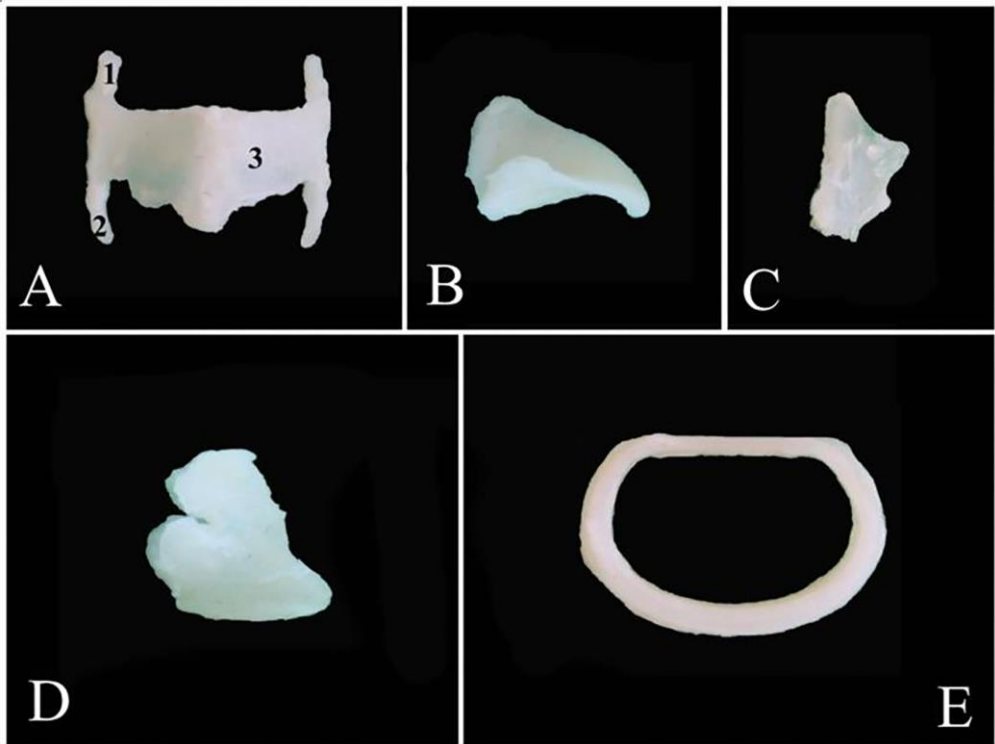


Fig (1): Larynx cartilages and transverse sections of cartilago trachealis. A: Cartilago thyroidea, 1. Cornu caudale, 2. Cornu rostrale, 3. Lamina thyroidea, B: Cartilago epiglottica, C: Cartilago arytenoidea, D: Cartilago cricoidea, E: Cartilago trachealis (the upper 1/3)

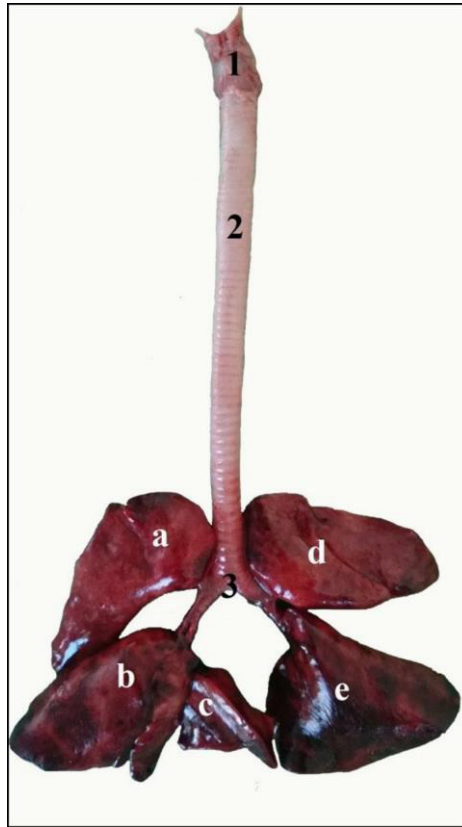


Fig (2):The dorsal image of the larynx, trachea and lung in marten. 1. Larynx, 2. Trachea, 3. Bifurcatio trachea, a. Lobus cranialis pulmonis dextri, b. Lobus caudalis pulmonis dextri, c. Lobus accessorius pulmonis dextri, d. Lobus cranialis pulmonis sinistri, e. Lobus caudalis pulmonis sinistri

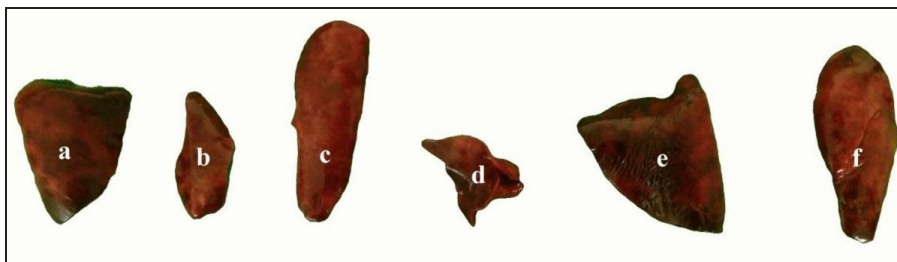


Fig (3): The image of the separated pulmonary lobes (lobus pulmonis). a. Lobus caudalis pulmonis dextri, b. Lobus medius pulmonis dextri, c. Lobus cranialis pulmonis dextri, d. Lobus accessorius pulmonis dextri, e. Lobus caudalis pulmonis sinistri, f. Lobus cranialis pulmonis sinistri.

Animal species in this Issue

Martens (*Martes foina*)



Kingdom: Animalia & Phylum: Chordata & Class: Mammalia & Order: Carnivora & Suborder: Caniformia & Family: Mustelidae & Subfamily: Mustelinae, Genus: ***Martes*** & Species: ***N. foina***

The **beech marten** (*Martes foina*), also known as the **stone marten**, **house marten** or **white breasted marten**, is a species of marten native to much of Europe and Central Asia, though it has established a feral population in North America. While the pine marten is a forest specialist, the beech marten is a more generalist and adaptable species, occurring in a number of open and forest habitats.

The beech marten has a somewhat longer tail, a more elongated and angular head and has shorter, more rounded and widely spaced ears. Its nose is also of a light peach or grey colour, whereas that of the pine marten is dark black or greyish-black.

the beech marten moves by creeping in a polecat-like manner, whereas the pine marten and sable move by bounds. The beech marten's fur is coarser than the pine marten's, with elastic guard hairs and less dense underfur. Its summer coat is short, sparse and coarse, and the tail is sparsely furred. The colour tone is lighter than the pine marten's. Unlike the pine marten, its underfur is whitish, rather than greyish. The tail is dark-brown, while the back is darker than that of the pine marten.

Source: Wikipedia, the free encyclopaedia

Morphological and Craniometric Features of the Skull of African Savanna Hare (*Lepus microtis*) Found in North-Central Nigeria

Fatima O. Oyelowo¹, Ifukibot I. Usende^{1*}, Idris A. Azeez² and Abdulsalam E. Aminu¹

¹*Department of Veterinary Anatomy, University of Abuja, Federal Capital Territory, Nigeria

²Department of Veterinary Anatomy, University of Jos, Plateau state, Nigeria

With 6 figures & one table

Received August, accepted for publication September 2017

Abstract

African savanna hare (*Lepus microtis*) belonging to the family *Leporidae*, is a placental mammal with vast economic and scientific importance ranging from the major source of protein for the teeming population to models of laboratory and genetic studies as well as valued game reserve. The aim of this study was to investigate the morphology and craniometric features of the skull of African savanna hare found in North-central Nigeria in an attempt to provide basic anatomical data of this wild rodent. The African savanna hare used were sampled from Gwagwalada area council, Federal capital territory, Abuja, Nigeria. Morphological and craniometric measurements were conducted on six skulls. Results

showed a foramen on the nasal bone and a non-serrated lateral margin of the margo supraorbital process of the frontal bone. The maxilla was trabeculated while the temporal bone was spongy-like in appearance. The palatine appeared perforated in a W-shape. For craniometric results, the skull weight was 13.4g with the mandible and 9.5g without the mandibles. While the dorsal and ventral skull length was 10.5 ± 0.8 and 7.3 ± 0.9 , the dorsal and ventral skull width was 3.1 ± 0.2 and 4.0 ± 0.2 with a dorsal and ventral skull index of 29.52 and 54.79 respectively. The orbital and cranial capacities were 5.8 ± 0.6 and 11.2 ± 0.4 , and this could aid the vision and intelligence of this rodent. Our findings have provided baseline information on the skull morphology

and craniometrics of the African savannahare, which would be of benefit in understanding morphofunctional and paleontological studies with emphasis on adaptive features necessary for domestication of this rodent.

Keywords: Morphology, Morphometrics, Orbits, Peculiarities, *Lepus microtis*, Cranial and Facial.

Introduction

African Savanna Hare (*Lepus microtis*) belongs to the family *Leporidae* and order *Lagomorpha* (Kryger et al., 2004). They are placental mammals' varying in size from small to medium sized (Chapman and Flux, 1990; Mengoni, 2011). They are generally herbivorous and long eared and constitute the base of many predator-prey interactions (Chapman and Flux, 1990; Mengoni, 2011). They are fast runners and although they typically live solitarily, can shift hundreds of kilometres in response to environmental changes or in search of food (Kryger et al., 2004).

African Savanna hares have been reported to be of economic and scientific importance due to their role as a major food source of protein, a model of laboratory animals, valued game reserve and can provide scientific insight into entire trophic systems (Chapman and Flux, 2008).

Also serve as a model for population genetics (Alves et al., 2008). Recently, they have been seen as the subject of numerous international translocation (Moores et al., 2012) and traditional medicine for curing nearly 11 different ailments including diarrhoea, stomach ache, burns and wound (Magige, 2015).

Moores and Brown (2013) emphasized the need for research by both professionals and amateur biologists on this rodent as its identification has posed problems. In Africa, different species of hares have been identified based on their morphological traits (Suchentrunk et al., 2006; Palacios et al., 2008) such as body size, ratio of width of mesopterygoid space to minimum length of the hard palate, teeth features and quantity of black coloration in the ear (Kingdon, 2013). Basically, the basis for its identification despite the conspecific report on their taxonomy and distribution globally (Petter 1959; Slimen et al., 2005; Slimen et al., 2008) is the obvious russet area on the nape of the neck and its more coloured and roughed fur (Moores et al., 2012) but no particular emphasis has been placed on the skull morphology; a good anatomical area of species identification and to the best of our knowledge is non-existent in the literature.

The aim of the present study, therefore, was to investigate the skull

morphology and morphometry of the African savanna hare in an attempt to contribute to information in this emerging field of anatomical studies of this wild rodent.

Materials and Methods

Six (four males and two females) African Savanna hares were used for this study. They were live-trapped at Gwagwalada area council, Federal Capital Territory, Abuja, North central Nigeria. A veterinarian physically examined all the hare, and there was no osteological deformity. Ethical approval was obtained from Animal Care and Use Committee of the University of Abuja, Nigeria. Animals were transported in metal cages to the Department of Veterinary Anatomy, University of Abuja and immediately euthanized by lethal intraperitoneal injection of xylazine (10mg/kg) and ketamine (100mg/kg) (Usende *et al.*, 2016) and thereafter the heads were collected by cutting at the atlantooccipital joint. The heads were then processed, and skulls were prepared using cold water maceration techniques described by Ekeolu *et al.*, (2016) and Tahon *et al.*, (2013) with some modification. Briefly, the heads were soaked in cold water with ammonium solution and sodium hydroxide overnight to remove grease and soften the connective tissues and muscular attachment on

the bones. The solution was changed daily for seven days. Extraneous tissues on the bones were picked using thumb forceps, after brushing the muscle fibers and connective tissues attached to the bones with sponges (Ekeolu *et al.*, 2016). The bones were then washed in 0.5% sodium hypochlorite solution (bleach) for 24hours and removal of any remaining muscles and ligaments was done. The skulls were left in the above solution for two changes of 3 hours each and then left to dry in sunlight. Specimens were photographed using Olympus digital camera (FE-360). Digital venire caliper, ruler and thread were engaged in taking the linear measurement of the various parts of the skull bones and mandible to the nearest 0.01centimeters. All parameters measured were as described by Sarma (2006) and Saber and Gummow (2014).

1. Skull length (SL): taken as the distance between the highest point of the parietals to the middle of the rostral margin of the incisive bone. This was taken at the dorsal and ventral views and recorded as dorsal skull length and ventral skull length respectively.
2. Skull width (SW): taken as the distance between the two zygomatic arches. This

- was taken at the dorsal and ventral views and recorded as dorsal skull width and ventral skull width respectively.
3. Cranial length (CL): taken as the distance from the central point of the fronto-nasal suture to the middle point of the nuchal crest.
 4. Cranial width (CW): taken as the maximum distance between the highest points of the parietal bones.
 5. Facial length (FL): taken as the distance from the fronto-nasal suture to the centre of the incisive bone.
 6. Facial width (FW): taken as the distance between the caudal extents of the orbital rims.
 7. Mandibular length: taken as the distance between incisor and caudal border of the mandible
 8. Mandibular height: taken as the distance between the highest point of the coronoid process to the base of the mandible
 9. Skull weight with mandibles (SWM) and Skull weight without mandible (SWWM) was taken using sensitive bench top scale (LP 502A, China; with sensitivity of 0.1 to 5kg).
 10. Orbital capacity (OC): all foramina opening into the orbital cavity were plugged with plasticine, and the cavity filled with rice grains to the orbital rim and then contents emptied into a measuring cylinder.
 11. Cranial capacity (CC): similar to the orbital capacity, all foramina opening into the cranial cavity were plugged with plasticine, and the cavity was filled with rice grains and then content emptied into a measuring cylinder.
 12. Orbital height (OH): taken as the perpendicular distance between the supraorbital and infra-orbital margins of the orbit.
 13. Orbital width (OW): taken as the horizontal distance between the rostral and caudal margins of the orbital rim.
 14. Foramen magnum width (FMW): taken as the maximum distance between the mid lateral (horizontal) boundaries of the foramen magnum.
 15. Foramen magnum height (FMH): taken as the maximum distance between the mid vertical boundaries of the foramen magnum.
 16. Length of margo supraorbital (LMS): taken as the distance between the rostral and caudal extent of the margo supraorbital for the frontal bone.

17. Width of margo supraorbital (WMS): taken as the distance from most lateral to most medial of the margo supraorbital of the frontal bone. This was taken at three points: Rostral (RMS), Middle (MMS) and caudal (CMS).
18. For the skull, cranial, orbital and facial indices, the equation of Miller *et al.* (1964) was used and are given below:
 - a. Skull index = skull width/skull length X100
 - b. Cranial index = cranial width/cranial length X100
 - c. Orbital index = orbital width/orbital length X100
 - d. Facial index = facial width/facial length X 100
 - e. Foramen magnum index = foramen width/foramen height X 100

Statistical analysis

All numerical data generated from the craniometric studies were analyzed using Graph Pad prism version 6.0 (GraphPad Software, Inc., La Jolla, CA, USA) and presented as mean \pm standard deviation.

Results

The skull consists of the cranial bones, facial bones and hyoid apparatus. The cranial and facial bones give boundaries to the cranial and

nasal cavities respectively. The bones are either paired or unpaired and thus described as follows:

Os occipital (Occipital bone)

The occipital makes up the boundary that completely encircles the foramen magnum (passage of spinal cord) at the most caudal part of the skull. The supra-occipital or squamous part of the occipital (Fig 1/1) forms the dorsal boundary; the flat basioccipital (Fig 1/3) forms the ventral boundary while the exoccipital (Fig 1/2) forms the lateral boundary. The supra-occipital is a flat butterfly-like bone bearing a distinct nuchal crest (Figs 1/5, 2/20, 3/2) about its middle. It is fused with the interparietal (Fig 1/9) and paired parietal (Fig 1/10) rostrally forming both internal and external protuberances (Figs 1/6, 3/3). The external protuberance fuses with the nuchal crest.

The exoccipital flanks the foramen magnum on either side dorsally and ventrally, it bears two distinct occipital condyles (Fig 1/8) that articulate with the wings of the atlas. Lateral to these condyles are distinct jugular processes (Figs 1/7, 3/5). The hypoglossal fossa is located between each condyle and the jugular process bearing two hypoglossal canals (Fig 3/6).

The basilar part (basioccipital) (Figs 1/3, 3/10) is slightly shallow and

wide. It fuses with the laterals on either side and with the basisphenoid (Fig 3/11) rostrally.

Os basisphenoidale & Os Pre-Sphenoidale (Sphenoid bone)

The unpaired sphenoid bone is medially located and divided into two parts; the basisphenoid (Fig 3, 11) and presphenoid (Fig 3/14) which are separated by a distinct fissure.

Dorsally, the wide basisphenoid bears a slightly shallow longitudinal depression, which is continuous with the basioccipital. It also bears a cranio-pharyngeal canal (Fig 3/13) that opens into the hypophyseal fossa. Ventrally, it bears two distinct ridges that taper rostrally towards the presphenoid bone. The presphenoid is much narrower, triangular and thickened caudally. Both basi- and presphenoid bear alasphe-noids and orbitosphenoid respectively, which are wing projection from the body that extends into the caudal border of the orbital wall. An orbital foramen is located between the two wings. The alasphe-noid fuses with the frontal bone and pterygoidhamulus of the pterygoid bone. The orbitosphenoid is fused with the frontal bone dorsally, ethmoid cranially and palatine ventrally. The ethmoid foramen (Fig 4/27) is situated at the frontosphenoid suture.

Os parietale (Parietal bone)

These are paired flat bones (Figs 1/10, 2/3, 4/18) that make up the dorsal boundary of the cranial cavity and unite at the midline by the interparietal suture. Slightly convex in shape, it forms a fusion with the frontals and squamous part of temporal laterally on either side. Caudally it fuses with the interparietal and occipital bones.

Os interparietale (Interparietal bone)

These are two tiny oval plates (Figs 1/9, 2/18, 4/20) situated between the parietals, squamous and lateral parts of the occipital bones. It is slightly spongy in nature.

Os frontale (Frontal bone)

The frontal bone (Figs 1/13, 2/2,) is made up of narrow, long pair of bones making up part of the dorsal wall of the cranial cavity. It fuses with the parietals caudally. It is made up of two parts: the slightly convex horizontal plate and a vertical plate. The margo supraorbital (Figs 1/14, 2/7, 3/20, 4/14) located on the lateral margin of the horizontal plate extends rostrally and caudally over the orbit forming the rostral (Fig 2/10, 4/15) and caudal (Figs 2/11, 4/16) supraorbital incisures and processes respectively against the frontal bone. The caudal incisura is twice the length of the rostral one. Rostrally, the nasal processes

(Fig 4/17) of the frontal bone fuse with the paired nasal bones (Figs 2/1, 4/1). The shape of the nasal processes of either side ends at an angle forming an isosceles triangular shape. Furthermore, the frontal bone bears a thin lateral process.

Orbita (Orbits)

These are incomplete circular bony structures located on either side of the skull about its middle. It consists of frontal on its dorsal boundary, ethmoid as its rostromedial surface, alaspheoid and orbitospheoid forming the mediocaudal surface. The temporal (Figs1/15, 4/19) forms the caudal surface, while the zygomatic arch (Fig 4/35) makes up the lateral boundary. The lacrimal (Fig 4/13) forms the proximal rostral boundary while the maxillary tuber (Fig 4/8) forms the distal rostral boundary.

A pterygopalatine fossa is present between the orbital median surface and the maxillary tuber. This fossa bears three foramina namely: the most proximal maxillary foramen which leads to the infraorbital canal, the sphenopalatine foramen that leads to the nasal cavity and the caudal palatine that leads into the palatine canal

The two orbits are separated by a thin median bony septum. The rostral part of the bony septum bears a

large optic foramen (Fig 4/28) through which the two orbits communicate.

Os lacrmale (Lacrimal bone)

These form the rostral boundary of the orbit on its proximal end. These are paired small, thin bones bearing a nasolacrimal foramen (Fig 4/12) that leads into the nasolacrimal canal for passage of lacrimal duct from the gland. Above the foramen is the laterally situated lacrimal hamulus.

Os temporale (Temporal bone)

This is a paired bone located between the parietal dorsally, rostrally with frontal and sphenoid ventrally. It has four parts: the squama, mastoid, tympanic and petrous. The squama is bordered by the squamous occipital dorsocaudally and the other 3 parts. The squama is irregular in shape, contributing most to the lateral wall of the cranial cavity. Rostrally it gives out a zygomatic process (Fig4/31) forming the lateral wall of the orbit. The ventral part of this process bears a mandibular fossa to which the condyle of the mandible articulates. A small tubercle projects above the zygomatic process.

Ventral to the squama is the mastoid part (Fig 4/30) that is spongy-like in appearance. It is attached to

the occipital caudally and tympanic part of temporal distally. Ventral part of the temporal bone bears the bulbous tympanic bulla (Figs3/7, 4/25) that gives exit to the external acoustic meatus (Figs1/11, 2/15, 4/24), which is a short tube-like structure. The retrotympanic process (Fig 4/22) is located dorso-caudally to the base of the external acoustic meatus. Ventral to this is the styloid process. The petrosal part is behind the mastoid part, and the small jugular process is located about the middle and ventral border of the bulla respectively. The large prominent carotid canal is situated at the ventromedial part of the bulla towards the basisphenoid.

Os ethmoidale (Ethmoid bone)

This bone forms the rostral and caudal boundaries of the cranial and nasal cavities respectively. It bears a sieve-like cribriform plate and a perpendicular plate. The olfactory nerves emanating from olfactory bulb of the brain pass through the cribriform plate, while the bony nasal crest makes up the perpendicular plate. A narrow crista galli divides the cribriform plate into 2 parts. The plate also bears scattered large foramina. The perpendicular plate forms the caudal nasal septum in conjunction with the vomer bone (Fig 3/15).

Turbinates bones

These are scroll-like bony plate projections in the nasal passage from the cribriform plate of ethmoid that projects rostrally.

Os nasale (Nasal bone)

These are paired bones located rostrally to the frontals and elongated rostrally. Each nasal bone is fused with the frontal caudally and the nasal process of the incisive (Figs2/4, 4/3 throughout its length laterally. Dorsally the bone is smooth horizontally and tapers or declines ventrally midway of its length. About 2/3 the length, it bears a nasoincisive notch which is slightly convex lateroventrally. This notch bears a foramen (Fig4/29). Rostrally, the nasals end as a curved shape to conform to the nasal openings. The openings are divided into two halves by a median cartilaginous nasal septum that extends caudally to meet the ethmoid bone.

Os incisivum (Incisive bone)

The incisive bones (Figs 3/28, 4/2) are paired bones that make up the most rostral aspect of the skull. It presents a body, two surfaces and three processes. The palatine surface is slightly concave while the labial surface is slightly convex. The nasal process (Fig 4/3) is long, thin and does not fuse with the nasal and maxillary bones (Fig 4/4). How-

ever, it makes up part of nasal cavity lateral wall. The palatine process (Fig 3/28) is very much thinner and fuses with the other rostrally only, close to the incisor teeth and further fuse again towards the first premolar. The alveolar process (Fig 3/32) is very short. Each alveoli process bears alveolar sockets for four incisor teeth with 2 being most rostral.

Maxilla

The upper jaw is mainly made up of the paired maxilla (Fig 4/4). The body bears two surfaces, which present a trabeculae-like appearance made up of numerous foramina lateromedially. The infraorbital foramen (Fig 4/7) is situated amongst the foramina at the base of the zygomatic arch. Immediately behind the foramen is the zygomatic process (Fig 4/9) of the maxilla, which bears a prominent facial crest. The medial surface is concave dorsoventrally forming part of the nasal cavity wall. The thin dorsal border fuses with the nasal process of incisive and lateral process of frontal bones while the thick, strong ventral border is somewhat straight and smooth. The latter extends caudally and widens mediolaterally as the alveolar process (Fig 4/33) to accommodate the alveolar canals for the two premolar and four molar teeth.

A narrow bony palatine process of the maxilla (Fig 3/26) is situated rostrally to the horizontal plate of the palatine (Fig 3/18). Both the maxilla and palatine fuses together to form part of the hard palate.

The maxilla extends caudally towards the orbit to form a medial maxillary tuber (Fig 4/8) and a lateral facial tuber (Fig 4/6). The maxillary tuber is thick and wide rostrocaudally as it presents a pterygopalatine fossa against the orbital median surface.

The facial tuber is very small, fuses with the temporal process of zygomatic (Fig 1/12) bone to form the zygomatic arch alongside the zygomatic process of temporal bone (Fig 4/31).

Os zygomaticum (Zygomatic bone)

The zygomatic bones (Fig 4/11) are two small bones that make up part of the lateral boundary of the orbit. It has two surfaces, the flat orbital and concave malaris surfaces. It fuses with the maxilla by its zygomatic process rostrally and the zygomatic process of the temporal bone caudally. The suture line between the bones is fused. The temporal process of the zygomatic bone runs caudally towards the zygomatic process of temporal bone. The temporal process has a projection (Fig

4/32) caudally at the end of the zygomatic arch.

Os palatinum (Palatine bone)

The paired palatine has both perpendicular part (Fig 3/17) and horizontal part (Fig 3/18). The horizontal part forms the caudal hard palate at which the soft palate attaches. It also bears the major palatine foramen (Fig 3/27), which is rostral and minor palatine foramen. The perpendicular part in conjunction with basisphenoid and pterygoid process makes up the dorsal and lateral walls of the nasopharyngeal meatus, choanae (Fig 3/19) and nasal cavity opening into the nasopharynx. The rostral part of this plate overlaps the alveolar process of the maxillae. The caudal part forms 2 lateral processes of which the external process overlaps the pterygoidhamulus, and the internal process overlaps the pterygoid process of sphenoid bone.

Os pterygoideum (Pterygoid bone)

These are paired, tiny bony plates between the palatine rostrally and the sphenoid caudally. It is made up of the squamous part and pterygoid hamulus. The squamous part is convex and makes up part of the lateral and ventral walls of the cranial cavity. It is located caudally and fuses with the tympanic bulla of the

temporal bone. It also fuses with the pterygoid process of sphenoid bone. It forms the Pterygoid hamulus, which is a thin hook-shaped process on its free margin. This makes up pterygoid fossa between the two laminae of the bone.

Vomer

This is a thin single bony plate that makes up the ventral part of the nasal septum. It is a bent arch, located rostrally at the palatine process sulcus and caudally at the rostral margin of presphenoid bone.

Mandibula (Mandible)

This makes up the lower jaw (Fig 5). It consists of two halves, each made up of a body (Figs 5/1, 5/2) and a vertical ramus (Fig 5/3). The thick body can be subdivided into rostral and caudal parts. The rostral incisive part (Fig 5/1) is convex on its labial surface (Fig 5/7) and concave on its lingual surface. The most rostral part bears alveolar sockets for the incisor pair of teeth. The molar caudal part bears sockets on its dorsal border to accommodate the roots of the five cheek teeth (Fig 5/18) and a small oval mandibular foramen.

The molar part (Fig 5/2) bears a mandibular foramen on its lingual surface, which is continuous cranially toward the incisive part and exit as the mental foramen (Fig 5/13),

which is made up of two openings. Pitted small numerous foramina (Fig 5/10), which are numerous and also seen in this region.

The thin, flat, vertical ramus bears masseteric (Fig 5/4) and pterygoid fossae on the lateral and medial surfaces respectively. Caudal to the body and ventral to the ramus is the rounded angle of the mandible (Fig 5/15). Proximal to this is the angular process (Fig 5/16), which bears a sharp pointed edge. Proximal to the angular process is a wider edge called the condyloid process (Fig 5/9) where the TMJs are situated. Mandibular notch (Fig 5/6) separates the condyloid process from a rostral smaller coronoid process (Fig 5/5).

Morphometrics

Some of the morphometric parameters taken are represented in figure 6 and the results of the morphometric measurements are presented in table 1. The dorsal skull length was 10.5 ± 0.8 while the ventral was 7.3 ± 0.9 . The dorsal width of the skull was 3.1 ± 0.2 whereas the ventral was 4.0 ± 0.2 . On the other hand, the cranial length and width were 7.1 ± 0.4 and 3.5 ± 0.1 respectively while the facial length and width were 3.3 ± 0.2 and 3.2 ± 0.1 respectively. Orbital height and width were 3.4 ± 0.3 and 2.8 ± 0.3 respectively.

Discussion

We report that the skull of African savanna hare (*Lepus microtis*) consists of the cranial bones, facial bones and hyoid apparatus. Similar findings have been documented for the domestic rabbit (*Oryctolagus cuniculus*) (Farang *et al.*, 2012).

Concerning the occipital bone of the African savannah hare, four parts were observed in this study; supraoccipital, basioccipital and two exoccipital similar to reports of Farang *et al.*, (2012) and Crabb (1931) in domestic rabbit. Again we reported a notched foramen magnum corroborating the work of Farang *et al.*, (2012). The supraoccipital is a flat butterfly-like bone. However, the condyles and jugular process are typical of other mammals (Shawulu *et al.*, 2011).

For the basisphenoid, we observed a perforated rostrorhynchogaleal canal that opens into the hypophyseal fossa (Sisson and Grossman 1975, Shawulu *et al.*, 2011). This observation is consistent with that of domestic rabbit Farang *et al.*, (2012). However, while the canal was centrally located in the domestic rabbit, we observed a lateral located canal in the African savannah hare. The hypophyseal fossa accommodates the hypophyseal gland (Sisson and Grossman 1975; Shawulu *et al.*, 2011).

Our observations on the parietal bone simulate the report of Farag *et al.*, (2012) in domestic rabbit and lack the zygomatic process. Earlier, Shawulu *et al.* (2011) suggested that prominence of the interparietal suture could predispose to fracture. This is a possibility in the African savanna hare. The parietal bone also bears a smooth external surface, which is in line with the findings of Cabon-Raczynska, (1964). The interparietal bone on the other hand composed of slightly spongy two bony plates. This simulates the findings of Cabon-Raczynska, (1964) in the European hare as being porous in structure.

On the frontal bone, we observed a non-serrated margin of the margo supraorbital process in African savanna hare skull. Although Farag *et al.*, (2012) observed this feature in domestic rabbit, to be serrated. In addition, the caudal incisura is twice the length of the rostral one. Our observation on museum specimen of the skull of other domestic mammals used during Veterinary anatomy practical showed the absence of this incisura.

The orbits of African savanna hare are similar to that described by Farag *et al.*, (2012) for the domestic rabbit. The thin median bony sep-

tum observed that separate the two orbits could be a point of fracture in this species.

The mastoid part of the temporal bone presents spongy-like appearance at the ventrolateral part, which also forms the part of the cranial cavity. This has not been reported in domestic mammals. A large prominent carotid canal was also observed on the temporal bone of the skull of African savanna hare that simulates the work of Farag *et al.*, (2012) for the domestic rabbit.

Our study of the nasal bone showed a foramen on the naso-incisive notch. This foramen has not been reported in domestic and wild animals. We venture to call it nasal foramen (of Oyelowo and Usende).

It was observed in this study that the nasal process of incisive bone does not fuse with the nasal and maxillary bones as in other domestic species. The zygomatic bone was also observed to have a flat orbital and concave malaris surfaces. Although it simulates the study of Cabon-Raczynska, (1964), this is different from other domestic species.

Morphometric data are useful for the theoretical importance of functional

morphology as well as either absolute or relative size of particular interest (Saber and Gummow 2014), and we present for the first time, data on the morphometrics of the African savanna hares. In our report, the dorsal and ventral skull index of the African savanna hare were 29.52 and 53.79 respectively. Saber and Gummow (2014) showed the skull index of koala, wombat and wallaby to be 48.78, 111.21 and 74.75 respectively. Although their study only looked at the dorsal skull index, comparing their report with our present report of 29.52 for dorsal skull index, this was relatively lower compared to the report of Saber and Gummow (2014). Similarly, we reported a facial index of 96.97 for the African savanna hare while Saber and Gummow (2014) reported 186.11, 175.24 and 114.29 for koala, wombat and wallaby respectively.

Concerning the cranial capacity, Saber and Gummow (2014) reported 20.0 ± 2.4 , 61.7 ± 11.8 and 33.5 ± 37 for koala, wombat and wallaby respectively. Earlier, Sarma (2006) showed the cranial capacity of akagani goat to be 113 while Yahaya *et al*, (2012) reported 487.92 ± 7.55 for one hump camel. Interestingly, Hajnis (1962) stated that skull capacity is in no way dependent on the form of the skull. However, in

koala, about 40% of the cranium is filled with cerebrospinal fluid (Saber and Gummow, 2014). In the Wombat, the cranial index has been reported to be 50.961 (Saber and Gummow, 2014). This is higher than the 46.67 reported in our work for African savanna hare.

Brain capacity/size in relationship to intelligence in school children (Estabrooks, 1928) and animals (Hicks and Dougherty, 2013) have been studied and in wombats and wallabies could reflect their intelligence for getting food and water, managing territory, offences and in defence (Saber and Gummow, 2014).

Our findings have provided baseline information on the skull morphology and morphometrics of the African savanna hare, which would be of benefit in understanding morpho-functional and paleontological studies with an emphasis on adaptive features necessary for domestication of this rodent.

References

Alves PC, Melo-Ferreira J, Freitas H, Boursot P (2008): The ubiquitous mountain hare mitochondria: multiple introgressive hybridization in hares, genus *Lepus*. *Philosophical transactions of the Royal Society of London. Series B, Biological sciences*, 363: 2831–2839.

- Cabon-Raczynska K (1964):** Studies on the European Hare. III. Morphological variation of the skull. *Actatheriologica* 9(17): 249-285
- Chapman JA, Flux JEC (1990):** Rabbits, Hares and Pikas. Status Survey and Conservation Action Plan. IUCN/SSC Lagomorph Specialist Group, Gland, Switzerland.
- Chapman JA, Flux JEC (2008):** Introduction to the Lagomorpha. In *Lagomorph Biology*. Springer Berlin Heidelberg, Germany. Pg. 1-9.
- Crabb, E.D. (1931):** Principles of functional anatomy of the rabbit. P. Blackstone's son & co., Inc., 1931.
- Ekeolu OK, Usende IL, Adejumobi OA, Azeez AI, Orolu-Adedeji MO. (2016):** Comparative morphometric study of the right and left pectoral and pelvic bones of cattle egret (*Bubulcus ibis*). *Inter J Vet Sci*, 5(4): 285-289.
- Estabrooks GH (1928):** The relationship between cranial capacity, relative cranial capacity and intelligence in school children. *Journal of Applied Psychology*, 12(5): 524-529
- Farag FM, Daghsh SM, Mohamed EF, Hussein MM, and Hagrass SM (2012):** Anatomical studies on the skull of the domestic rabbit (*Oryctolagus cuniculus*) with special reference to the hyoid apparatus. *J. Vet Anat.* 5(2):49-70
- Hajnis K. (1962):** Evaluation of different methods of calculation of skull capacity for lineal measurements. *Ceskolov. Merfol.*, 10: 220-233
- Hicks K, Dougherty M. (2013):** Finding the intelligence of an animal. Field study presented to STEM Teacher Academy, Rider University. <http://riderstem.weebly.com/cranial-volume-intelligence.html>
- Kingdon J. (2013):** Mammalian evolution in Africa. In: Kingdon JS, Happold D, Hoffmann M et al (Eds.), *The Mammals of Africa, Introductory chapters and Afrotheria*, Bloomsbury, Amsterdam, 1:75–100
- Kryger U, Robinson TJ, Bloomer P (2004):** Population structure and history of southern African scrub hares, *Lepussaxatilis*. *Journal of Zoology*, 263: 121–133.
- Magige FJ. (2015):** Traditional medicinal uses of small mammal products: a case study of the African savannah hares, crested porcupines and rock hyraxes in Serengeti District, Tanzania. *Tanzania Journal of Science*. 14(1): 64-71
- Mengoni C. (2011):** Phylogeny and genetic diversity of Italian species of

hares (genus *Lepus*) PhD thesis. Università di Bologna, Bologna.

Moores R, Brown D. (2013): African Savannah Hare *Lepusmircrotis* near Tantan – a new mammal species for North Moroccan Atlantic Sahara. *Go-South Bulletin*, 10: 263-265

Moores, R, Brown D, Martin R, Lees AC. (2012): Status and identification of hares *Lepus* sp. in Western Sahara and Southern Morocco *Go-South Bulletin* 9: 126-130.

Palacios, F.; Angelone, C.; Alonso, G.; Reig, S. (2008): Morphological evidence of species differentiation within *Lepus capensis* Linnaeus, 1758 (*Leporidae, Lagomorpha*) in Cape Province, South Africa. *Mammalian Biology – Zeitschrift für Säugetierkunde*, (73): 358–370.

Petter, F. (1959): Eléments d'une révision des lièvres africains du sous-genre *Lepus*. *Mammalia* (23): 41-67.

Saber, A.S. and Gummow, B. (2014): Morphometric studies on the skull in three marsupial species (Koala, Wombat, Wallaby). *J. vet. Anat.* 7(2):117-131

Sarma, K. (2006): morphological and craniometrical studies on the skull of kagani goat (*capra hircus*) of

Jammu region. *Int. J. Morphol* 24(3):449-455

Shawulu, J.C.; Kwari, H.D.; Olopade, J.O. (2011): Morphology of the Bones of the Skull in the Sahel Ecotypes of Goats (*Capra hircus*) in Nigeria. *J. Vet. Anat.* 4(2): 1 - 13

Sisson S, Grossman JD. (1975): The Anatomy of the Domestic Animals. Vol.2, 5th ed. W. B. Saunders Company, Philadelphia.

Slimen, HB, Suchentrunk F, Memmi A, Ben Ammar Elgaaied A. (2005): Biochemical genetic relationships among Tunisian Hares (*Lepus* species), South African Cape Hares (*L. capensis*), and European Hares (*L. europaeus*). *Biochemical Genetics*.43: 11-12.

Slimen HB, Suchentrunk F, Stamatis C, Mamuris Z, Sert H, Alves PC, Kryger U, Shahin AB, Elgaaied ABA. (2008): Population genetics of cape and brown hares (*Lepus capensis* and *L. europaeus*): A test of Petter's hypothesis of conspecificity. *Biochemical Systematics and Ecology* 36(1): 22–39

Suchentrunk F, Slimen HB, Stamatis C, Sert H, Scandura M, Apollonio M, Mamuris Z. (2006): Molecular approaches revealing prehistoric, historic, or recent translocations and introductions of hares

(genus *Lepus*) by humans. *Hum Evolution* 21:151–165

Tahon RR, Ragab SA, Abdel Hamid MA, Rezk HM. (2013): Some anatomical studies on the skeleton of chicken, A PhD thesis. Anatomy and Embryology, Faculty of veterinary medicine, Cairo University

Usende IL, Leitner DF, Neely E, Connor JR, Olopade JO. (2016):

The Deterioration Seen in Myelin Related Morpho-physiology in Vanadiumexposed Rats is Partially Protected by Concurrent Iron Deficiency. *Nigeria Journal of Physiological Sciences*,31(1): 11-22.

Yahaya A, Olopade JO, Kwari D, Wiam IM. (2012): Osteometry of the skull of one-humped camels. Part I: immature animals. *IJAE*, 117: 23-33.

Corresponding author

Dr. Usende, Ifukibot Levi
Department of Veterinary Anatomy,
University of Abuja, FCT
Nigeria.
Email: ifukibot.usende@uniabuja.edu.ng

Table (1): Mean±SD of skull parameters of African savanna hare (*Lepus microtis*) found in North central Nigeria

SN	Parameter	Mean±SD
1	Skull weight with mandibles (g)	13.4
2	Skull weight without mandibles (g)	9.5
3	Dorsal skull length	10.5±0.8
4	Ventral skull length	7.3±0.9
5	Dorsal skull width	3.1±0.2
6	Ventral skull width	4.0±0.2
7	Dorsal skull index	29.52
8	Ventral skull index	54.79
9	Cranial length	7.1±0.4
10	Cranial width	3.5±0.1
11	Cranial index	46.67
12	Cranial capacity	11.2±0.4
13	Facial length	3.3±0.2
14	Facial width	3.2±0.1
15	Facial index	96.97
16	Orbital height	3.4±0.3
17	Orbital width	2.8±0.3
18	Orbital index	82.35
19	Orbital capacity	5.8±0.6
20	Length of margo supraorbital	1.9±0.2
21	Rostral distance between margo supraorbital	2.2±0.4
22	Mid distance between margo supraorbital	2.5±0.3
23	Caudal distance between margo supraorbital	3.0±0.7
24	Foramen magnum height	1.8±0.1
25	Foramen magnum width	1.9±0.3
26	Foramen magnum index	105.5
27	Mandibular length	6.0±0.9
28	Mandibular height	3.2±0.7

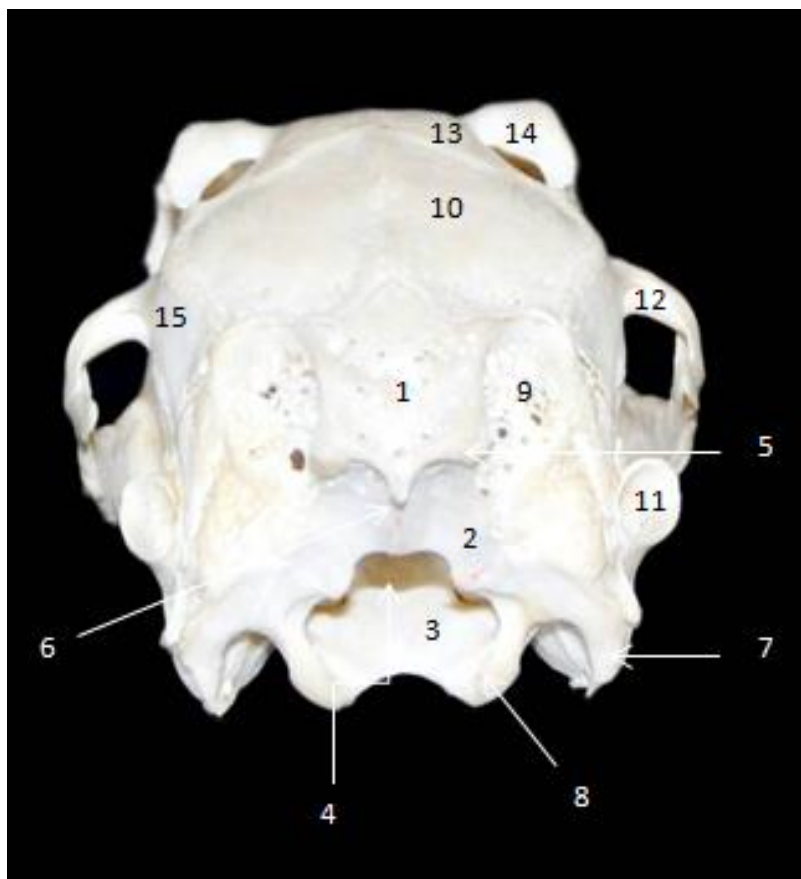


Fig (1): Dorsocaudal view of the skull of African Savanna Hare

1 Squamous part of occipital bone, 2 Exoccipital of occipital bone, 3 Exoccipital of occipital bone, 4 Basilar part of occipital bone, 5 Foramen magnum, 6 Nuchal crest, 7 External occipital protuberance, 8 Jugular process, 9 Occipital condyle, 10 Inter-parietal bone, 11 Parietal bone, 12 External acoustic meatus, 13 Temporal process of zygomatic bone, 14 Frontal bone, 15 Supraorbital process,

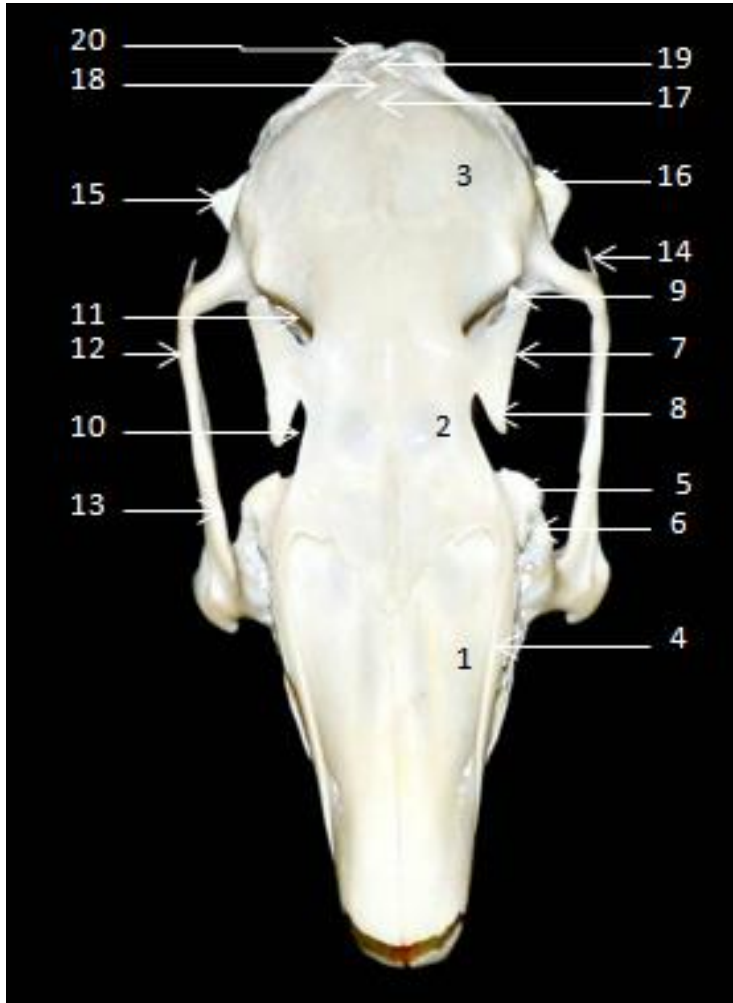


Fig (2): Dorsal view of the skull of African Savanna Hare

1 Nasal bone, 2 Frontal bone, 3 Parietal bone, 4 Nasal process of incisive bone, 5 Lacrimal bone, 6 Facial tuber, 7 Supraorbital margin, 8 Rostral branch of 7, 9 Caudal branch of 7, 10 Rostral supraorbital incisures, 11 Caudal supraorbital incisures, 12 Zygomatic process of maxilla bone, 13 Zygomatic process of temporal bone, 14 Zygomatic bone, 15 External acoustic meatus, 16 Squamous part of temporal bone, 17 External sagittal crest, 18 Interparietal bone, 19 Squamous part of occipital bone, 20 Nuchal crest

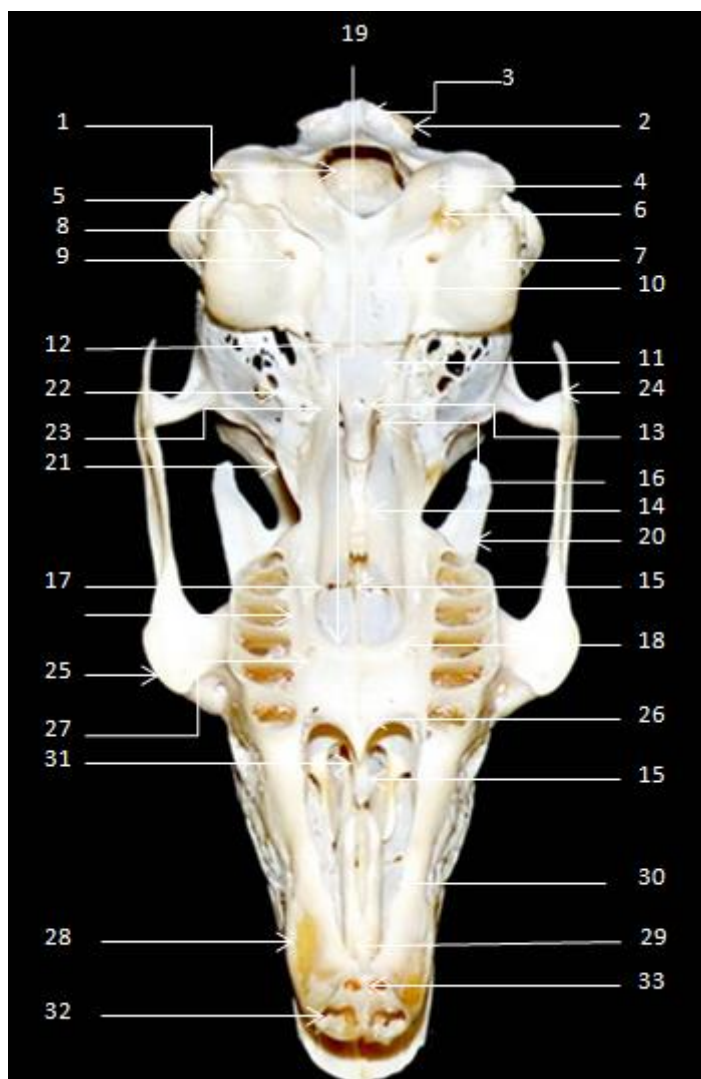


Fig (3): Ventral view of the skull of African Savanna Hare

1 Foramen magnum, 2 Nuchal crest, 3 External occipital protuberance, 4 Occipital condyle, 5 Jugular process, 6 Hypoglossal nerve canal, 7 Tympanic bulla, 8 Jugular foramen, 9 Carotid canal, 10 Basilar part of occipital bone, 11 Basisphenoid bone, 12 Basilar tubercle, 13 Craniopharyngeal canal, 14 Presphenoid bone, 15 Vomer, 16 Orbital fissure, 17 Perpendicular plate of palatine bone, 18 Horizontal plate of palatine bone, 19 Choana, 20 Supraorbital margin, 21 Pterygoid fossa, 22 Alapresphenoid, 23 Pterygoid process, 24 Zygomatic bone, 25 Facial tuber, 26 Palatine process of maxilla bone, 27 Major palatine foramen, 28 Body of incisive bone, 29 Palatine process of 28, 30 Ventral nasal concha, 31 Palatine fissure, 32 Dental part of 28, 33 Alveolar process of 28.



Fig (4): Left lateral view of the skull of African Savanna Hare

1 Nasal bone , 2 Body of incisive bone, 3 Nasal process of incisive, 4 Body of maxilla, 5 Perforated Facial surface of 4, 6 Facial tuber, 7 Infraorbital foramen, 8 Maxilla tuber, 9 Zygomatic process of 4, 10 Alveolar process of 4, 11 Zygomatic bone, 12 Lacrimal foramen, 13 Nasolacrimal bone, 14 Supraorbital margin, 15 Rostral supraorbital incisure, 16 Caudal supraorbital incisure, 17 Nasal margin of frontal bone, 18 Parietal bone, 19 Temporal bone, 20 Interparietal bone, 21 Nuchal crest, 22 Retrotympanic process, 23 Mastoid process, 24 External acoustic meatus, 25 Tympanic bulla, 26 Stylomastoid foramen, 27 Ethmoidal foramen, 28 Optical canal, 29 Nasal foramen of 1, 30 Mastoid part of 19, 31 Zygomatic process of 19, 32 Projected portion of temporal process of 11, 33 Alveolar process of 4, 34 Occipital condyle, 35 Zygomatic arch, 36 Jugular process

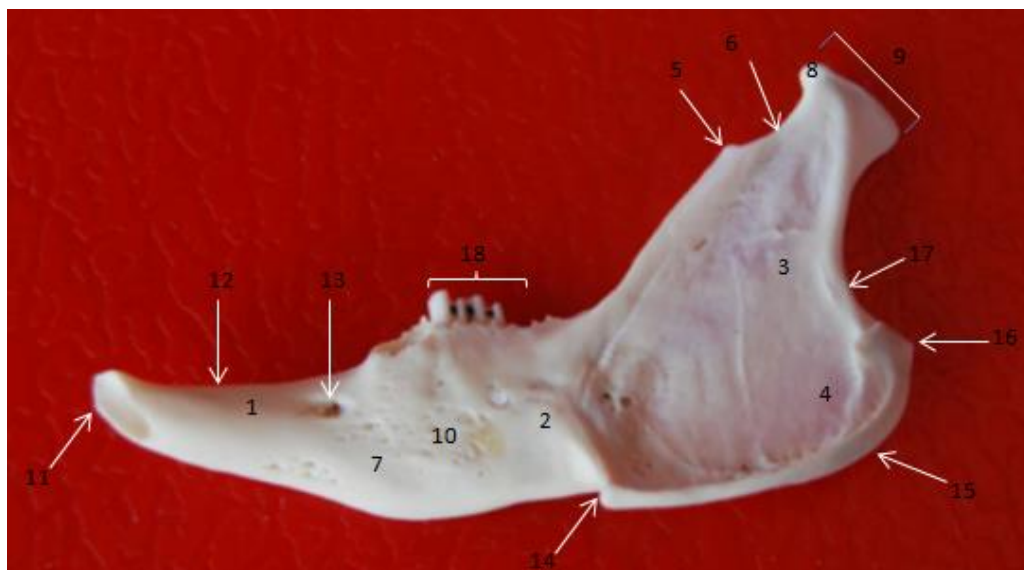


Fig (5): Lateral view of the left half of the mandible of Africana Savanna hare

1 Body of mandible- incisive part, 2 Body of mandible- molar part, 3 Mandibular ramus, 4 Masseter fossa, 5 Coronoid process, 6 Mandibular notch, 7 Labial surface, 8 Head of condyloid process, 9 Condyloid process, 10 Numerous foramina, 11 Mandibular incisure, 12 Inter-alveolar margin, 13 Mental foramen, 14 Vasorum incisure, 15 Angle of mandible, 16 Angular process, 17 Mandibular collum, 18 Premolar and molar teeth

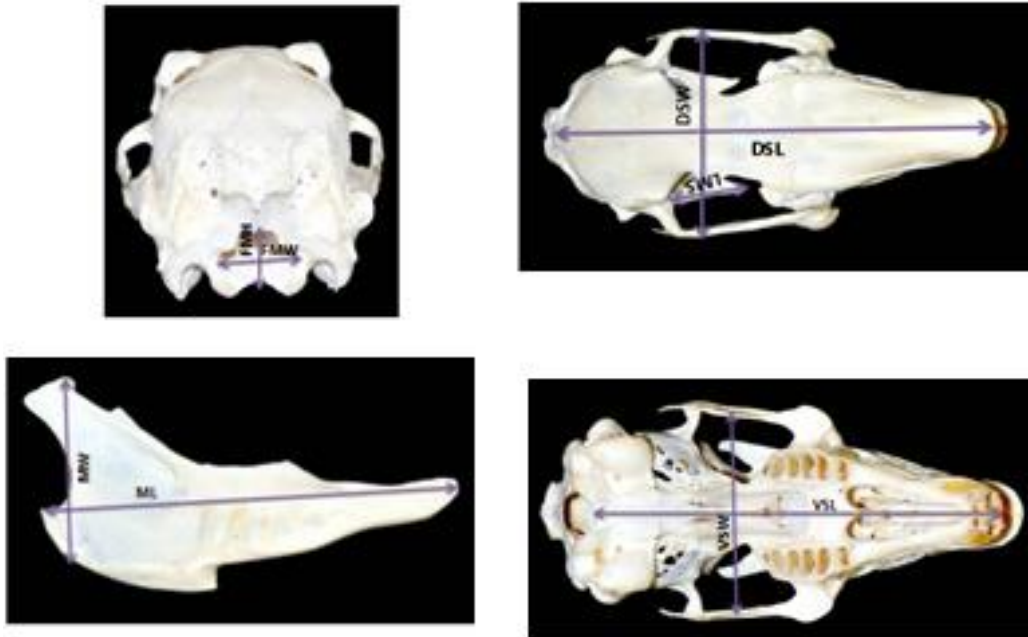


Fig (6): Some of the morphometric parameters of Africana Savanna hare. ML- Mandibular length, MH- Mandibular height, DSL- Dorsal skull length, VSL- Ventral skull length, DSW- Dorsal skull width, VSW-Ventral skull width, LMS-Length of margo supra-orbital, FMH-Foramen magnum height, FMW-Foramen magnum width.

Animal species in this Issue

African savanna hare (*Lepus microtis*)



Kingdom: Animalia & Phylum: Chordata & Class: Mammalia & Order: Lagomorpha & Family: Leporidae & Genus: *Lepus* & Species: *L. microtis*

The **African savanna hare** (*Lepus microtis*) is a species of mammal in the family Leporidae, native to Africa. It is native to diverse regions and habitats of Africa, including savannas and the Sahel. It is found in: Algeria, Botswana, Burundi, Chad, the Democratic Republic of the Congo, Ethiopia, the Gambia, Guinea, Guinea-Bissau, Kenya, Libya, Mali, Mauritania, Morocco, Mozambique, Namibia, Niger, Rwanda, Senegal, Sierra Leone, South Africa, Sudan, Tanzania, Tunisia, Uganda, and Zambia. The IUCN has listed its conservation status as being of "least concern".

The African savanna hare is a medium-sized species growing to a length of 41 to 58 cm with a weight of 1.5 to 3 kilograms. The ears have black tips, the dorsal surface of head and body is greyish-brown, the flanks and limbs are reddish-brown and the under parts are white. The general colouring is richer in tone than other hares, especially in mountain regions where the hares are a rather darker shade. The tail is black above and white below. This hare looks very similar to the Cape hare in appearance but can be told apart by its distinctively grooved incisors.

Source: Wikipedia, the free encyclopaedia

Development of the Rabbit (*Oryctolagus cuniculus*) Metanephros

W. Gaber

Department of Anatomy, Histology and Embryology, Faculty of Veterinary Medicine, Assiut University, Assiut, Egypt.

With 34 figures & 1 table

Received August, accepted in September 2017

Abstract

Thirty-seven rabbit embryos at embryonic days (E) 10-30 were used to study the morphogenesis of the metanephros by light microscope. The primordium of the metanephros appears at E 12 within the pelvic cavity as a spherical ureteric bud capped by metanephrogenic tissue. The nephrogenic spherules and the renal vesicles develop at E 15 while formation of the renal tubules and differentiation of the glomerular capsule take place at E 16. At E 18, differentiation of the glomerular capillaries occurs and the proximal and distal convoluted tubules are clearly first time demarcated. Positive alkaline phosphatase activity and PAS-positive material are confined to the metanephric corpuscles and the luminal border of the proximal convoluted tubules. In addition, the collecting tubules show large masses of intracytoplasmic PAS-positive granules. The rabbit metanephros is smooth unipapillary with indistinct renal columns and pyra-

mids. It undergoes migration until reaches its permanent position at E 30 where the right metanephros is located opposite to the level of the 2nd – 4th lumbar vertebrae and the left one is situated opposite to the level of the 3rd – 5th lumbar vertebrae. This migration is accompanied by rotation for about 135 degrees resulting in a dorsomedially located hilus. In conclusion, the stages of development of the rabbit metanephros are similar to those in other mammals but they maintain a delayed sequence.

Keywords: Rabbit, Metanephros, Development, Embryos.

Introduction

Metanephros is the primordium of the permanent kidney. It develops from two sources; ureteric bud (metanephric diverticulum) which forms the collecting part and metanephrogenic mass of intermediate mesoderm which gives the secretory part i.e. nephron (Huber, 1905;

Hamilton and Mossman, 1976; Kaufman, 1992; Imam, 2005). Many aspects of the development of the metanephros have been investigated by histologists and embryologists in different species; (Aoki, 1966; Rao and Padmini, 2012) in human, Canfield (1980) in bovine, Imam (2005) in camel and (Abbas and Rabie, 2012; Fayez et al., 2014) in rabbit.

The rabbit is the only known mammal in which the tubules can be separated from kidney slices with the basement membrane intact, a factor that has justified its use in many studies involving renal tubule physiology. Information about the known differences between the kidney of the rabbit and the kidneys of other mammals is therefore of special importance (Brewer, 2006). This article represents a light microscopic study on the development of the metanephros in rabbits during the prenatal life and aims to focus on its origin, early development and migration, in addition to the histological and histochemical changes of the nephron and the duct system during different embryonic stages.

Materials and Methods

Thirty seven normal New Zealand white rabbit embryos at embryonic days (E) 10-30 were collected from the Research Farm of Faculty of Agriculture, Assiut University, Egypt

(Table 1). Ethical approval was obtained from Animal Care and Use Committee of Assiut University. The pregnant rabbits were sacrificed at various periods of gestation and the embryos were removed shortly after evisceration. The embryos were fixed in 10% neutral buffered formalin or Bouin's fluid. For histological and histochemical studies, the embryos aged 10-26 days were taken as a whole while in those aged 28 and 30 days, only the metanephri were used. The fixed specimens were dehydrated in graded alcohol series, cleared, embedded in paraffin and serially sectioned at 3-5 μm thick. The obtained sections were stained with the following stains: Harris haematoxylin and eosin stain (Harris, 1900) for general histological studies, Periodic Acid Schiff reaction (PAS) (McManus, 1946) for detection of glycoproteins and Gomori calcium method (Gomori, 1952) for detection of alkaline phosphatase activity. The prepared sections were demonstrated by light microscope. For studying the position of the metanephri at full term, 3 embryos at E 30 were dissected.

Results

At E 10 and E 11, the ureteric bud could not be observed at the pelvic part of the mesonephric duct.

At E 12, the primordium of the metanephros could be observed as a

spherical ureteric bud capped by metanephrogenic tissue. The ureteric bud arises from the dorsal aspect of the caudal part of the mesonephric duct before its entrance into the urinary bladder. The metanephros primordium is located within the pelvic cavity, caudal to the mesonephros for some distance and is related dorsally to the aorta, ventrally to the rectum and ventrolaterally to the umbilical artery. The metanephrogenic tissue consists of an overcrowded inner layer and a loose outer layer of mesenchyme. This mesenchyme consists of small branched cells with little amount of cytoplasm and large oval nuclei (Fig. 1).

At E 13, the primordium of the metanephros extends more cranially to be located just caudal to the mesonephros. The metanephros becomes enlarged and elongated craniocaudally. The first division of the ureteric bud could be observed consisting of cranial and caudal branches surrounded by the metanephrogenic tissue. These branches are lined by simple columnar epithelium with rounded or oval basally located nucleus and acidophilic cytoplasm (Fig. 2). It becomes stratified in some areas and many mitotic divisions could be noticed.

At E 14, the metanephros is compressed between the last lumbar somites dorsally and the caudal end

of the mesonephros ventrally (Fig. 3). It is bean shaped where it has dorsal and ventral surfaces, cranial and caudal extremities, convex lateral border and slightly concave medial border. The ureter leaves the middle of the medial border. The two metanephri are opposite to each other craniocaudally and dorsoventrally. They are related medially to the aorta and projected laterally into the celomic cavity (Fig. 4). The ureteric bud gives off the second division. Each branch of the ureteric bud is capped by its own metanephrogenic tissue and all are surrounded by loose mesenchyme containing some red blood cells. The metanephros is surrounded externally by a thin layer of mesenchyme, which represents the prospective renal capsule (Fig. 5). The branches of the ureteric bud showed positive PAS reaction while the metanephrogenic tissue was PAS negative (Fig. 6).

At E 15, the metanephros is located dorsal to the mesonephros, just caudal to its middle (Fig. 7). The right metanephros is situated somewhat cranial and dorsal to the level of the left one (Fig. 8). The metanephros differentiates into an outer dense cortex and an inner loose medulla. The medulla contains few collecting tubules surrounded by large amount of intertubular mesenchyme. Each group of

the collecting tubules is capped by its own metanephrogenic tissue forming together the primitive renal lobes, which are separated from each other by interlobar mesenchyme containing many red blood cells. Outgrowths of the collecting tubules extend within the cortex with their terminal branches breaking down the metanephrogenic tissue into smaller separate portions. The cells of the metanephrogenic tissue around the collecting tubules are arranged in several layers. They are closely packed with large deeply stained nuclei. At the angle between the collecting tubule and its terminal branches, there are small nephrogenic spherules. Some of these spherules develop a narrow lumen in its center forming renal vesicles (Fig. 9). The collecting tubules showed PAS-positive material while the metanephrogenic tissue, the nephrogenic spherules and the renal vesicles were PAS negative.

At E 16, the metanephros extends a bit cranially to be located dorsal to the middle of the mesonephros. The nephrogenic tissue of the adjacent primitive renal lobes becomes completely fused forming a continuous outer nephrogenic layer giving the metanephros a smooth outer surface. Within the cortex, most of the metanephrogenic spherules develop into renal vesicles while; others remain solid and somewhat peripher-

ally located. Some of the renal vesicles become elongated into renal tubules and acquire different shapes; comma-shape and S-shape. Few of the ends of these tubules, which are close to the terminal branches of the collecting tubules, are continuous with them (Fig. 10). The other ends become ampullated and invaginated by mesenchymal mass to form a crescent-shaped glomerular capsule. This mesenchymal mass contains some red blood cells. The glomerular capsule has an outer parietal and an inner visceral layer with glomerular cavity inbetween. This cavity shows different width. The epithelium of the parietal layer is simple squamous while that of the visceral layer is low columnar (Fig. 11).

The renal tubules have narrow lumen and are lined by simple columnar epithelium with oval basally located nuclei and deeply stained cytoplasm. The terminal branches of the collecting tubules within the cortex are small, have wide lumen and lined by simple low columnar epithelium with oval basally located nuclei and pale cytoplasm. The intertubular mesenchyme contains some red blood cells. The part of the renal tubule nearby the glomerular capsule is the prospective proximal convoluted tubule. The other part near the terminal branches of the

collecting tubule is the prospective distal convoluted tubule and the middle part will form the loop of Henle.

The medulla contains stems of the collecting tubules surrounded by large amount of loose mesenchyme. These collecting tubules are large, have wide lumen and lined by high columnar epithelium with oval centrally located nuclei and pale cytoplasm. The cells of the collecting tubules showed masses of PAS-positive intracytoplasmic granules while the metanephrogenic tissue, the nephrogenic spherules, the renal vesicles as well as the renal tubules showed negative PAS reaction.

At E18, the cranial two thirds of the metanephros become cranial to the level of the mesonephros therefore; it is related ventrally to the liver on the right side and the stomach on the left (Figs. 12&13). The hilus becomes located somewhat dorsomedially (Fig. 14).

The metanephros is covered externally by connective tissue capsule. The outer layer of the cortex is represented by a thin layer of metanephrogenic tissue followed by the renal tubules. The peripheral renal tubules remain undifferentiated while the inner ones, towards the medulla, become differentiated into proximal convoluted tubules, loop of

Henle and distal convoluted tubules. The undifferentiated renal tubules have narrow lumen and are lined by simple columnar epithelium with large oval vesicular nuclei and dark cytoplasm (Fig. 15). The proximal convoluted tubules are numerous, large and lined by large cuboidal epithelium with rounded vesicular nuclei and eosinophilic cytoplasm with uneven luminal border. The distal convoluted tubules are few, smaller, have wide lumen and lined by cuboidal epithelium with dark cytoplasm.

Near the medulla, the mesenchymal mass, which invaginates into the glomerular capsule is differentiated into glomerular capillaries, some contain red blood cells. The visceral layer of glomerular capsule becomes lined by podocytes, which come in contact with the endothelium of the glomerular capillaries. The glomerulus and the glomerular capsule forming the metanephric corpuscles (Fig. 16).

The terminal branches of the collecting tubules between the undifferentiated renal tubules are lined by simple low columnar epithelium with oval basally located nuclei and pale cytoplasm while, that deeper in the cortex are lined by simple columnar epithelium with rounded centrally located nuclei and pale cytoplasm. The renal pelvis is lined by simple columnar epithelium with

rounded apically located nuclei and pale cytoplasm. In some areas, the epithelium was stratified (Fig. 17). Masses of PAS-positive granules could be seen within the cytoplasm of the collecting tubules. There was a slight PAS-positive material in the luminal border of some proximal convoluted tubules while the metanephric corpuscles, the distal convoluted tubules, the loop of Henle and the undifferentiated renal tubules showed negative PAS reaction (Fig. 18). Slight alkaline phosphatase activity was confined to the luminal border of the proximal convoluted tubules, the visceral epithelium of the glomerular capsule and the endothelium of the glomeruli (Fig. 19).

At E 20, the metanephros is related caudally to the degenerated mesonephros, cranially to the liver on the right side and the stomach on the left. Ventrally, it is related to the liver on the right side and the intestine on the left. The hilus is located dorsomedially. The layer of the metanephrogenic tissue in the outer part of the cortex becomes thinner and interrupted by renal tubules. The proximal and distal convoluted tubules increase in density on the expense of the outer undifferentiated renal tubules.

The renal pelvis gives off papillary ducts which branch into stems of

the collecting tubules (Fig. 20). In the mesenchyme close to the renal pelvis, some small renal tubules lined by cuboidal epithelium could be observed. Transitional epithelium could be detected in some areas of the lining epithelium of the renal pelvis. It consists of; basal layer of high cuboidal cells with rounded apically located nuclei, middle layer consists of several layers of polyhedral cells, the most outer one consists of pear-shaped cells, and a superficial layer of large cuboidal cells with dome-shaped apical surface (Fig. 21). The collecting tubules showed large masses of PAS-positive granules in their cytoplasm. Moderate PAS reaction and alkaline phosphatase activity could be observed within the luminal border of all proximal convoluted tubules as well as the juxtamedullary metanephric corpuscles.

At E 23 and E 24, the demarcation between the cortex and the medulla is well distinct (Fig. 22). The layer of the metanephrogenic tissue could not be observed. The medullary rays could be detected extending in the cortex towards the renal capsule forming the radiated part of the cortex, which alternates with the convoluted part of the cortex (Fig. 23). The interlobar blood vessels and the renal columns are indistinct consequently; the renal pyramids could not be detected. Within the medulla,

the arteria recti could be observed extending between the collecting tubules towards the renal pelvis (Fig. 24). The relative position of the main structures in the hilus is that the renal artery is located cranio-dorsally and the ureter is caudoven- trally while the renal vein is in- between (Figs. 25&26).

At E 26 and E 28, the metanephros reaches the adult structure. The ra- diated and convoluted parts of the cortex become well distinct (Fig. 27). The interlobar blood vessels could be clearly observed while the renal columns are still indistinct. The stems of the collecting tubules are directed towards the renal pelvis to open into the papillary ducts, which open on a common renal papilla that is projected within the large re- nal pelvis (Fig. 28). The stems of the collecting tubules and the papil- lary ducts are lined by tall columnar epithelium with centrally located nu- cleus (Fig. 29). The epithelium of the common renal papilla and the renal pelvis is transitional in type (Fig. 30).

At E 24 and E 26, strongly positive alkaline phosphatase activity and much PAS-positive material were confined to the metanephric corpus- cles and the luminal border of the proximal convoluted tubules (Figs. 31&32). The collecting tubules showed very large masses of intra-

cytoplasmic PAS-positive granules (Fig. 33).

At E 30, the right metanephros is located opposite to the level of the 2nd – 4th lumbar vertebrae within the renal impression of the liver, which is very deep and formed by the caudate process only. The left met- anephros is situated opposite to the level of the 3rd – 5th lumbar verte- brae (Fig. 34).

Discussion

The stages of development of the metanephros in rabbit are similar to those in other mammals but they maintain a delayed sequence where, according to the present study, the primordium of the meta- nephros is firstly observed at E 12 (about the end of the first half of gestation) consisting of ureteric bud surrounded by metanephrogenic tissue. The ureteric bud originates from the mesonephric duct before its entrance in the urinary bladder while, in human according to Sadler (2000), the primitive metanephros appears so early at the fifth week of gestation as an outgrowth from the mesonephric duct before its en- trance in the cloaca. Due to late de- velopment of the metanephros in rabbit, the cloaca has been differen- tiated into rectum, urinary bladder and urogenital sinus therefore, at this time; in rabbit the mesonephric duct opens in the urinary bladder

but not in the cloaca as in human. At early stage of development (E 12), the metanephros is spherical in shape and at E 13, it is elongated therefore, it has cranial and caudal ends. At E 14, the metanephros acquires its adult bean shape where, at this age it is compressed between the lumbar somites and the mesonephros so it has dorsal and ventral surfaces. In addition, due to the differential growth of its borders, the medial border becomes slightly concave and the lateral border becomes convex.

Nickel et al. (1973) stated that, during development of the metanephros, the type of the kidney depends upon the degree of fusion of the cortex and medulla of the adjacent lobes. If the fusion of the cortex is incomplete, the kidney becomes fissured as in ox but if the fusion is complete, the kidney becomes smooth as in horse, dog and small ruminants. On the other hand, if the papillae of the adjacent lobes are partially fused, the kidney is multipapillary as in ox and pig but in that of the horse, dog and small ruminants, the papillae are completely fused therefore; the kidney is unipapillary. In this respect, the results of the current work reveal that the kidney of the rabbit is smooth unipapillary as horse, dog and small ruminants where at E 15, the nephrogenic tissue of the adjacent

primitive lobes of the kidney is separated by interlobar mesenchyme but at E 16, this nephrogenic tissue completely fuses forming an outer smooth surface. On the other hand, at E 26, the papillae are completely fused forming a common renal papilla i.e. unipapillary kidney. These results are in accordance with Abbas and Rabie (2012) in rabbit fetuses.

The kidney undergoes a remarkable change in position during its development. It migrates from the pelvic to the lumbar region (Gruenwald, 1943; McGeady et al., 2006) and this is considered an exception to the general rule in developmental topography, since it migrates upward along the vertebral column, instead of downward like the other viscera (Jackson, 1909; Arey, 1965). Many authors have studied the migration of the kidney; Leeson and Baxter (1957) in rabbit, Canfield (1980) in bovine and Imam (2005) in camel. There is a great controversy about the mechanism of displacement of the kidney. Some authors assume that it is an active growth as the anlage elongates, extending forward along the line of least resistance in the loose mesenchyme of the space bounded by the aorta dorsally, the rectum ventrally, and the umbilical arteries laterally (Jackson, 1909), others believe that this displacement is probably due to a

diminution of the body curvature (Gruenwald, 1943), while others stated that in addition to being an active cranial migration it is also due to differential growth of the skeletal and muscular structures in the lumbo-sacral region (Patten, 1953; Arvey, 1965; McGeady et al., 2006).

Concerning migration, according to the current study, the metanephros of rabbit embryos is located in the pelvic cavity at E12 but at E 14, it is located dorsal to the caudal end of the mesonephros i.e. in the caudal part of the lumbar region then at E 15 it extends a bit cranially to be situated just caudal to the middle of the mesonephros while, Leeson and Baxter (1957) in the same animal stated that at E 15 the metanephros is present in the pelvis. In our study, we found that the metanephros of rabbit reaches the middle of the mesonephros at E 16 and at E18, the cranial two thirds of the metanephros become cranial to the level of the mesonephros then at E 20 it migrates more cranially to set cranial to the degenerated mesonephros and at E 30, it reaches its permanent position at the middle part of the sublumbar region. The rate of migration is not the same for both kidneys where, from E 12 to E 14, both kidneys have the same rate of migration as at E 14, they lie opposite to each other then after, the rate of migration of the right kidney is more rapid than the left one. Con-

sequently, at E 30 the right kidney is located more cranial, opposite to 2nd – 4th lumbar vertebrae while, the left is situated opposite to 3rd – 5th lumbar vertebrae. These results support the statements of El-Hagri (1967) and Nickel et al. (1973) who stated that, the right kidney of all domestic animals except the pig is somewhat more cranial than the left kidney.

In rabbit embryos, as the right kidney is cranial to the level of the left one, it is located in the renal impression of the liver. This impression is very deep and is formed only by the caudate process of the liver; the right lobe of the liver does not share in its formation. This result is in agreement with Gaber (2013) in rabbit. On the other hand, in the dog, ruminants and horse, the renal impression is formed by the caudate process and the right lobe of the liver (Nickel et al., 1973).

The position of the hilus of the rabbit kidney differs in the different stages of development and it depends upon the degree of rotation of the kidney along its longitudinal axis. At E 12, the ureter is connected to the ventral aspect of the primitive metanephros. At E 14, the hilus is located medially as the kidney rotates medially for about 90 degrees along its long axis. At E 18, the hilus is situated somewhat dorsomedially and at E 20, it is placed dorsomedially as a result of its rotation dorsally for about 45 degrees. In the same

respect, according to Patten (1953) and Arey (1965) the kidneys of human, during their migration, undergo a rotation of 90 degrees, so that the original dorsal border becomes the convex lateral border and the hilus faces medially rather than ventrad. Nickel et al. (1973) stated that, the hilus in horse is located ventrally, that of small ruminants and dog medially but in the left kidney of ox, it is located dorsally. In camel, the hilus is directed ventrally (Imam, 2005).

In rabbit, the renal artery, vein and ureter enter the hilus where, their arrangement to each other differ in different stages of development but this arrangement reaches its adult form at E 23 as, the renal artery is located craniodorsally and the ureter is caudoventrally while the renal vein is inbetween. This arrangement is similar to that present in horse and large ruminants but in small ruminants and dog, the ureter is located in the middle while in pig, the ureter is the most dorsal (El-Hagri, 1967).

According to the present article, the renal pelvis of rabbit is relatively large as the kidney is unipapillary but its lining epithelium differs according to the stage of development from simple columnar to transitional epithelium.

The present results reveal that at E 15 i.e. the half of gestation period,

the terminal branches of the collecting tubules break down the metanephrogenic tissue into small nephrogenic spherules and some of these spherules develop into renal vesicles while in human, the first vesicle is formed at the end of the seventh week (Mishra et al., 2006) and in bovine, nephron induction starts as early as 4-6 weeks gestation (Canfield, 1980). At E 16, some of the renal vesicles become elongated into renal tubules and few of the ends of these tubules, which are close to the terminal branches of the collecting tubules, are continuous with them. The other ends become ampullated and invaginated by mesenchymal mass to form a crescent-shaped glomerular capsule. Differentiation of the proximal and distal convoluted tubules takes place at E 18 but in human, the proximal and distal convoluted tubules are clearly first time demarcated at 17 weeks of fertilization (Tank et al., 2012).

This study is in agreement with Aoki (1966) in human who stated that, the early migration of erythrocytes into the vesicular invagination occurs before the glomerular capillaries are completely developed. Similarly, in rabbit we found that, the glomerular capillaries differentiate at E 18 while red blood cells could be observed within the mesenchymal

mass invaginating the glomerular capsule at E 16 and within the loose mesenchyme surrounding the branches of the ureteric bud and the interlobar mesenchyme earlier at E 14 and E 15.

At E 23 and E 24, the medullary rays could be detected extending in the cortex towards the renal capsule forming the radiated part of the cortex. Within the medulla, the arteria recti could be observed extending between the collecting tubules towards the renal pelvis. At E 26 and E 28, the interlobar blood vessels could be clearly observed while the renal columns are indistinct consequently; the renal pyramids could not be detected.

According to our observations, positive alkaline phosphatase activity and PAS-positive material were confined to the metanephric corpuscles and the luminal border of the proximal convoluted tubules and the intensity of these reactions increased with increase in fetal age. This similarity in the distribution of alkaline phosphatase and PAS-positive material was mentioned before by Moog and Wenger (1952) and Leeson and Baxter (1957) in rabbit. In addition, we found that the collecting tubules showed large masses of intracytoplasmic PAS-positive granules throughout all the developmental stages. Localization of alkaline phosphatase in the lu-

minal border of the proximal convoluted tubules was also observed by Chida (1993) in rat kidney. Alkaline phosphatase is involved in the reabsorption of glucose in the tubules of the kidney (Lundsgaard, 1935) and the distinctive distribution of the alkaline phosphatase in the luminal border of the proximal convoluted tubules is indicative of functional ability (Bradfield, 1950) that the distinctive distribution of the alkaline phosphatase in the luminal border of the proximal convoluted tubules is indicative of functional ability. Davies (1953) mentioned that, presence of PAS positive granules in the tubule cells of the metanephros may be indicative of protein which had crossed the glomerular membrane and had been reabsorbed by proximal tubule cells. I suggest that reabsorption of protein takes place in the collecting tubules in addition to the proximal convoluted tubules.

References

- Abbas, J.G. and Rabie, F.O. (2012):** Histomorphological study of tubular system and collecting tubules in domestic rabbit's fetuses. Kufa journal for veterinary medical sciences, 3 (1): 67-76.
- Aoki, A. (1966):** Development of the human renal glomerulus. Anat. Rec., 155: 339-352.
- Arey, L.B. (1965):** Developmental anatomy. A textbook and laboratory

manual of embryology. 7th Ed. W. B. Saunders Co. Philadelphia. London.

Bradfield, J.R.G. (1950): The localization of enzymes in cells. *Biol. Rev.*, 25: 113-157.

Brewer, N.R. (2006): Biology of the rabbit. *Journal of the American Association for Laboratory Animal Science*, 45: 8-24.

Canfield, P. (1980): Development of the bovine metanephros. *Zbl. Vet. Med. C. Anat. Histol. Embryol.*, 9: 79-107.

Chida, K. (1993): Immunohistochemical detection of alkaline phosphatase in formalin-fixed and paraffin-embedded rat organs by means of avidin-biotin peroxidase complex method. *Okajimas Folia Anat. Jpn.*, 70 (5): 203-208.

El-Hagri, M.A.A. (1967): Splanchnology of domestic animals. The public organization for books and scientific appliances. Cairo Univ. Press.

Fayez, S.E.; Sayed-Ahmed, A.; Abo-Ghanema, I.I. and Elnasharty, M.A. (2014): Morphogenesis of rabbit kidney pre-and postnatal. *Alexandria Journal of Veterinary Sciences*, 41: 47-61.

Gaber, W. (2013): Prenatal developmental studies on the rabbit liver. Ph.D. Thesis, Assiut University, Assiut, Egypt.

Gomori, G. (1952): Histochemistry of estrases. *Int. Rev. Cytol.*, 1: 323.

Gruenwald, P. (1943): The normal changes in the position of the embryonic kidney. *Anat. Rec.*, 85: 163-176.

Hamilton, J.W. and Mossman, H.W. (1976): Human embryology. 9th Ed. Macmillan Press Ltd., London.

Harris, H.F. (1900): On the rapid conversion of haematoxylin into haematein in staining reactions. *J. Appl. Microsc. Lab. Methods*, 3: 777-780. Cited by Bancroft et al. (1996).

Huber, G.C. (1905): On the development and shape of uriniferous tubules of certain of the higher mammals. *American Journal of Anatomy*, 4 (4): 1-98.

Imam, H.M.A. (2005): Early embryonic development of the camel metanephros. *Assiut Vet. Med. J.*, 51: 12-20.

Jackson, C.M. (1909): On the developmental topography of the thoracic and abdominal viscera. *Anatomical record*, 3 (7): 361-396.

Kaufman, M.H. (1992): The atlas of mouse development. Academic Press. Harcourt Brace Jovanovich, Publishers, London. San Diego. New York. Boston. Sydney. Tokyo. Toronto.

Leeson, T.S. and Baxter, J.S. (1957): The correlation of structure and function in the mesonephros and metanephros of the rabbit. *J. Anat., Lond.*, 91: 383-390.

Lundsgaard (1935): The effect of phloridzin on the isolated kidney and isolated liver. *Skandinav. Arch. f. Physiol.*, 72: 265-270.

McGeady, T.A.; Quinn, P.J.; Fitzpatrick, E.S. and Ryan, M.T. (2006): *Veterinary embryology.* Blackwell Publishing. Ltd, Oxford.

McManus, J.F.A. (1946): Histological demonstration of mucin after periodic acid. *Nature (London)*, 158: 202.

Mishra, S.; Dinesh, A. and Kaul, J.M. (2006): Morphological and morpho-metrical study of human renal development during mid-gestation period. *J. Anat. Soc. India*, 55 (2): 5-10.

Moog, F. and Wenger, E.L. (1952): The occurrence of a neutral muco-

polysaccharide at sites of high alkaline phosphatase activity. *Amer. J. Anat.*, 90: 339-377.

Nickel, R.; Schummer, A. and Seiferle, E. (1973): *The viscera of the domestic mammals.* Verlag Paul Parey Berlin. Hamburg.

Patten, B.M. (1953): *Human embryology.* 2nd Ed., McGraw-Hill Book Company, Inc. New York, Toronto, London.

Rao, B.N. and Padmini, M.P. (2012): Prenatal histogenesis of kidney in human fetuses. *International Journal of Basic and Applied Medical Sciences*, 2 (2): 144-147.

Sadler, T. W. (2000): *Langman's Medical Embryology.* 6th Ed., Williams and Wilkins.

Tank, K.C.; Saiyad, S.S.; Pandya, A.M.; Akbari, V.J. and Dangar, K.P. (2012): A study of histogenesis of human fetal kidney. *Int J Biol Med Res.*, 3(1): 1315-1321.

Corresponding author:

e-mail: wafaa.anatomy@gmail.com

Table (1): Age and number of used embryos.

Age (day)	10	11	12	13	14	15	16	18	20	23	24	26	28	30
Number	4	3	4	3	3	4	2	4	2	1	1	1	1	4

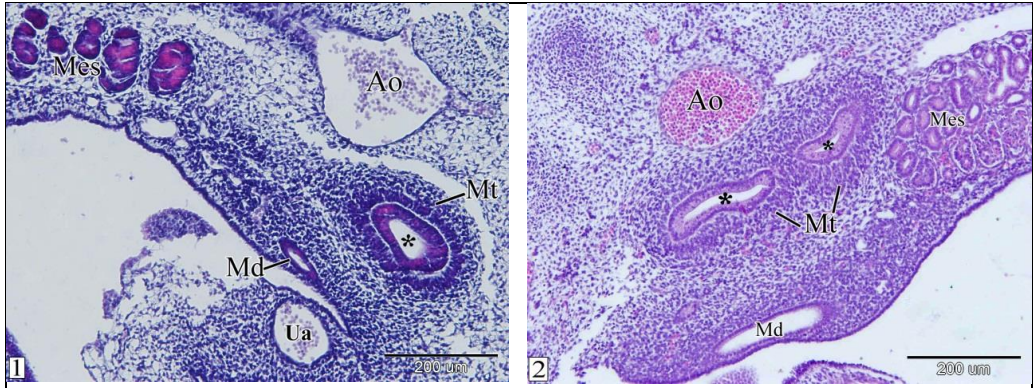


Fig (1): Sagittal section in a rabbit embryo at E 12 showing the primordium of the metanephros. Ureteric bud (*), metanephrogenic tissue (Mt), mesonephric duct (Md), mesonephros (Mes), aorta (Ao) and umbilical artery (Ua). (H&E, X 100).

Fig (2): Sagittal section in a rabbit embryo at E 13 showing the branches of the ureteric bud (*) surrounded by the metanephrogenic tissue (Mt). Mesonephric duct (Md), mesonephros (Mes) and aorta (Ao). (H&E, X 100).

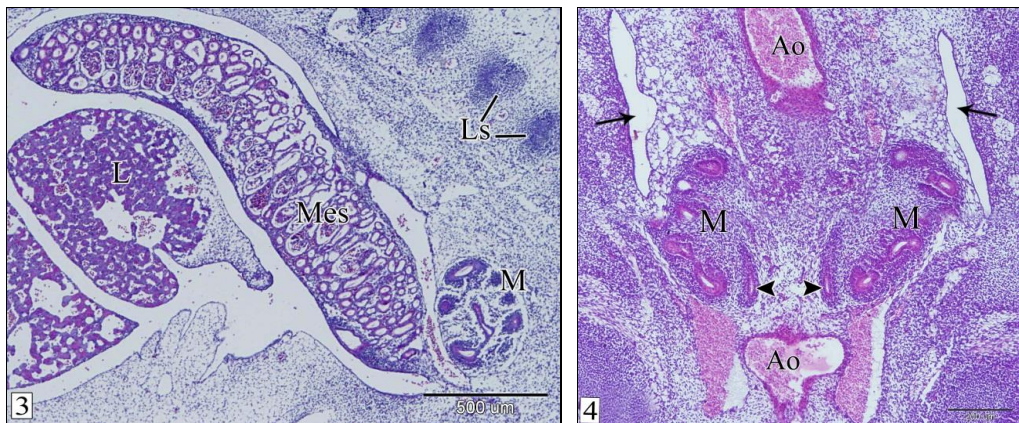


Fig (3): Sagittal section in a rabbit embryo at E 14 showing the metanephros (M) is located dorsal to the caudal end of the mesonephros (Mes). Lumbar somites (Ls) and liver (L). (H&E, X 40).

Fig (4): Frontal section in a rabbit embryo at E 14 showing the metanephri (M) are bean shaped and located opposite to each other. Ureter (arrowhead), aorta (Ao) and celomic cavity (arrow). (H&E, X 100).

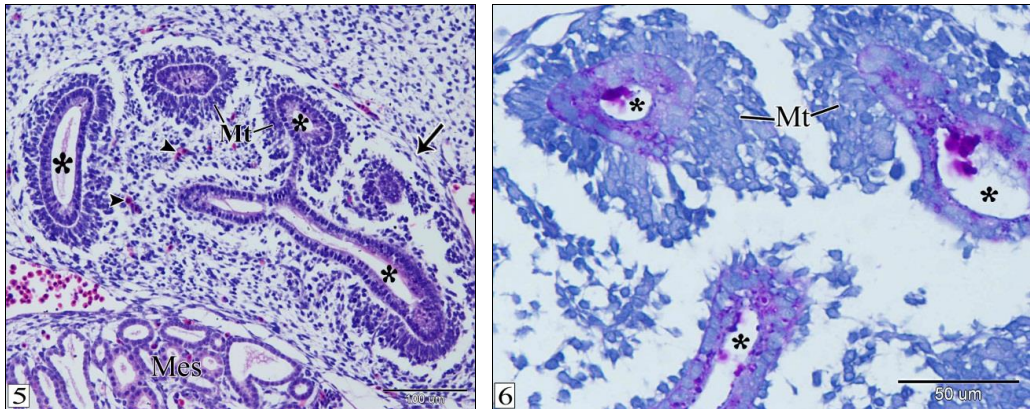


Fig (5): Sagittal section in a rabbit embryo at E 14 showing the structure of the meta-nephros. Branches of the ureteric bud (*), metanephrogenic tissue (Mt), red blood cells (arrowheads), prospective renal capsule (arrow) and mesonephros (Mes). (H&E, X 200).

Fig (6): Sagittal section in a rabbit embryo at E 14 showing positive PAS reaction in the branches of the ureteric bud. Notice, the metanephrogenic tissue has negative PAS reaction. Branches of the ureteric bud (*) and metanephrogenic tissue (Mt). (PAS-Haematoxylin, X 400).

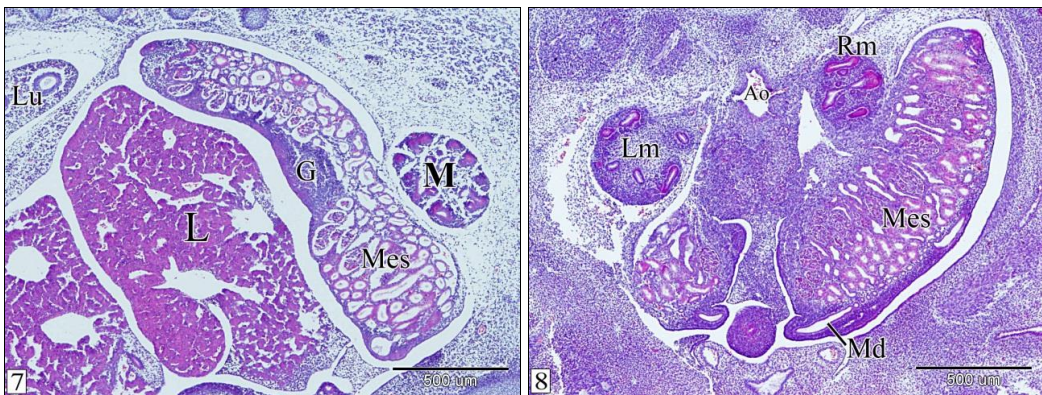


Fig (7): Sagittal section in a rabbit embryo at E 15 showing the metanephros (M) is located dorsal to the mesonephros (Mes), just caudal to its middle. Gonad (G), liver (L) and lung (Lu). (H&E, X 40).

Fig (8): Frontal section in a rabbit embryo at E 15 showing the right metanephros (Rm) is located somewhat cranial to the left metanephros (Lm). Mesonephros (Mes), mesonephric duct (Md) and aorta (Ao). (H&E, X 40).

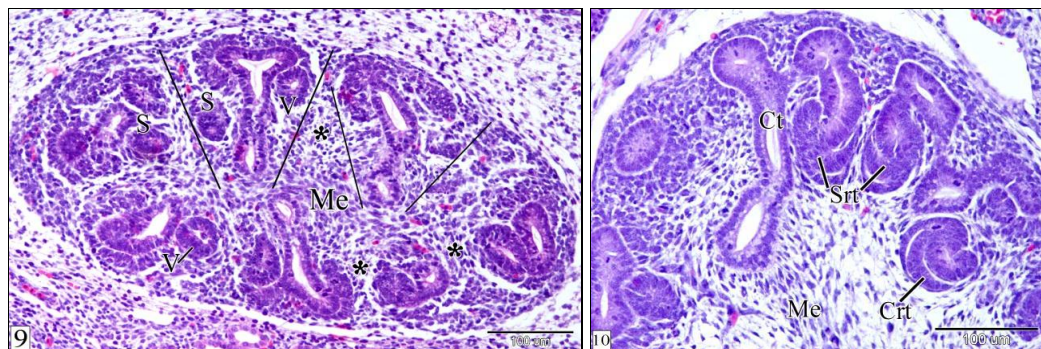


Fig (9): Sagittal section in a rabbit embryo at E 15 showing the structure of the metanephros. Primitive renal lobes (selected areas), interlobar mesenchyme (*), nephrogenic spherules (S), renal vesicles (V) and medulla (Me). (H&E, X 200).

Fig (10): Sagittal section in a rabbit embryo at E 16 showing the smooth surface of the metanephros and the different shapes of the renal tubules. Notice, the connection between the S-shape renal tubule (Srt) and the collecting tubule (Ct). Comma-shape renal tubule (Crt) and medulla (Me). (H&E, X 200).

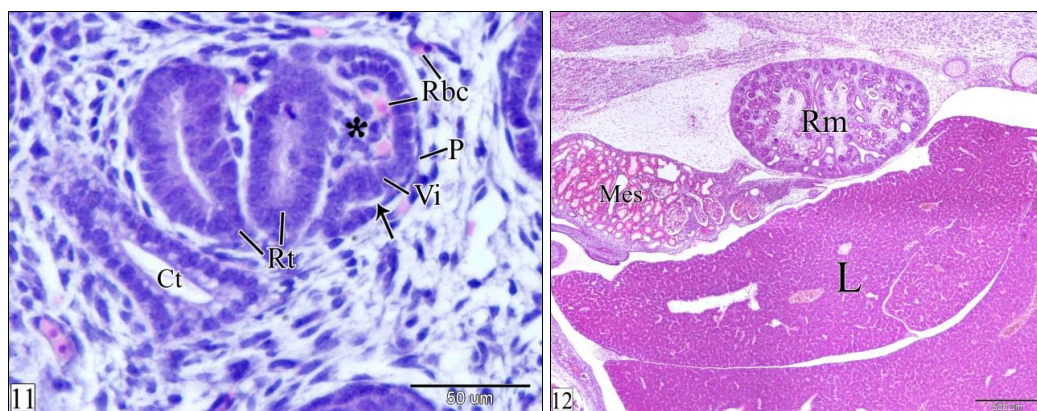


Fig (11): Sagittal section in a rabbit embryo at E 16 showing the ampullated end of the renal tubule invaginated by mesenchymal mass (*) forming glomerular capsule. Parietal layer of glomerular capsule (P), glomerular cavity (arrow), visceral layer of the glomerular capsule (Vi), red blood cells (Rbc), renal tubule (Rt) and collecting tubule (Ct). (H&E, X 400).

Fig (12): Sagittal section in a rabbit embryo at E 18 showing the right metanephros (Rm) is related ventrally to the liver (L). Mesonephros (Mes). (H&E, X 40).

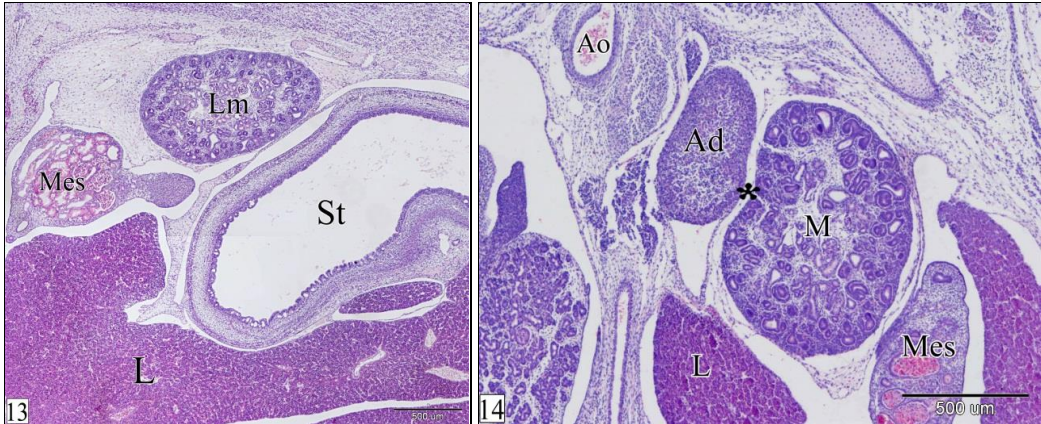


Fig (13): Sagittal section in a rabbit embryo at E 18 showing the left metanephros (Lm) is related ventrally to the stomach (St). Mesonephros (Mes) and liver (L). (H&E, X 40).

Fig (14): Transverse section in a rabbit embryo at E 18 showing the hilus of the meta-nephros (*) is somewhat dorsomedially located. Metanephros (M), mesonephros (Mes), liver (L), adrenal gland (Ad) and aorta (Ao). (H&E, X 40).

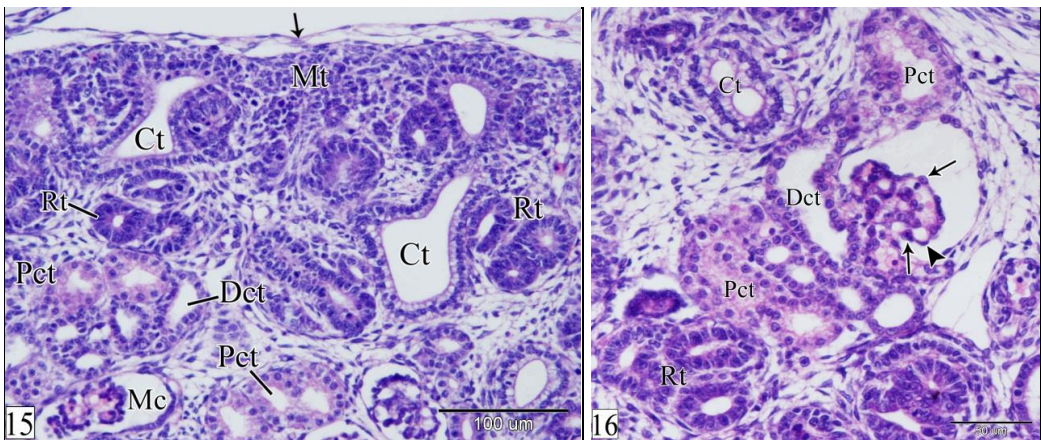


Fig (15): Sagittal section in a rabbit embryo at E 18 showing the structure of the meta-nephric cortex. Renal capsule (arrow), metanephrogenic tissue (Mt), collecting tubule (Ct), renal tubule (Rt), proximal convoluted tubules (Pct), distal convoluted tubules (Dct) and metanephric corpuscle (Mc). (H&E, X 200).

Fig (16): Sagittal section in a rabbit embryo at E 18 showing the structure of the deep part of the metanephric cortex. Proximal convoluted tubules (Pct), distal convoluted tubules (Dct), podocytes (arrows), endothelium of the glomerular capillaries (arrow head), renal tubule (Rt) and collecting tubule (Ct). (H&E, X 400).

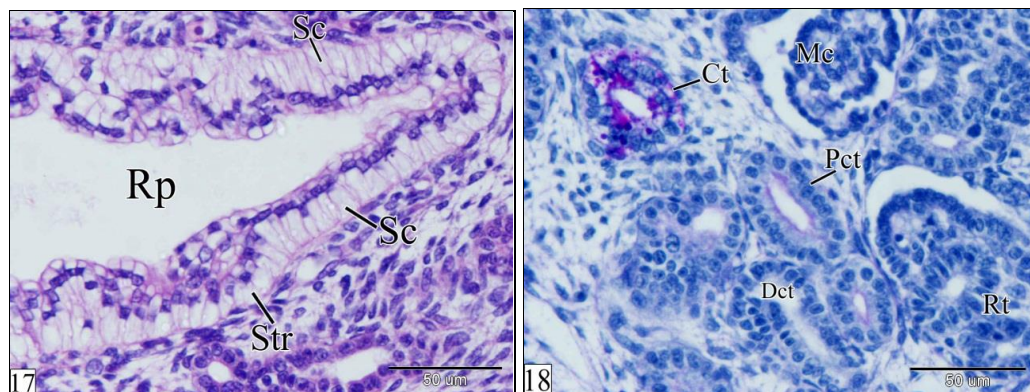


Fig (17): Sagittal section in a rabbit embryo at E 18 showing the lining epithelium of the renal pelvis (Rp). Simple columnar epithelium (Sc) and stratified epithelium (Str). (H&E, X 400).

Fig (18): Sagittal section in a rabbit embryo at E 18 showing masses of PAS-positive granules in the cytoplasm of the collecting tubules (Ct) and a slight PAS-positive material in the luminal border of some proximal convoluted tubules (Pct). Metanephric corpuscles (Mc), distal convoluted tubules (Dct) and renal tubules (Rt). (PAS-Haematoxylin, X 400).

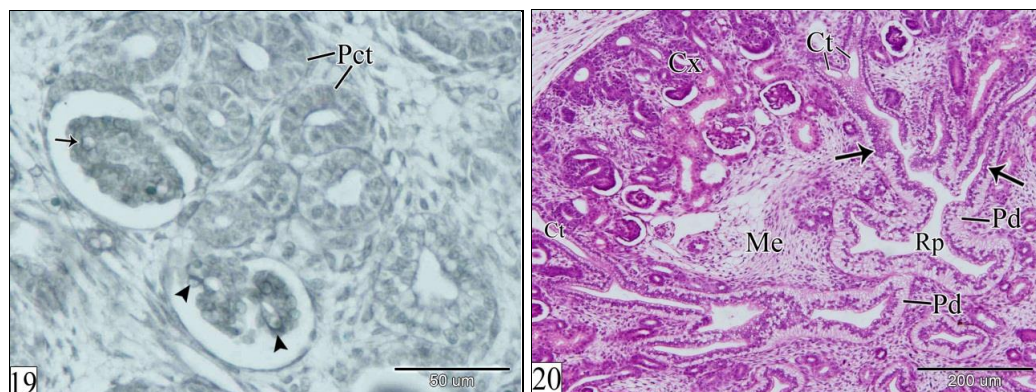


Fig (19): Sagittal section in a rabbit embryo at E 18 showing Slight alkaline phosphatase activity in the luminal border of the proximal convoluted tubules (Pct), the visceral epithelium of the glomerular capsule (arrow heads) and the endothelium of the glomeruli (arrow). (Gomori calcium method, X 400).

Fig (20): Transverse section in a rabbit embryo at E 20 showing the renal pelvis (Rp) gives off papillary ducts (Pd). Stems of the collecting tubules (arrows), collecting tubules (Ct), cortex (Cx) and medulla (Me). (H&E, X 100).

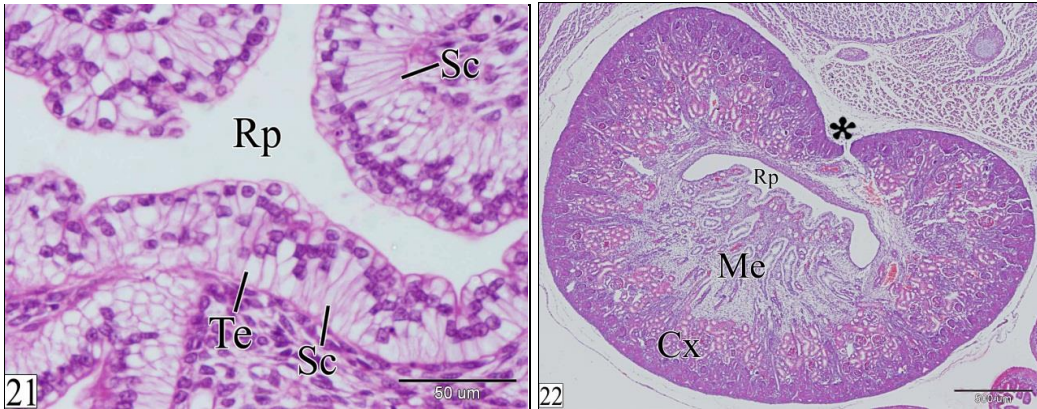


Fig (21): Transverse section in a rabbit embryo at E 20 showing transitional epithelium (Te) in some areas of the lining epithelium of the renal pelvis (Rp). Simple columnar epithelium (Sc). (H&E, X 400).

Fig (22): Transverse section in a rabbit embryo at E 24 showing increase the demarcation between the cortex (Cx) and the medulla (Me). Renal pelvis (Rp) and hilus (*). (H&E, X 40).

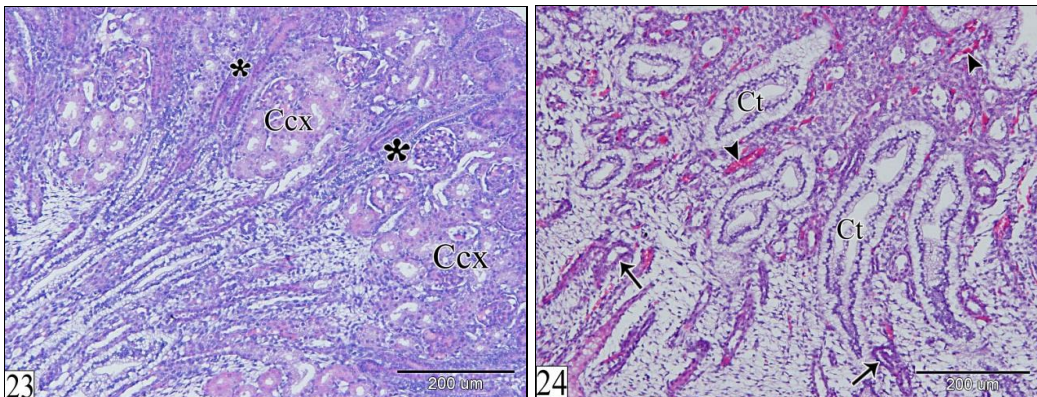
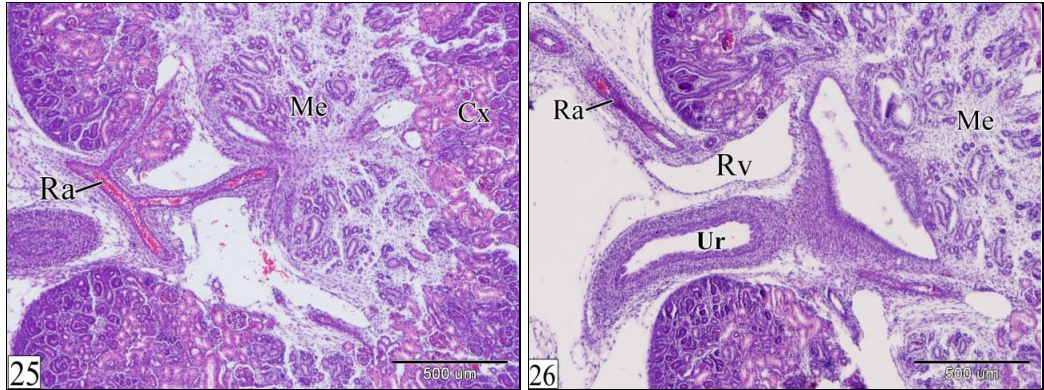


Fig (23): Transverse section in a rabbit embryo at E 24 showing the medullary rays (*) extending in the cortex. Convoluted part of the cortex (Ccx). (H&E, X 100).

Fig (24): Transverse section in a rabbit embryo at E 24 showing the arteria recti (arrow heads) between the collecting tubules (Ct). Loop of Henle (arrows). (H&E, X 100).



Figs (25 & 26): Frontal sections in a rabbit embryo at E 23 showing the relative position of the main structures in the hilus. Renal artery (Ra), renal vein (Rv), ureter (Ur), cortex (Cx) and medulla (Me). (25) is a more dorsal level than (26). (H&E, X 40).

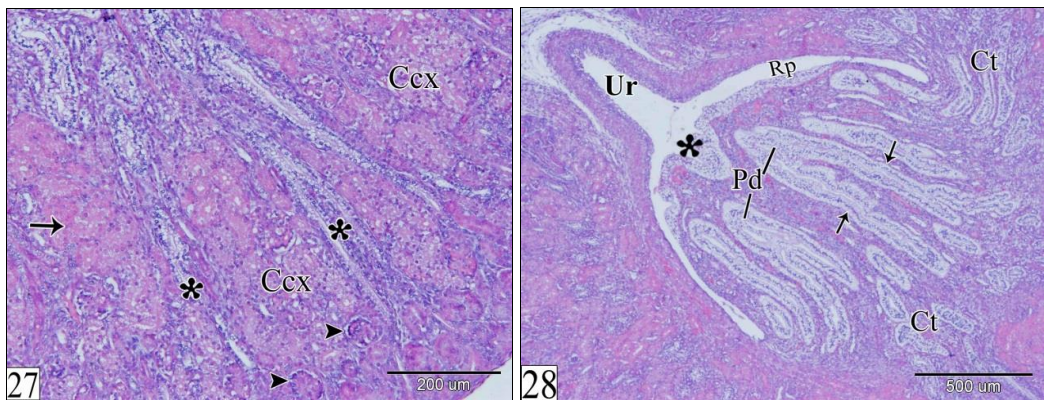


Fig (27): Transverse section in a rabbit embryo at E 26 showing the radiated and convoluted parts of the cortex. Radiated part (*), convoluted part (Ccx), metanephric corpuscles (arrow heads) and convoluted tubules (arrow). (H&E, X 100).

Fig (28): Transverse section in a rabbit embryo at E 26 showing the meta-nephros is unipapillary. Ureter (Ur), renal pelvis (Rp), common renal papilla (*), papillary ducts (Pd), stems of the collecting tubules (arrows) and collecting tubules (Ct). (H&E, X 40).

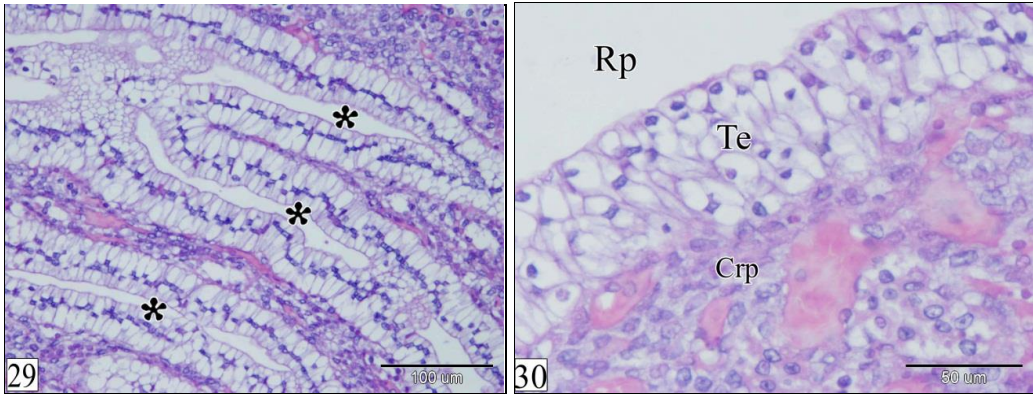


Fig (29): Transverse section in a rabbit embryo at E 26 showing the stems of the collecting tubules (*) are lined by tall columnar epithelium with centrally located nucleus. (H&E, X 200).

Fig (30): Transverse section in a rabbit embryo at E 26 showing the common renal papilla (Crp) is covered by transitional epithelium (Te). Renal pelvis (Rp). (H&E, X 400).

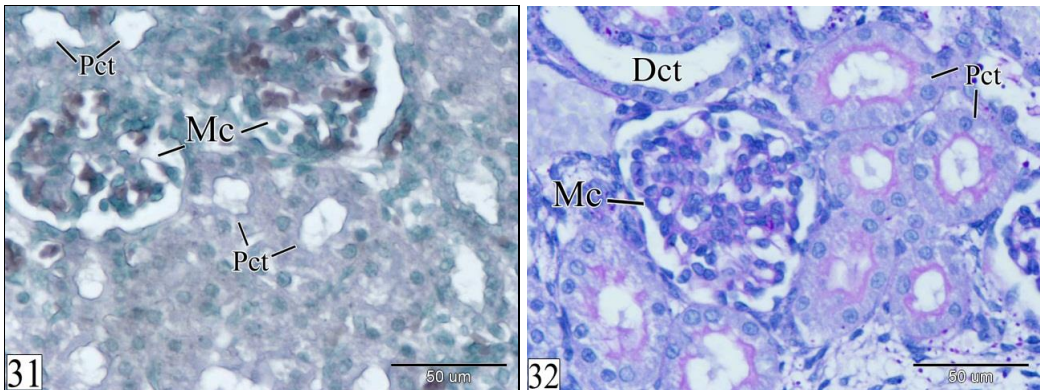


Fig (31): Transverse section in a rabbit embryo at E 24 showing strongly positive alkaline phosphatase activity within the metanephric corpuscles (Mc) and the luminal border of the proximal convoluted tubules (Pct). (Gomori calcium method, X 400).

Fig (32): Transverse section in a rabbit embryo at E 24 showing strong PAS-positive material within the metanephric corpuscles (Mc) and the luminal border of the proximal convoluted tubules (Pct). Notice, the distal convoluted tubules (Dct) are PAS-negative. (PAS-Haematoxylin, X 400).

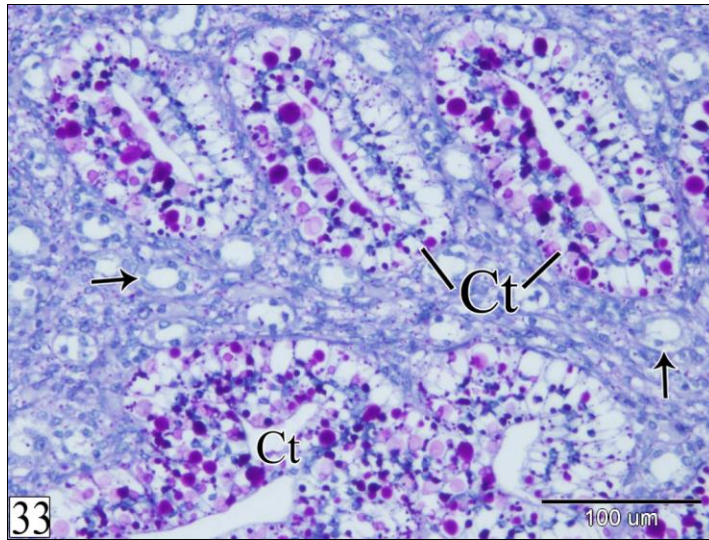


Fig (33): Transverse section in a rabbit embryo at E 26 showing very large masses of PAS-positive granules in the cytoplasm of the collecting tubules (Ct). Notice, the loop of Henle (arrows) is PAS-negative. (PAS-Haematoxylin, X 200).

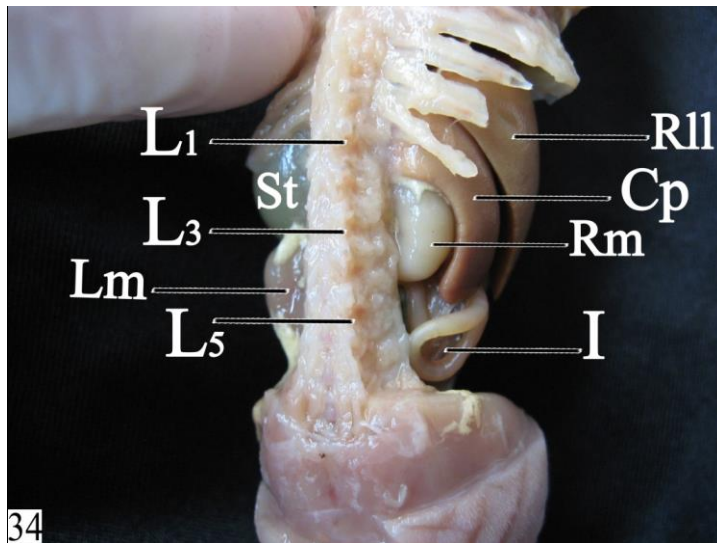


Fig (34): Photograph of a rabbit embryo at E 30 showing the position of the metanephros. Right metanephros (Rm), left metanephros (Lm), right lobe of the liver (Rl1), caudate process (Cp), intestine (I), stomach (St), first lumbar vertebra (L₁), third lumbar vertebra (L₃) and fifth lumbar vertebra (L₅).

Instruction to Contributors (Journal of Veterinary Anatomy)

The Journal of African Association of Veterinary Anatomists is published by half-Yearly from Asila for Design and Publishing , 32 Mohamed Awad Str. Nasr City, Cairo , EGYPT. It is in digital print size of 20.5x27.5 cm in two columns with a print area of 17x22 cm. It will be known as **Journal of Vet. Anat.** with **Volume** number on yearly basis and Number on issues per volume basis (in exceptional cases there can be more than two issues in a volume).

Nature of coverage: This journal is dedicated to disseminate scientific information in form of: Original research articles in , histology, embryology, teratology, cell biology and learning veterinary anatomy.

Submission of manuscript: Mail two copies of the Manuscript and two complete sets of figures to Prof. Dr. A . S. Saber, editor, Journal of Vet. Anat., Department of Anatomy & Embryology, Faculty of Veterinary Medicine, Sadat City Branch, Menoufiya University, EGYPT.

The manuscript should be sent in a heavy paper envelope and photographs or illustrations should be enclosed in a cardboard to avoid damage during mail handling. The Manuscript should be accompanied by a covering letter from the author responsible for correspondence. It should also contain a statement that manuscript has been seen and approved by all co-authors. Editor and members of the editorial board are not responsible for the opinions expressed by authors and reserves the right to reject any material or introduce editorial changes. Material will be accepted for publication on the understanding that it has not been published in any other form and is not being considered elsewhere. Any material once accepted for publication may not be republished in any form without prior permission of the author.

Manuscripts can also be accepted on CD, computers, PM5 or PM6 Microsoft-Word-5 or compatibles, Microsoft-Excel-4, Cricket Graph-4 Statview-4 or compatibles. It would be in the interest of authors to accompany a hard copy.

Preparation of the manuscript: Manuscript should be typed on white bond paper (A4 or 5 size) with a margin of 4 cm on right side, 3 cm on left side, top and bottom. British English, spellings and generic names of drugs should be used. International Code of Zoological Nomenclature, *Nomina Anatomica Veterinaria*, International Code of Nomenclature of Bacteria, International Code of Botanical Nomenclature and International Standards should be strictly followed. All terms should be identified by their scientific names and for easy comprehension common terms/names can be used.

Each of the following sections should be types on separate pages:

Title page: This page should contain title of the article, name of the department/institution where work has been done, present postal address of each author and name of author to whom reprint request should be addressed. Following is the example:

Example: Cardiac Looping and Formation of the Heart Regions in Japanese Quail Embryo (Coturnix coturnix):

A.S. Saber, K.M. Shoghy, A.M. Erasha and M.M.Nada

Department of Anatomy & Embryology, Faculty of Vet. Med., Sadat City Branch, Menoufiya University, EGYPT

Send Reprint Request to Prof. Dr. A. S. Saber

Abstract and Key words: The abstract should begin with title of the article (in upper case), and have brief procedures, salient results and conclusions not more than 225 words, in one paragraph on second page. Proprietary names and abbreviations should be avoided. Provide four to six key words below the abstract for indexing services. Abstract is not necessary for short communications, case reports, news items etc.

Text: The proper text of the paper should start from third page and should again begin with title of the article (in upper case). The text should be divided into sections with headings, introduction, materials and methods, results, discussion, tables/illustrations and references.

Introduction: The logic of the introduction is to introduce the specificity and relevance of the topic to the readers. It should include the objective of the work in brief and most important related reference(s). Materials and Methods: Should contain details regarding materials and brief account of procedures used.

However, sufficient details must be included to reproduce the results. For established or routine methods only related reference(s) can be cited. Any deviation from routine procedures should be specifically mentioned. Only

generic names of the drugs and chemicals should be used in the running text. The trade names, source or other necessary related information should be mentioned in parenthesis there in.

In case reports, the case record sheet should also be included in materials and methods.

Statistical methods if used should be briefly described along with reference. If any analysis is done with the help of a computer programme, its complete name and source should be mentioned, however, it does not mean to exclude the mention of methods, level of significance and other relevant information.

Results and Discussion should be presented in logical sequence with implications of findings about other relevant studies. The data or information easily attainable from the tables or graphics need not be repeated in the results. Only important observations need to be summarized. Undue repetition of the text from results to discussion has to be avoided. To preclude it, depending on article, results and discussion can be combined. In discussion only significant results should be discussed. One should not always stick to the term 'statistically significant' data rather biological importance or significance of any variation should be given due importance in discussion. Discussion should always end in conclusions linked with objectives of the study mentioned in the introduction and unqualified statements should be avoided.

Tables: Each table should be typed on separate sheet. Large tables should be avoided and should not exceed one page. Each table should be numbered in Indo-Arabic numerals according to their sequence in the text that refers to it. In the text it should be referred as proper noun e.g., Table 1. The title of the table should be brief and self-explanatory. Footnotes can be included to enhance understanding ability of the contents of the table.

Illustrations and Legends: All illustrations should be submitted in duplicate and about twice the size desired for reproduction that is 17 cm for double column or 8.3 cm for single column. Photographs and photomicrographs should be printed on glossy paper with excellent details and contrast. Drawings and diagrams should be in India ink (Black) on smooth white paper. All illustrations should be referred as figures in the text and should also be numbered in Indo-Arabic numerals e.g., Fig 1. Legends of all these figures should be typed on a separate sheet. Each legend should be clear, concise and informative. A statement of magnifications or reductions should be given where it is applicable. Nothing should be written with pen or typed on the back of any illustration except it bears running title of the paper, figure number and arrow indicating top edge with light pencil. All graphs should be supported with data on a separate sheet to redo them (in certain special cases) according to format of the journal.

References: References to the work should be cited in the text with author's surname and year of publication in the parenthesis e.g., Saber (1995) or Saber *et al.* (1995) or (Saber *et al.* 1995), depending upon construction of the sentence. In case there are two authors the conjunction 'and' or its symbol '&' should be used according to construction of the sentence.

References should be arranged in alphabetical order. Authors should not modify the title of the references. Mention full name of the journal. Examples of correct forms of references are given below:

Reprints: There is no provision for free reprints. Author or person in correspondence has to pay EL 300 (for Egyptian Citizens only) or US \$ 100 or £ 55 or Euro 70, in advance for 10 reprints. Additional reprints in multiples of 10 may be requested and will be charged at the same rate but with minimum order of 30 reprints and every request for extra reprints should be made, if required, before 30th May or November every year.

Charges for colour and black and white pictures: Author(s) has to pay for production of colour plates in his/her manuscript. More than 4 black and white picture will be charged from the author(s) towards printing charges.

Copyright: The copyright of the article will remain with the owner, Prof. Dr. A.S.Saber and will be governed by the Egyptian Copyright Act.

AFRICAN



**Journal of
Veterinary Anatomy**

www.vetanat.com